2016

Performance evaluation of continuity connections for use in modular construction

Andrew J. Putz
Iowa State University

Performance evaluation of continuity connections for use in modular construction

by

Andrew J. Putz

A thesis submitted to the graduate faculty

in partial fulfillment of the requirements for the degree of

MASTER OF SCIENCE

Major: Civil Engineering (Structural Engineering)

Program of Study Committee:
Brent M. Phares, Major Professor
Jiehua Jay Shen
Jennifer Shane

Iowa State University

Ames, Iowa

2016

TABLE OF CONTENTS

LIST OF FIGURES iv

LIST OF TABLES vi

ACKNOWLEGEMENT vii

ABSTRACT viii

CHAPTER 1. INTRODUCTION 1
1.1 Background 1
1.2 Scope and Objectives 4
1.3 Report Format 6

CHAPTER 2. LITERATURE REVIEW 7

CHAPTER 3. EXPERIMENTAL PROCEDURE 12
3.1 Overview 12
3.2 Test A: Longitudinal Joints 16
3.2.1 Specimen Details 16
3.3.2 Fabrication Procedure 21
3.2.3 Instrumentation Plan 26
3.2.4 Curing and Ponding Tests 28
3.2.5 Strength Tests 29
3.3 Test B: Transverse Joints 31
3.3.1 Specimen Details 31
3.3.2 Fabrication Procedure 36
3.3.3 Instrumentation Plan 39
3.3.4 Strength Tests 41

CHAPTER 4. RESULTS AND DISCUSSIONS 45
4.1 Test A: Longitudinal Joints 45
4.1.1 Curing and Ponding Tests 45
4.1.2 Crack and Failure Patterns 46
4.1.3 Comparison of Surface Preparation Techniques 49
4.1.4 Load, Strains, and Deflections 50
4.2 Test B: Transverse Joints 63
4.2.1 Crack and Failure Patterns 64
4.2.2 Loads, Strains, and Deflections 69

CHAPTER 5. SUMMARY, CONCLUSIONS, AND RECOMMENDATIONS 82
5.1 Longitudinal Joints 82
5.1.1 Curing and Ponding Tests 83
5.1.2 Crack and Failure Patterns 83
5.1.3 Surface Preparation Techniques 84
5.1.4 Loads, Strains, and Deflections 85
5.2 Transverse Joints 85
5.2.1 Crack and Failure Patterns 86
5.2.2 Loads, Strains, and Deflections 87

CHAPTER 6. REFERENCES 88

LIST OF FIGURES

Figure 3-1. Specimen Design Locations 14
Figure 3-2. Cross Section of the Little Siler Creek Bridge 14
Figure 3-3. Constructed Little Silver Creek Bridge 15
Figure 3-4. Longitudinal Joint Detail 17
Figure 3-5. Cross Section of Left Deck Panel 17
Figure 3-6. Cross Section of Right Deck Panel 17
Figure 3-7. Reinforcing Steel Layout of Left Deck Panel 18
Figure 3-8. Reinforcing Steel Layout of Right Deck Panel 19
Figure 3-9. Cross-Section of Jointless Specimen 22
Figure 3-10. Reinforcing Steel Layout of Jointless Specimen 22
Figure 3-11. Steel Reinforcement and Formwork Fabrication 23
Figure 3-12. Fabrication of Three Different Joint Options 24
Figure 3-13. Placement of HPC for the Deck Panels 25
Figure 3-14. Formwork Construction and Placement of Joint Material 25
Figure 3-15. Surface Mounted Instrumentation 27
Figure 3-16. Embedded Instrumentation for Jointed Specimens 27
Figure 3-17. Embedded Instrumentation for Jointless Specimens 28
Figure 3-18. Setup for Curing and Ponding Tests 29
Figure 3-19. Enclosure for Ponding Test 29
Figure 3-20. Setup for Strength Tests 30
Figure 3-21. Continuous Strength Testing Setup 31
Figure 3-22. Details of the Compression Block 32
Figure 3-23. Fabricated Compression Block 33
Figure 3-24. Reinforcing Steel Layout for Deck of both Specimens 34
Figure 3-25. Details of Specimen I 35
Figure 3-26. Details of Specimen II 36
Figure 3-27. Cross Section Details 36
Figure 3-28. Placement of Shear Studs 37
Figure 3-29. Diaphragm End of Girders 38
Figure 3-30. Formwork Construction 39
Figure 3-31. Embedded and Surface Mounted Gauges 39
Figure 3-32. Embedded Instrumentation for Specimen I 40
Figure 3-33. Embedded Instrumentation for Specimen II 40
Figure 3-34. Surface Mounted Instrumentation for Specimen I 41
Figure 3-35. Surface Mounted Instrumentation for Specimen II 41
Figure 3-36. Testing Setup for Specimen I 42
Figure 3-37. Testing Setup for Specimen II 42
Figure 3-38. Laboratory Test Setup 43
Figure 3-39. West and East Side Loading Configuration 44
Figure 4-1. Examination of Ponding Test 45

Figure 4-2. Crack Patterns 47
Figure 4-3. Flexural Cracking 48
Figure 4-4. Failure Cracks 48
Figure 4-5. Joint Investigation 49
Figure 4-6. Comparison of Joint Surfaces 50
Figure 4-7. Load vs. Strain - Specimen C1 (1st Test) 52
Figure 4-8. Load vs. Strain - Specimen C1 (2nd Test) 52
Figure 4-9. Load vs. Strain - Specimen C2 53
Figure 4-10. Load vs. Strain - Specimen C3 53
Figure 4-11. Load vs. Strain - Specimen J1 (Plastic Formliner-UHPC) 54
Figure 4-12. Load vs. Strain - Specimen J2 (Form-Retarder-UHPC) 54
Figure 4-13. Load vs. Strain - Specimen J4 (Rubber Formliner-UHPC) 55
Figure 4-14. Load vs. Strain - Specimen K1 (Form-Retarder-K-UHPC) 55
Figure 4-15. Load vs. Strain - Specimen K2 (Plastic Formliner-K-UHPC) 56
Figure 4-16. Load vs. Strain - Specimen K3 (Rubber Formliner-K-UHPC) 56
Figure 4-17. Load vs. Deflection for all Test A Specimens 63
Figure 4-18. Crack Formations on Deck Slab for Each Specimen 66
Figure 4-19. Diaphragm Cracks on Short Side for Each Specimen 67
Figure 4-20. Diaphragm Cracks on Long Side for Each Specimen 67
Figure 4-21. Localized Failure of Specimen II Under the Loading Point 68
Figure 4-22. Reinforcing Steel Examination 68
Figure 4-23. Cracking of Diaphragm for Specimen I 69
Figure 4-24. Revised Loading Configuration of Specimen I 69
Figure 4-25. Load vs. Strain 6 in. West of the Diaphragm - Specimen I 71
Figure 4-26. Load vs. Strain 6 in. West of the Diaphragm - Specimen II 71
Figure 4-27. Load vs. Strain Center of the Diaphragm - Specimen I 72
Figure 4-28. Load vs. Strain Center of the Diaphragm - Specimen II 72
Figure 4-29. Load vs. Strain 6 in. East of the Diaphragm - Specimen I 73
Figure 4-30. Load vs. Strain 6 in. East of the Diaphragm - Specimen II 73
Figure 4-31. Strain Values 6 in. West of the Diaphragm 76
Figure 4-32. Strain Values Center of Diaphragm 76
Figure 4-33. Strain Values 6 in. East of the Diaphragm 76
Figure 4-34. Load vs. Strain on Girder at Midpoint 78
Figure 4-35. Load vs. Strain on Girder 6 in. Outside of Diaphragm 78
Figure 4-36. Load vs. Strain on Compression Block 79
Figure 4-37. Load vs. Displacement of both Specimens 81
Figure 4-38. West vs. East Loading Rates 81

LIST OF TABLES

Table 4-1. Summary of all Test A Results 58
Table 4-2. Testing Results for each Surface Preparation Technique 58
Table 4-3. Summary of Results by Joint Material 60
Table 4-4. Compressive Strength Testing Results for Joint Materials 62
Table 4-5. Compressive Strength Tests Results 64
Table 4-6. Distance from Loading to Gauge Locations 64
Table 4-7. Summary of Tests Results at Each Cross-Section 74
Table 4-8. Summary of Critical Tests Results 80

ACKNOWLEGEMENT

There are several people I would like to thank who have made this research possible. I want to start by thanking my committee chair, Brent Phares, and committee members, J. Jay Shen, and Jennifer Shane for their advice along the course of this research. I want to thank Doug Wood for his expertise and assistance in the laboratory. I also want to extend my thanks to Yaohua Deng (Jimmy) for his continued guidance and support throughout the whole research process. Lastly, I would like to thank my family and friends. Without their support and encouragement, this thesis would not have been possible.

ABSTRACT

With the growing concern of our nation's aging infrastructure, several new ideas and concepts are being developed and implemented throughout several state departments. These turnkey innovative designs are being introduced into a rapid renewal technique called Accelerated Bridge Construction (ABC). ABC was developed under the Second Strategic Highway Research Program (SHRP 2), which targeted strategic solutions to improve several aspects of transportation including, safety, congestion, and renewal methods for roads and bridges. Prefabricated bridge elements and systems (PBES) is one technique often associated with ABC. It incorporates the use of prebuilt modules, which include part of the girder system and a portion of the bridge deck. Some of the most critical components in a modular system are the closure pours required to connect each prefabricated module. High performance materials (HPM) such as Ultra High Performance Concrete (UHPC) are often being used for the longitudinal connections today. The transverse closure joints are used over the piers and connect each adjacent module. In this particular study, a steel compression block was placed on the piers and positioned tightly between the two adjacent modules to attempt to reduce the compressive forces that were transferred through the diaphragm.

To assess the performance of the longitudinal and transverse joint details that were designed for use on a demonstration bridge, several specimens were constructed with a replica of the joint detail and ran through a series of lab tests to determine the strength and constructability. There were also specimens designed and constructed as a

standard cast-in-place bridge deck that served as a baseline for comparison purposes. It was proven that the performance of the longitudinal joint detail was very consistent to the continuity that is provided by a monolithic slab. Two different materials were tested for use as the longitudinal joint material, Ductal UHPC and Korean UHPC. Both materials had comparable results throughout testing. As for the transverse joints, the inclusion of the steel compression block showed to effectively alter the performance, as the specimen was able to withstand a larger moment prior to ultimate failure.

CHAPTER 1. INTRODUCTION

1.1 Background

Historically, the construction of bridges did not interfere with public transportation. This was primarily due to the fact that these bridges were brand new and constructed simultaneously as the roadway. Nowadays, the already established roadway infrastructure in the United States is deteriorating rapidly. Specifically speaking, the United States roadway infrastructure consists of over 600,000 bridges and approximately 25% of those bridges are in need of repair or replacement (American Society of Civil Engineering (ASCE), 2015). Currently, the average age of bridges is 44 years old and they were typically designed for a life expectancy of 50 years (Federal Highway Administration, 2014). And, currently over 20% of bridges in the state of Iowa alone are considered structurally deficient, meaning that deterioration is prominent in one or more components, but is not yet unsafe to use (Mulholland, 2015). This makes Iowa the third worst in the country in terms of structurally sound bridges (Shoup, Donohue, & Lang, 2011). With approximately 24,000 bridges throughout the state, repairing all of the deficiencies would not be feasible using traditional construction practices. New techniques are currently being studied to help manage all the required bridge construction throughout the United States needed in the next few years. These new techniques are providing greater safety in the work-zone, fewer impacts on the area surrounding construction, minimizing traffic disturbances, and greatly reducing construction time. Among these techniques is Accelerated Bridge Construction (ABC), which was being

developed and studied under the Second Strategic Highway Research Program (SHRP 2) (Federal Highway Administration, 2014) and elsewhere.

ABC techniques taking advantage of prefabricated bridge elements and high performance materials are more and more commonly being utilized for bridge replacement projects resulting in minimal road closure time/traffic interruption and re-construction of long-lasting highway bridges. Moving towards increased adoption, these techniques have been utilized in several demonstration bridge projects. For instance, the goal of the SHRP 2 Project R04 was to develop standards and codified language for ABC and to also provide for the construction of demonstration bridges like the Keg Creek Bridge which consisted of several prefabricated steel beam/concrete deck components connected with both transverse and longitudinal closure pours. To address design concerns about performance in the negative moment region, lab tests were conducted to evaluate the Ultra-high performance concrete (UHPC) transverse full-depth deck joint over the pier of the demonstration bridge (Hartwell, 2011).

As part of the State of Iowa's growing program to utilize ABC technologies and approaches, there are current plans to construct even more of the bridge system originally used for the Keg Creek Bridge. This continued evolution of promising concepts is a demonstration of the Iowa DOTs commitment to enhancing bridge construction. The second-generation bridge system was utilized to replace a bridge located on Iowa 92 over Little Silver Creek in Pottawattamie County, Iowa. For this project, prefabricated bridge elements were placed adjacently on the substructure and connected using closure pour connections.

State-of-the-art planning and design along with advanced construction techniques and materials allows ABC to provide safe and economical solutions. Prefabricated bridge elements and systems (PBES) are becoming more often incorporated into the ABC design. Having the ability to fabricate several of the bridge elements off-site ensures high quality products and greatly reduces construction time, which in turn reduced road closures. Typically, the elements are delivered to the site during the construction of the substructure. The elements are then lifted into place and connected to one another by closure pours. At this time one of the most common materials used to complete the longitudinal joints in ultra high performance concrete (UHPC), which is an ideal closure material due to its high durability, high strength, superior bond action, very low permeability, and short development lengths for reinforcement. Transverse connections are generally completed using high performance concrete (HPC). HPC is predominantly used to help counter environmental effects that lead to premature deterioration, which is done through chemical admixtures. The HPC is placed between two adjacent elements over the pier locations to form the diaphragm and bridge deck. This location of a bridge is of particular importance due to the forces that are imposed at this connection.

Due to heavy traffic loads and growing span lengths, the forces that are transferred over the pier locations continue to increase. The induced tensile forces are primarily accounted for by the reinforcement in the bridge deck. Additional reinforcing bars are added to this location to reduce potential problems and control cracking. A recent study by the Bridge Engineering Center specifically studied negative moment reinforcement (Bridge Engineering Center, 2015). It was found that current Iowa

Department of Transportation (Iowa DOT) requirements for negative moment reinforcement were satisfactory and the supports do not have any issues with significant cracking.

Traditionally, the concrete diaphragm was the only component used as the compressive force transfer mechanism. The idea came to embed a steel section in the diaphragm between two adjacent girders. The steel section resembled the design of a concrete cinder block and would be referenced to as a steel compression block. Again, the purpose of this block is to better transfer the compressive forces through the concrete diaphragm while eliminating excessive compressive stress seen in the concrete.

1.2 Scope and Objectives

The objective of this research was to evaluate and improve the design of two types of joints that will be used on a replacement project for a bridge located on Iowa 92 over Little Silver Creek in Pottawattamie County, Iowa. The new bridge demonstrates the use of PBES and high performance materials (HPM). Both a longitudinal joint and a transverse joint detail were evaluated. The principal goal for the longitudinal joint was to determine the continuity and strength of the UHPC joint as well as the constructability of the detail that was used. As for the transverse joint, the goal was to see how the compressive forces were altered due to the addition of the steel compression block that was embedded between the two adjacent bridge beams. To accomplish this research, the following five tasks were followed.

Task 1: Literature Review

An in-depth literature search pertaining to relevant information, such as that related to ABC, longitudinal connection joints, transverse connection joints, and high performance materials started off the research. Another part of the literature review included looking at recommendations from past research projects to determine the most efficient methods to use while conducting the experimental testing.

Task 2: Specimen Design

Two different specimen types were designed for this research. All of the designs that were to be used for this project were drawn to scale in AutoCAD and checked to make sure all of the sections aligned correctly. An important consideration that went into the designs was planning ahead and making sure the specimens would line up with the required spacing in the laboratory needed for the strength tests.

Task 3: Specimen Construction

Do to the size of the full-scale specimens and the availability of lab space; the construction of the specimens was separated into different phases. Phase one consisted of all nine longitudinal specimens, and phase two included the two transverse specimens.

Task 4: Laboratory Testing

Laboratory Testing was also split up into the same two phases. The longitudinal specimens were tested in three days, with three specimens tested each day. Only one transverse specimen could be tested in a day, resulting in a total of two test days for these specimens.

Task 5: Draw Conclusions and Write Report

The last step of the research consisted of evaluating all of the data, drawing conclusions based on what was seen, and developing a report based on these findings.

1.3 Report Format

This report has been divided into chapters and subsections to facilitate navigation for the reader. Following Chapter 1, a literature review pertaining previous joint designs and related research findings is presented in Chapter 2. Chapter 3 starts with an overview of the experimental procedure and then goes into detail about the specimen designs. Chapter 3 is also the first chapter that starts separating the longitudinal and transverse joints in the subsections. This format for the subsections will continue through Chapter 5. Chapter 4 provides the results that were gathered from the experimental testing. Lastly, the summary and conclusions are provided in Chapter 5.

CHAPTER 2. LITERATURE REVIEW

Numerous methods have been studied throughout the years in an attempt to improve steel bridge construction. Recently, several surrounding state departments have started implementing the use of simple span configurations, which have often been called simple-made-continuous (SMC) (Johnson, 2015). These designs utilize an initial simply supported layout where the girders are eventually turned continuous through transverse closures involving the concrete diaphragm, bridge deck, and longitudinal reinforcement. In this setup, the simply supported sections support the dead loads and then once the concrete diaphragm cures all other loads are transferred throughout the system. The construction sequence to allow for this is as follows (Culmo, 2009):

- First, erect the beams and allow them to span from support to support, but leave a slight gap at each support.
- Cast the bridge deck, besides over the support locations near the beam-ends.
- Complete the pier closure pour by casting a block of concrete between the beam-ends.
- Lastly, cast the remaining section of the bridge deck, which can be cast with the pier closure pours.

This system is intended to replace the old system where the girders were field spliced. The bolted or welded field splice adds additional time to construction and significantly increases the labor cost. Several surrounding states have taken interest in this concept and a few of the findings will be reviewed.

A recent study performed at the University of Nebraska Lincoln by Dr. Azizinamini, Yakel, and Farimani looked into new methods for steel girder bridges (Azizinamini, 2005). New connection details were developed in the study, which allowed the girders to be placed on the supports acting as simple spans under the construction loads. The girders would later become continuous by means of the reinforcing steel, concrete deck and diaphragm. Three specimens were tested in the study and designed based on a study by the National Bridge Research Organization (NBRO). The designs were selected to examine how the compressive forces were being transferred between two adjacent steel girders over the piers. There were 3 specimens designed and fabricated for this study.

Specimen #1 consisted of the most complex design. It involved welding the bottom flanges of the two adjacent girders together, adding bearing plates that were welded to the ends of each girder, and a triangular gusset plate, which was welded above the bottom flange on each girder. The most distinguishing factor in this design is the continuity that's provided by attaching the bottom flanges. This detail allows the specimen to transfer large compressive forces without crushing the concrete diaphragm. Specimen #2, the simplest design, solely consisted of placing the girders on the piers and casting them in the concrete diaphragm. There was no additional steel attached to the girders for this specimen. Specimen #3 was very similar to specimen #1 besides the bottom flanges of the girders were not connected together. It only consisted of the bearing plates welded to the ends of the girders.

These three methods were analyzed through a series of fatigue testing followed by ultimate load testing. The results for crack load, yielding load, and ultimate load were compared as well as the deflection at these loads. Due to test errors in the strain gauges, some results were missing for Specimen #3. The strain data that was used for analysis revealed that both the cracking and yielding load for specimen #1 was slightly higher than that for Specimen #2.

The failure pattern of each specimen was also mentioned. First signs of damage for all of the specimens were noticed by cracks on the top surface of the deck near the edges of the pier. Failure was then dependent on the specimen details. Specimen #2 and #3 experienced brittle failures with the concrete crushing over the pier. Specimen #1 had a more desirable, ductile failure with the reinforcing steel in the deck all yielding prior to ultimate failure. It was made clear that the connection detail used for Specimen #1 served as an effective transfer mechanism for the pier.

A dissertation (Johnson, 2015) provided additional research and testing on SMC bridges with particular interest in the force transfer mechanism. The report presents results that were produced through lab testing and numerical analysis in the search of an alternative SMC design that used a steel diaphragm in lieu of the standard concrete diaphragm. Traditionally concrete has been the main material used for the diaphragms. However when comparing the two, steel appears to be advantages over concrete in several areas including cost, maintenance, and safety. Laboratory testing for this work was done at Colorado State University (CSU) Engineering Research Center. The testing setup consisted of two composite cantilevered girders, which were loaded at each end.

There was only one specimen tested for this study. The specimen design included two W33x152 girders that were cantilevered out from the reinforced pier that was also constructed for this study. Both of the girders were welded to a sole plate, which sat on a neoprene-bearing pad. A safety device was also incorporated into the design. It was essentially just a steel plate that was bolted down to the pier between the two bottom flanges to prevent any possible injuries. A W27x84 steel beam was selected to use for the steel diaphragm and provided the lateral stability of the specimen.

Load applicator beams were secured to the slab near both ends of the cantilevers. The sizes of these beams were selected to be able to distribute the whole load across the entire 72-inch width of the specimen. A 220 kip and two 110 kip actuators were used for the north and south end, respectively. Loading was initially controlled by displacement at a rate of .5 mm/minute. Instrumentation of the specimen was selected based on preliminary finite element analysis and included steel and concrete strain gages and string and linear potentiometers.

Due to shrinkage effects of the concrete, the expected applied load to failure increased from 90 to 98 kips. This corresponds to a design moment of 1172 ft-kip. Testing started and proceeded until a load of 85 kips was applied on each side. At this point testing was stopped due to what was described as “a loud bang”. Through inspections by visual examination it appeared there was no failure. Testing was resumed until reaching a load of 132 kips where testing was halted until the following day. Later that day it was discovered that the safety device was engaged due to axial and bending

deformation of the sole plate. The solution for the problem was to remove 1/16" off each side of the safety device and testing was restarted.

A much faster loading rate of .1 mm/second was used for the second day of loading. Additional load was added up until about 120 kips had been applied. At this point, another "loud bang" was heard. However this time, multiple failures were noticed in the thinner weld on the north girder. After examination, testing was recommenced one final time and continued until a load of 198 kips was applied. There was no additional evidence of failure at this point. Looking through the data it was noted that the reinforcing steel never became fully stresses. This means that the load transfer mechanism is critical to the success of the design. In this case, the sole plate was the most important and it was found that the weld size must be increased in order to transfer the full compressive forces that were developed. Lastly, it was found that the overall crack and failure patterns produced from testing correlated well with both the predicted results and those shown in similar tests.

CHAPTER 3. EXPERIMENTAL PROCEDURE

3.1 Overview

As mentioned previously, the purpose of this project is to evaluate the performance and benefits of using Prefabricated Bridge Elements and Systems (PBES) connected by closure pour connections. Prefabricated bridge elements fabricated in a controlled environment generally have a high level of quality. However, the closure pour connections commonly used in both the longitudinal and transverse directions can be the most critical components in a modular bridge due to potential issues related to serviceability, ductility, strength, and load transfer.

All specimen designs for this study came directly from the details specified for The Little Silver Creek Bridge, which is located on IA 92 in Pottawattamie Country, Iowa (Iowa Department of Transportation, 2016). The bridge is a second-generation design completed by the Iowa DOT for use in Accelerated Bridge Construction (ABC). The bridge, shown in Figure 3-1 through Figure 3-3, was designed as a skewed three-span modular rolled steel beam bridge with a length of 234 ft, a roadway width of 44 ft, and a skew angle of 15 degrees. The bridge span lengths are 91, 92, and 51 ft from the west to east. It is a second-generation design that included many of the same components of the first-generation bridge, the U.S. 6 Bridge over Keg Creek (Iowa Department of Transportation, 2016), but incorporated several additional challenges to evaluate the overall effectiveness of the technology and design. The Keg Creek Bridge won the category of Best Use of Innovation award for a small project in the America's

Transportation Awards competition (Bryant & Ford, 2013). America's Transportation Awards is used to recognize the best transportation projects across America and present the benefits they are creating in communities throughout the country.

The superstructure of the bridge contains 18 prefabricated modules, each consisting of two W40x149 girders and a 7 ft wide concrete deck panel. All of the modules were fabricated onsite in a staging area adjacent to the bridge site. After the substructure was completed, the modules were lifted into place and set in their final positions. Each module spanned from one substructure unit to the next adjacent one allowing the members to act as simply supported during the erection process. All of the modules were spaced 10 in. apart along the whole length of the bridge to allow for the longitudinal joints to be constructed between each adjacent module. The longitudinal joints (see Figure 3-1 and Figure 3-2) were specified to be completed using ultra-high performance concrete (UHPC) to establish continuity throughout the structure. For the transverse joints, the modules where placed against compression blocks, which were anchored into the piers. Section 3.3.1 Specimen Details discusses more of the details of the steel compression block, but its general appearance matched that of a concrete masonry unit (cinder block). Shims were used to fill any gaps between the compression blocks and the girder ends, which had steel plates welded to them to allow more surface area to come into contact with the blocks. The compression blocks were used in hopes to transfer compressive forces through the diaphragm to each adjacent module. The transverse closure pours for the diaphragms over the piers were completed using high performance concrete (HPC).

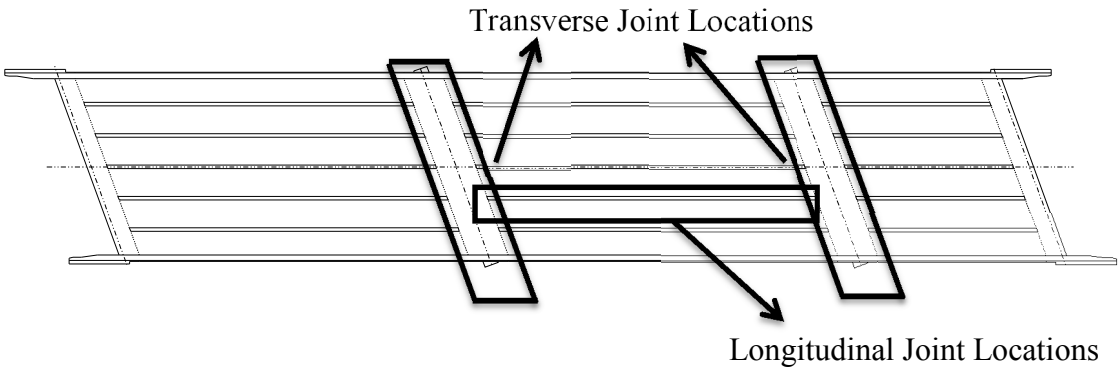

Figure 3-1. Specimen Design Locations

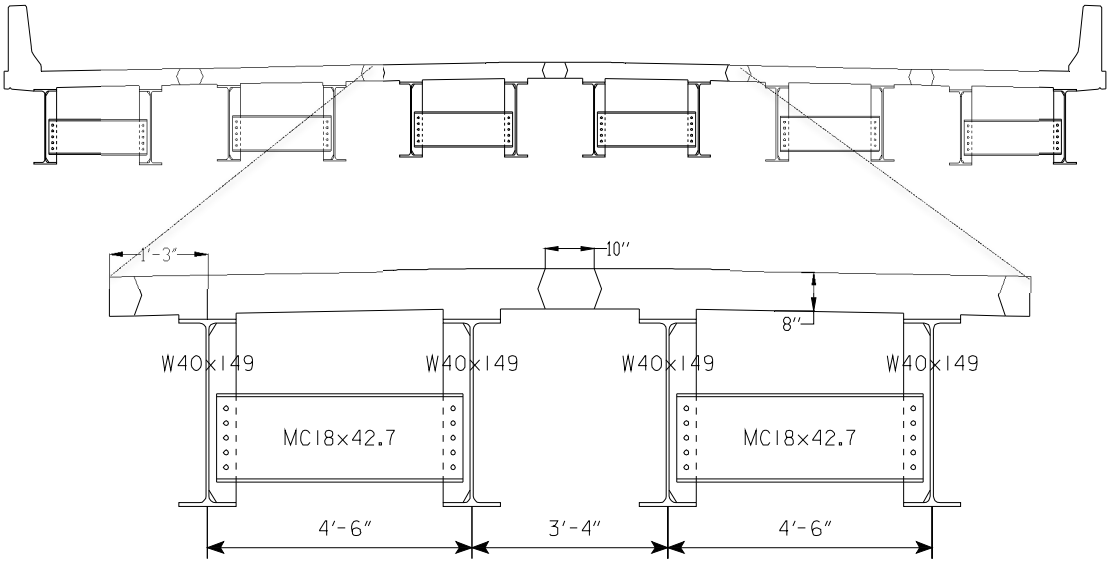

Figure 3-2. Cross Section of the Little Siler Creek Bridge

To evaluate the performance of the longitudinal and transverse joint details that were specified for the Little Silver Creek Bridge, 11 specimens were designed and tested. Nine of the specimens were used to evaluate the longitudinal joint detail. These nine specimens consisted of a reinforced concrete deck and were supported in a manner to simulate girder spacing's. The other two specimens were used to study the behavior and

performance of the transverse joints. These specimens included a steel bridge girder, reinforced concrete deck, and reinforced concrete diaphragm.

Figure 3-3. Constructed Little Silver Creek Bridge

The rest of Chapter 3 will cover in depth other information that was used for the experimental procedure. The chapter was broken up into subsections that will differentiate between the longitudinal joints and the transverse joints. The same information for both joint types is included in this chapter; design details, fabrication procedures, instrumentation plans, and the setup for the experimental tests.

3.2 Test A: Longitudinal Joints

An experimental program consisting of ponding and strength tests was designed and implemented to investigate the failure modes of flexural behavior of the longitudinal connections. These tests were completed to establish the behavior of the joint using various finish methods and materials.

3.2.1 Specimen Details

To investigate the failure modes and flexural behavior of the longitudinal joint detail, nine specimens were designed, fabricated, instrumented, and tested in the Iowa State University Structural Engineering Laboratory. The overall design of the specimen was based on the cross section of the demonstration bridge, shown in Figure 3-2. Six of these specimens were designed with a joint that replicated the specific Little Silver Creek Bridge detail, shown in Figure 3-4, provided by the Iowa Department of Transportation.

Three specimens were constructed using Ductal UHPC to complete the closure pour and three specimens were constructed using Korean-UHPC (K-UHPC) to complete the closure pour. Each specimen was designed as two separate precast modules (deck panels), shown in Figure 3-5 and Figure 3-6. The modular deck panels were specified to use standard Iowa DOT High Performance Concrete (HPC) with a compressive strength of 5 ksi. The dimensions for the two separate modules were the same, 7 ft wide, 3 ft long, and 8 in. deep as shown in Figure 3-5 through Figure 3-8. The modules were placed 10 in. apart to allow for the longitudinal joint connection as shown in Figure 3-4.

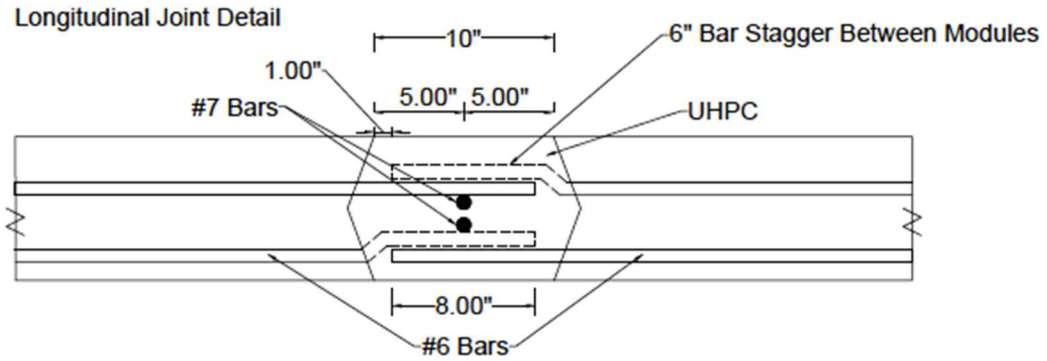

Figure 3-4. Longitudinal Joint Detail

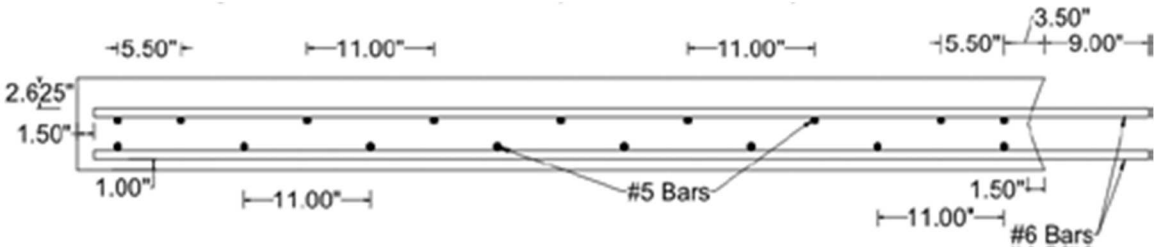

Figure 3-5. Cross Section of Left Deck Panel

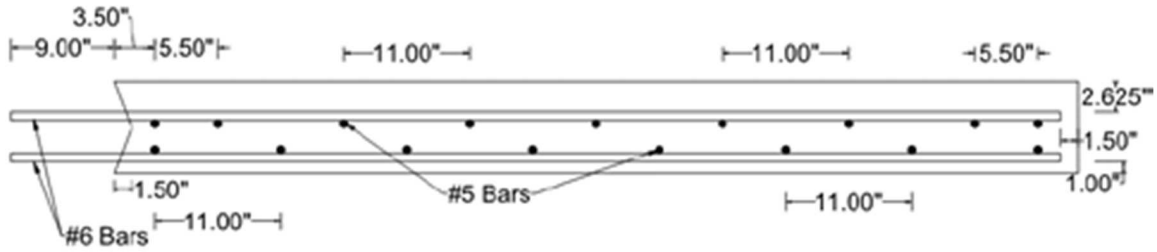

Figure 3-6. Cross Section of Right Deck Panel

Details for the reinforcement and cross-sections were determined based on the details from two adjacent modules (see Figure 3-1 and Figure 3-2). To facilitate testing only a portion of the deck was fabricated and tested. However, this partial deck section was fabricated full-scale matching the exact layout specified in the final bridge plans. The details for the jointed specimens, shown in Figure 3-4 through Figure 3-8, were established to match the overall size and reinforcing details used in the plans. As such, the results of the testing could be directly compared. Each jointed specimen had #5, #6,

and #7 bars. As shown in Figure 3-5 through Figure 3-8, the #6 bars ran along the width of the specimens (transverse direction), while the #5 bars ran along the length (longitudinal direction). A spacing of 11 in. was used for the longitudinal #5 bars and 1 ft for the transverse #6 bars. The longitudinal top and bottom bars were staggered every 5.5 in. There was no stagger between the top and bottom transverse reinforcement. All six #6 bars protruded 9 in. into the joint where they were staggered at 6 in. intervals from each module as shown in Figure 3-4 through Figure 3-8. This allowed for an 8 in. overlap length of each #6 bar in the 10 in. wide joint, which can be seen in Figure 3-4. Two #7 bars were used to longitudinally reinforce the joint and placed directly in the center. Concrete cover was as typically utilized in Iowa DOT bridges and can be seen in Figure 3-5 and Figure 3-6. Specifically, a clear cover of 1 in. was used for the bottom bars while 2 5/8 in. was used for the top bars.

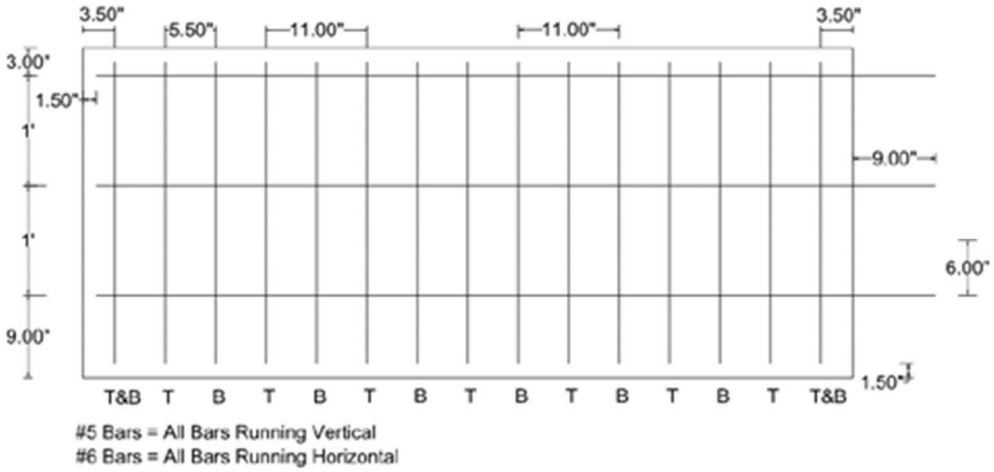

Figure 3-7. Reinforcing Steel Layout of Left Deck Panel

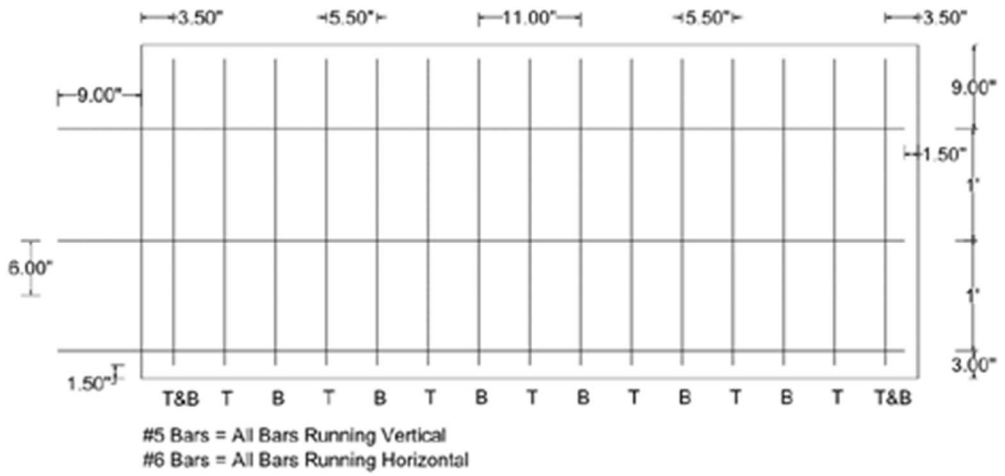

Figure 3-8. Reinforcing Steel Layout of Right Deck Panel

The only other difference between the six jointed specimens, besides the joint material, was the surface preparation in the joint. All the joints were texturized, but the joint surface preparation technique varied for each one. The textured surface was specified by the Iowa DOT to be a minimum concrete surface profile (CSP) 6. Three types of surface preparation techniques were utilized to texturize the joint surface of the three jointed specimens (two types of formliners {known as; rubber sandblast medium and plastic sandblast} and a form retarder). The rubber formliner was product #121 Sandblast #3 provided by Scott System. The plastic formliner was product #8001 Sandblast Medium provided by Customrock Formliner. There are two different types of form-retarders to choose from, a paint-like material that is applied directly to the forms, or a sprayable liquid that is applied on freshly placed concrete. The paint-like material was selected for this project. After the concrete had cured and the forms were removed, the surface with the form-retarder was power-washed to produce an exposed aggregate finish. Each of the three surface conditions were used once each for both the Ductal-

UHPC and the K-UHPC specimens. The different techniques were evaluated to determine the performance and feasibility of use with large-scale construction. The three surface treatments considered in this work met the designer's criteria of achieving a specified Concrete Surface Profile (CSP) level. As will be seen, since the loads considered in this work were much higher than the strength limit loads considered for design, the surface treatments selected didn't provide an interface bond higher than the concrete tensile capacity.

The other three specimens were designed based on the details of a continuous bridge deck, shown in Figure 3-9 and Figure 3-10. These jointless specimens consisted of a single deck panel (i.e., no longitudinal joint connection). The details of these specimens were designed to best represent the layout of a standard 'cast-in-place' bridge deck. These jointless specimens are, as much as anything, a "normal" baseline with which the jointed test results could be compared. Keeping the same size specimen was important for comparison purposes. As shown in Figure 3-9 and Figure 3-10, the dimensions for each of these specimens were 14 ft 10 in. wide, 3 ft long, and 8 in. deep. Only #5 and #6 bars were included in these specimens.

Details for the reinforcement and cross-sections remained fairly consistent in comparison to the jointed specimens. However, there were some variations between the two to best represent what a continuous slab layout looks like. The six transverse #6 bars ran the entire length of the specimen. Since the #6 bars are continuous with no stagger, a symmetrical distance of 6 in. was used for the spacing to the edge of the specimen as shown in Figure 3-9. #5 bars were used for the longitudinal direction and spaced evenly

at 11 in. along the entire width of the specimen. Four #5 bars at a spacing of 5.5 in. are designed at the "connection location" as shown in Figure 3-9 There was a 5.5 in. stagger between the top and bottom #5 bars as shown in Figure 3-10. There was no difference in the design between these three jointless specimens.

3.3.2 Fabrication Procedure

The specimens were fabricated in the Structural Engineering Laboratory at Iowa State University. All three of the jointless specimens were fabricated first, followed by the three jointed Ductal-UHPC specimens, and finally the three jointed K-UHPC specimens. The specimens all followed the same fabrication process, which is shown in Figure 3-11 through Figure 3-14. All of the bars were laid out and marked according to the specimen details. After everything was in the proper location, all the bars were tied together to form the mats. The specimen formwork was constructed using normal plywood. Plywood sheets were laid down and marked to the designed dimensions. As shown in Figure 3-11, the 8 in. tall sides were then attached on these lines. Before placing the steel reinforcing mats into the forms, uniaxial strain gauges were installed on the transverse bars near the joint location. The steel bars were installed and placed into the formwork.

All three jointless specimens were poured on the same day. The specimens had a 28-day cure time before they could be tested. During the curing process, the testing frame was constructed and all supports were put into place. The three jointless specimens were set up in a continuous line and tested within an 8-hour period. The concrete used for the jointless slabs had an average 28-day compressive strength of 5.2 ksi.

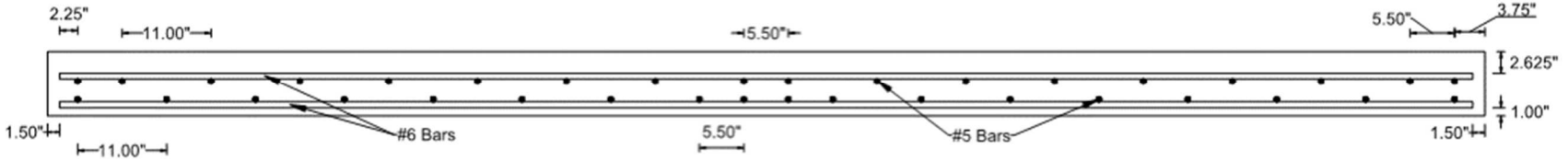

Figure 3-9. Cross-Section of Jointless Specimen

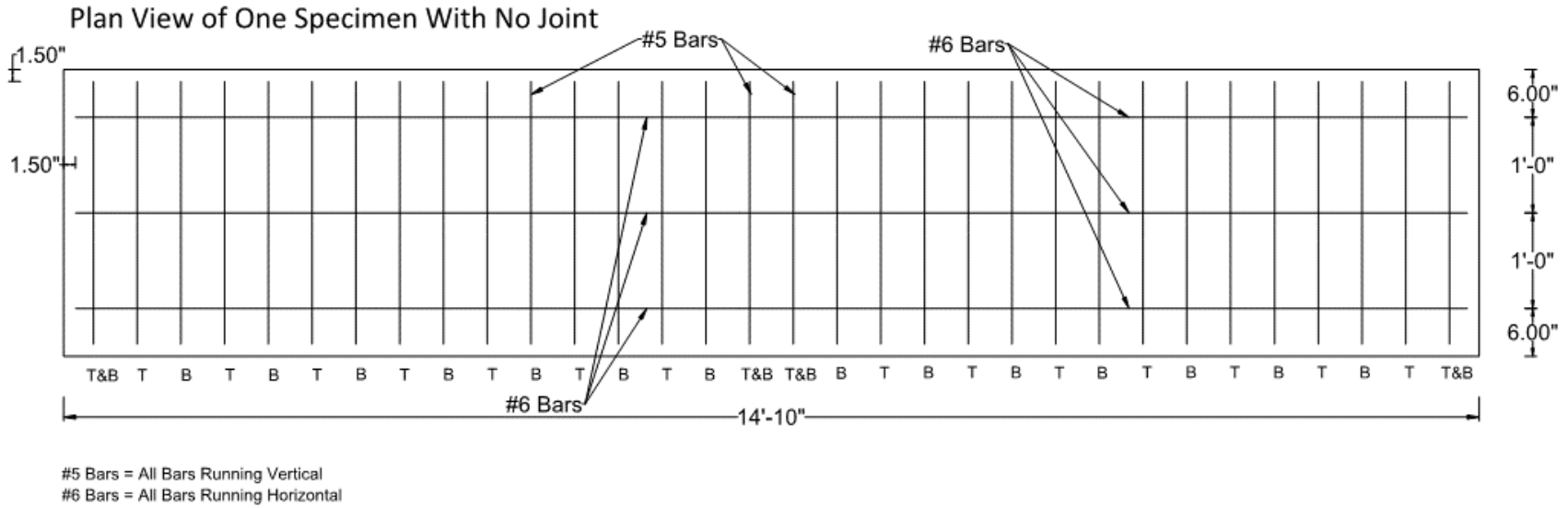

Figure 3-10. Reinforcing Steel Layout of Jointless Specimen

Figure 3-11. Steel Reinforcement and Formwork Fabrication

The formwork for the jointed specimens was slightly more complex due to the details of the joints. The joint detail included a 1.5 in. indent as well as six #6 bars that had to pass through the forms for each deck panel. After the center joint forms were constructed, the formliners were attached to their specific specimen as shown in Figure 3-12. Now all of the holes in the formwork could be drilled to allow the reinforcing steel to pass through. Right before the pour, either the formliners were rubbed down with a release agent or the form-retarder was applied. The HPC placement for the deck panels is shown in Figure 3-13. After the concrete reached sufficient strength, the modules were moved and placed in the final testing setup ensuring the dimensions between the two modules was correct.

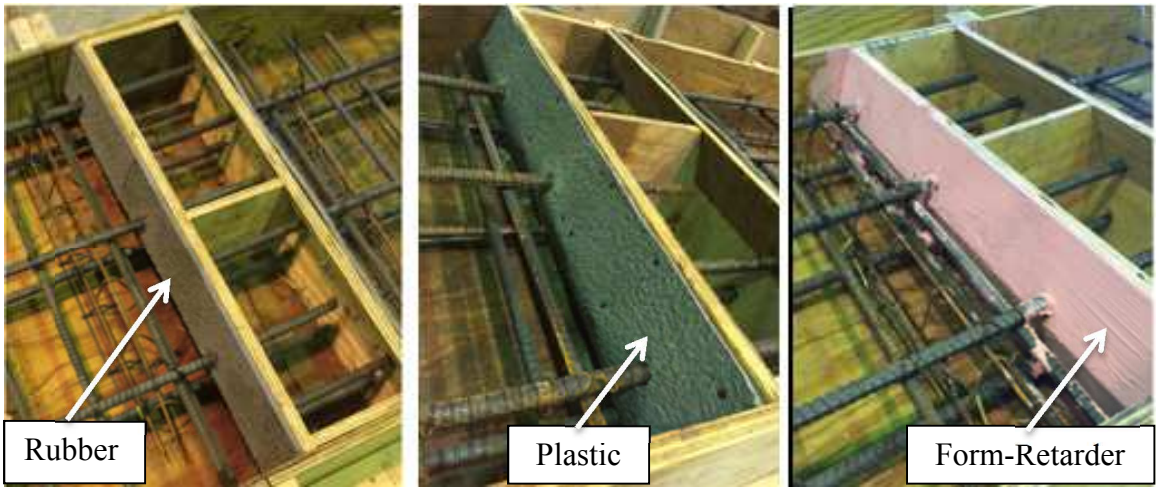

Figure 3-12. Fabrication of Three Different Joint Options

The deck panels for the Ductal-UHPC specimens were cast at the same time as the continuous slabs. After the continuous slabs were tested, the deck panels for the Ductal specimens were set in the test apparatus. New formwork was constructed at the joint location for the placement of the Ductal-UHPC, as shown in Figure 3-14. The UHPC was placed in the formwork and allowed to cure. Testing for these specimens was able to start as soon as the compressive strength of the UHPC reached 15 ksi, but no sooner than four days as four days is the minimum cure time specified by the IADOT. The Ductal-UHPC specimens were tested after 6 days with an average compressive strength of the UHPC around 15.5 ksi. All three specimens were tested on day 6 with all testing completed within 8 hours.

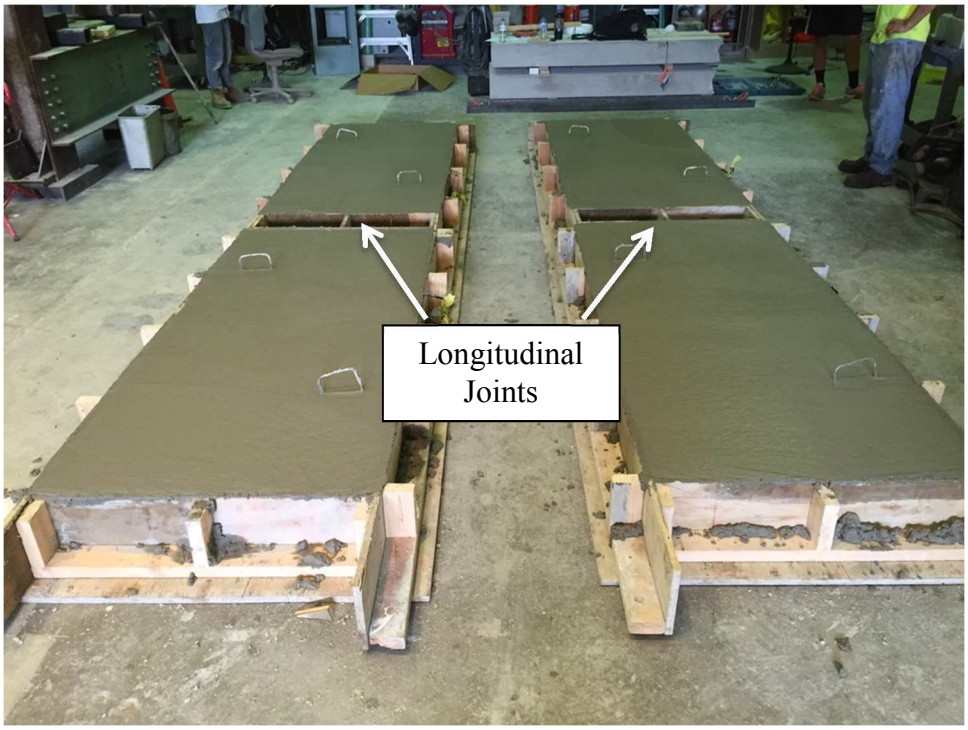

Figure 3-13. Placement of HPC for the Deck Panels

Figure 3-14. Formwork Construction and Placement of Joint Material

The last three specimens fabricated were the K-UHPC specimens. The same process was followed in preparation of testing. The deck panels were cast and cured for 28 days. By the 28-day mark, the specimens were in place with the joint formwork

constructed and ready for the K-UHPC to be placed. After placement of the K-UHPC, the test frame was setup and the testing started as soon as the strength requirement was reached. The average compressive strength of K-UHPC, after a 6-day cure, was measured at 15.7 ksi and the testing began the following day. As with the other tests, all three K-UHPC specimens were tested within an 8-hour period.

3.2.3 Instrumentation Plan

The instrumentation of all jointed specimens was exactly the same to ensure that the measured data from different specimens could be directly compared, and is shown in Figure 3-16. For each jointless specimen, the details of the gauge locations remained similar to the jointed specimens. However due to the difference of the geometry between the two types of specimens, the gauge locations were shifted to coincide with the reinforcing steel layout, as shown in Figure 3-17.

Two different types of strain gauges were used; embedded uniaxial gauges and concrete surface mounted gauges (BDI gauges). The embedded gauges were used to measure strain in the reinforcing steel throughout testing. The BDI gauges were attached to the bottom surface of the specimen and measured the strain in the concrete. The concrete gauges were removed prior to specimen failure to protect the gauges.

For the jointed specimens, the embedded gauges were installed on the bottom transverse reinforcing bars 2 inches outside the exterior line of the joint interface as shown in Figure 3-16. As shown in Figure 3-17, the placement of the embedded gauges for the jointless specimens was very similar. Each specimen was equipped with 4 embedded strain gages. Surface mounted BDI gauges were bridged over both the loading lines and the joint lines for jointed specimens. Details for the locations of the surface

mount gauges are shown in Figure 3-15. Eight surface mounted gauges were used for each specimen and the relative positions of each gauge remained the same for the continuous specimens.

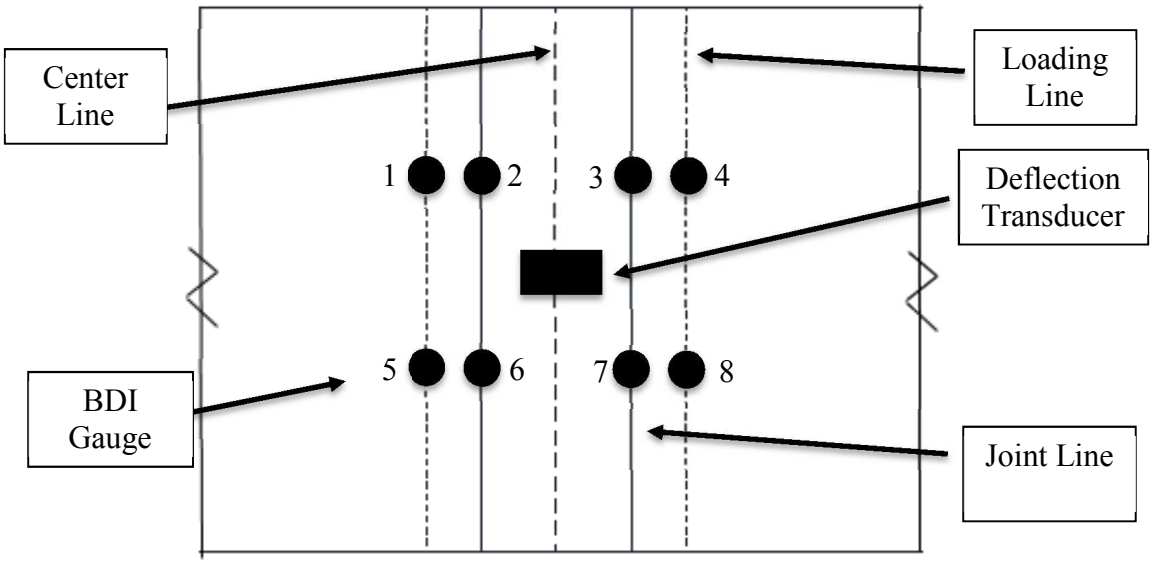

Figure 3-15. Surface Mounted Instrumentation

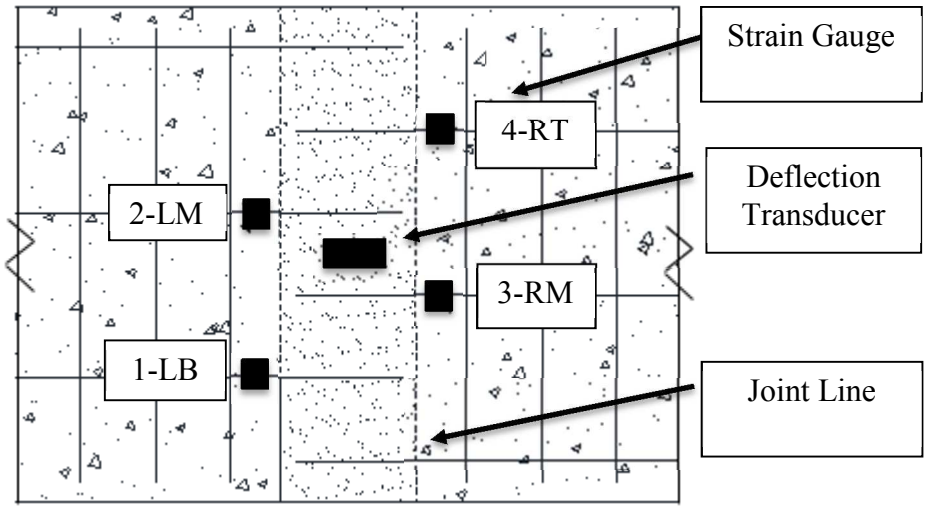

Figure 3-16. Embedded Instrumentation for Jointed Specimens

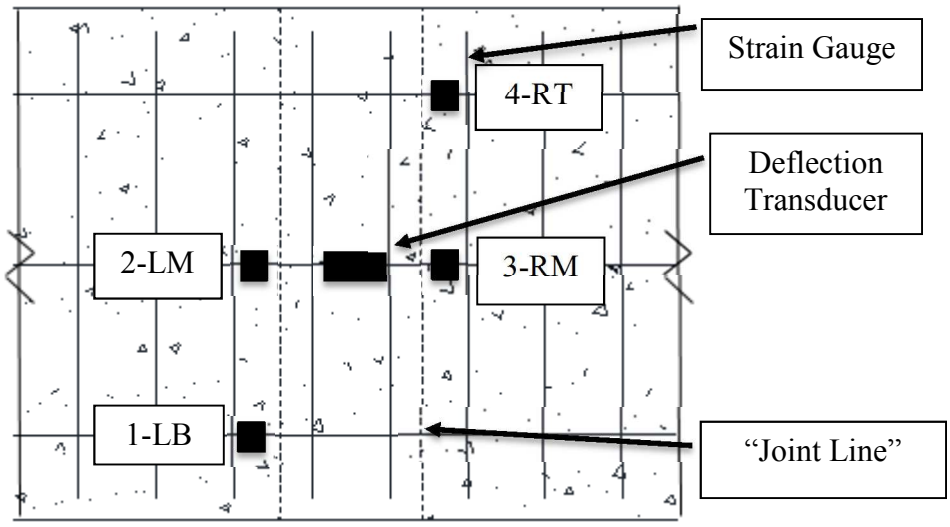

Figure 3-17. Embedded Instrumentation for Jointless Specimens

3.2.4 Curing and Ponding Tests

Ponding tests for a Ductal-UHPC and a K-UHPC jointed specimen were conducted to check if the UHPC connection developed cracks during curing. During both the placement and curing for the jointed specimens, vertical restraining forces, shown in Figure 3-18, were applied across the 3 ft length of the specimens at each end. These downward vertical forces were applied to simulate the transverse restraint provided by the girders. The tests setups were determined based on the bridge details. During the curing process, the interface between the UHPC and the normal concrete deck panels was visually observed to record any crack formation. On the 5th day after UHPC placement, a 24-hour ponding test was conducted on one of the jointed specimens. The ponding test was used to check if any leakage occurred at the connection and the interface. To form the pond, a 3 in. tall watertight wall was constructed all the way around the joint as shown in Figure 3-18 and Figure 3-19. Approximately 1 in. of water was placed in the pond (following Iowa DOT specified procedures). The specimen was observed for any

leakage and the water level was monitored throughout the testing period. This experimental ponding regimen followed the ponding regimen specified for construction of the actual bridge.

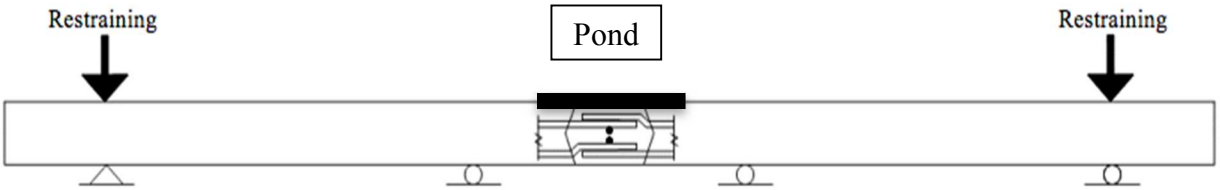

Figure 3-18. Setup for Curing and Ponding Tests

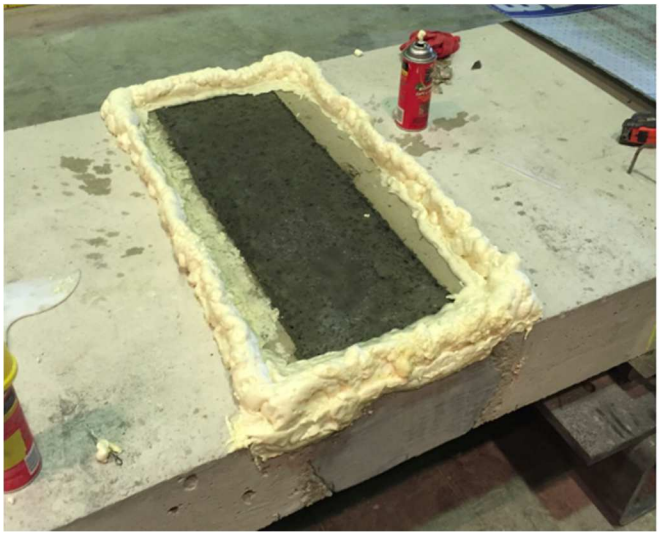

Figure 3-19. Enclosure for Ponding Test

3.2.5 Strength Tests

Strength tests were conducted on all nine specimens. The main goal was to determine if the jointed specimens had the same strength and performance as that of the baseline, jointless specimens. All specimens were setup and tested under the same loading and boundary conditions, shown in Figure 3-20. To simulate the actual boundary conditions of the bridge, supports were placed in a manner that simulates the girders from

adjacent modular units as shown in Figure 3-20. The configuration resulted in a center of span of 3 ft-4 in. and exterior spans of 4 ft-4 in. Additionally, an overhang of 1 ft-5 in. was used outside the exterior spans and is illustrated in Figure 3-20. All supports run the entire length of the specimen and the loading was achieved by using two hydraulic actuators that pushed down on a spreader beam. The spreader beam transferred the load to create two line loads; each placed 3.5 in. outside of the "connection interface". This loading pattern resulted in a spacing of 17 in. between the two loading lines. The same load spacing and support locations were replicated for the continuous slabs. The three-specimen setup is shown in Figure 3-21. The applied load was continuously measured using a load cell that was attached onto the hydraulic actuators. Visual crack mapping techniques were utilized to monitor and document crack formation in the deck panels, joint material, and interfaces during loading. Loading of each specimen was stopped and the cracks of each specimen were marked approximately every 50 kips, until the steel yielded. The loading continued until it was decided that each specimen had failed.

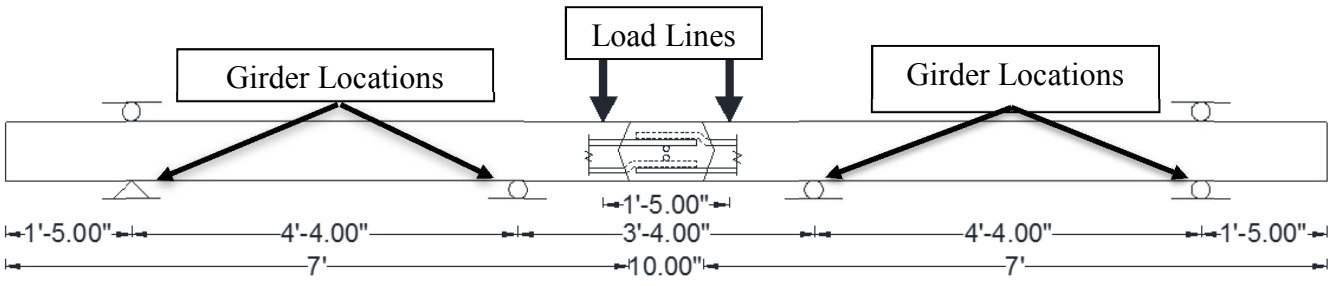

Figure 3-20. Setup for Strength Tests

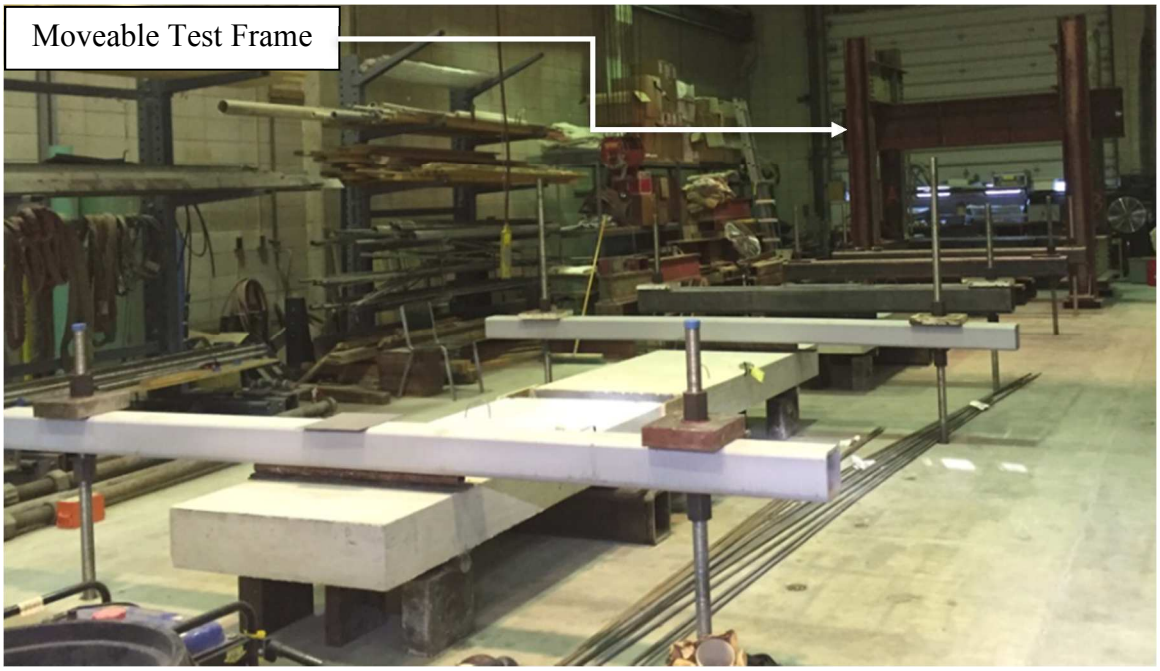

Figure 3-21. Continuous Strength Testing Setup

3.3 Test B: Transverse Joints

An experimental program consisting of strength tests on transverse connections was designed and implemented to evaluate the behavior, strength, and failure modes of the HPC transverse connection of the Little Silver Creek Bridge and to understand the importance of including the somewhat complex compression block in future designs.

3.3.1 Specimen Details

Two specimens were designed, fabricated, instrumented, and tested to evaluate the performance of the transverse joints with and without a compression block at the pier locations. The tests specimens were also designed based on the actual details of the Little Silver Creek Bridge. Note that the girders of each prefabricated module are spaced at 4 ft-6 in. and the adjacent girders between the two modules are spaced at 3 ft-4 in. as shown in Figure 3-2.

The first specimen, shown in Figure 3-25, was designed to exactly replicate the bridge details and included a compression block between the two longitudinally aligned girders (hereafter referred to as "Specimen 1"). The compression block was fabricated out of 1 in. thick steel plate. Figure 3-22 shows the details of the compression block and the actual compression block that was used is shown in Figure 3-23. The second specimen (hereafter referred to as "Specimen II") did not include a compression block, but has all other design details the same as Specimen I and is shown in Figure 3-26.

Each of the specimens consists of a deck panel, diaphragm, and two steel girders. The steel girders have a W40x149 cross-section, a length of 7 ft-6 in., and a 9 in. gap between them. The diaphragm has a length of 2 ft-9 in., a width of 3 ft-11 in., and a depth of 4 ft-1.5 in. The deck panel has a depth of 8 in. and a width the same as the diaphragm. Due to the varied girder spacing in the bridge design, the steel girders are offset 3.5 in. from the deck centerline resulting in one overhang being 7 in. wider than the other shown in Figure 3-27. The specimens were specified to use standard Iowa DOT High Performance Concrete (HPC-D) with a nominal compressive strength of 5 ksi.

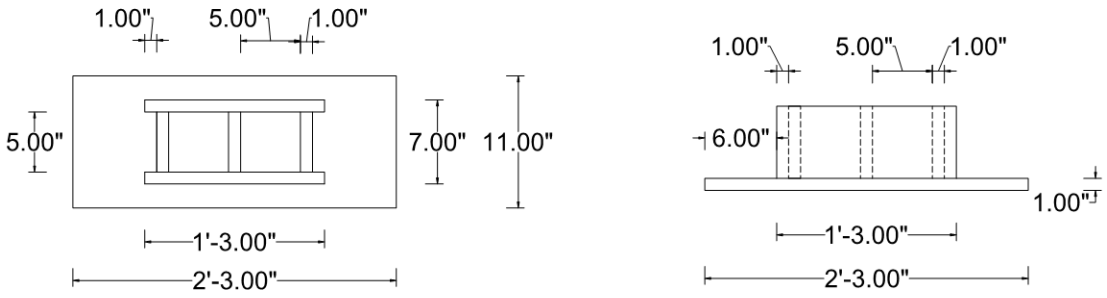

Figure 3-22. Details of the Compression Block

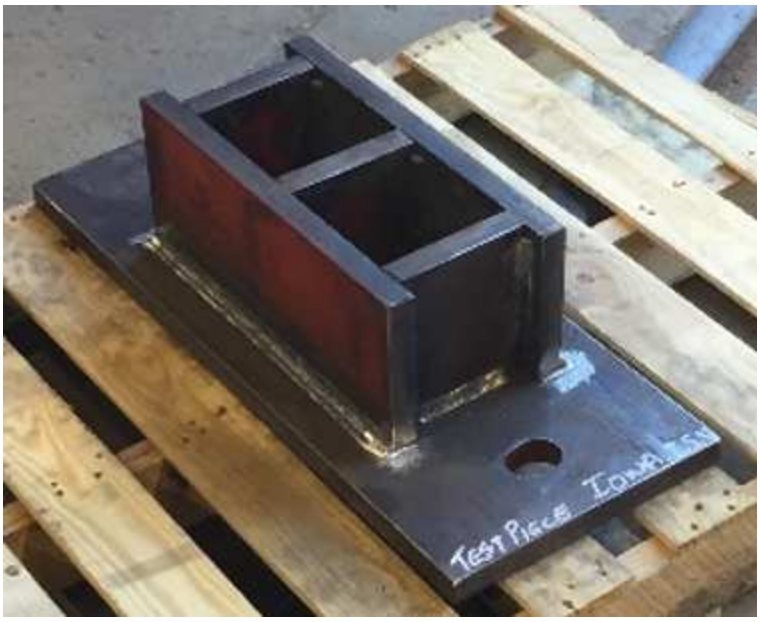

Figure 3-23. Fabricated Compression Block

Details for the reinforcement and cross-sections were determined based on two adjacent modules that were connected over the piers. Due to a variety of factors including material expenses and available space the specimens were shortened to a length of 7 ft-6 in. on each side of the pier. These sections remained full scale and the details that were specified in the bridge plans were used. The reinforcement of the deck panels consisted of two identical layers of reinforcement as shown in Figure 3-24. Each layer contained 8 #7 bars and 16 #6 bars. The #7 bars served as the longitudinal reinforcement and ran continuous along the whole length of the specimen, while the #6 bars served as the transverse reinforcement and ran continuous along the whole width of the specimen. A spacing of 5.5 in. was used for the longitudinal reinforcement and 1 ft for the transverse reinforcement. Both the top and bottom reinforcing steel mats for each specimen were the same except on the bottom mats the longitudinal reinforcement was on top while for the top mat it was on bottom. Concrete cover is shown in Figure 3-25 and Figure 3-26. A

distance of 1 in. was used for the bottom side of the slab and 2.75 in. was used for the top. 1 in. bolster chairs were used in-between the top and bottom reinforcing steel mats.

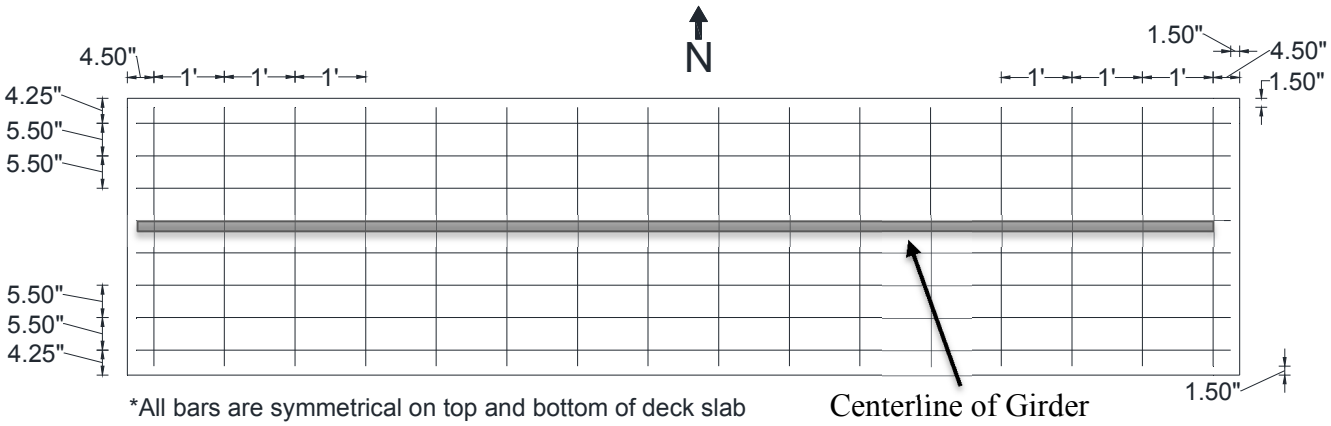

Figure 3-24. Reinforcing Steel Layout for Deck of both Specimens

The longitudinal diaphragm reinforcements were placed through 1 in. drilled holes in the girder webs. A spacing of 3 in. was used from the face of the diaphragm to the inside edge of the reinforcement. There were 3 holes drilled on each side of the diaphragm. The first hole was drilled 4 in. above the bottom flange of the girder. 1 ft was used for the spacing between the next two reinforcing bars. These dimensions were duplicated for all 4 reinforcement locations between the two specimens and are shown in Figure 3-25 and Figure 3-26. #5 bars were used for the longitudinal reinforcement in the diaphragm and measured a length of 3 ft 8 in. A total of four #5 bars were used for shear reinforcement in each diaphragm and the bent bar details are shown in Figure 3-25 and Figure 3-26.

Shear studs were incorporated into the specimens based on the specifications given in the plans. Three shear studs with a length of 6 in. and a diameter of 7/8 in. were welded across the width of the top flange. A spacing of 4-3/8 in. was used in-between the studs, leaving 1.5 in. to the outside of the flange as detailed in the plans and shown in

Figure 3-27. They were longitudinally spaced every 8 in. along the length of the beam. Each girder has stiffeners on each side of the web over the support location as well as underneath the loading point as shown in Figure 3-25 and Figure 3-26. It should be noted that only incorporating the compression block into one specimen, but keeping the rest of the design exactly the same made it possible to directly compare the results and determine the effect the compression block had on the performance of the transverse connection.

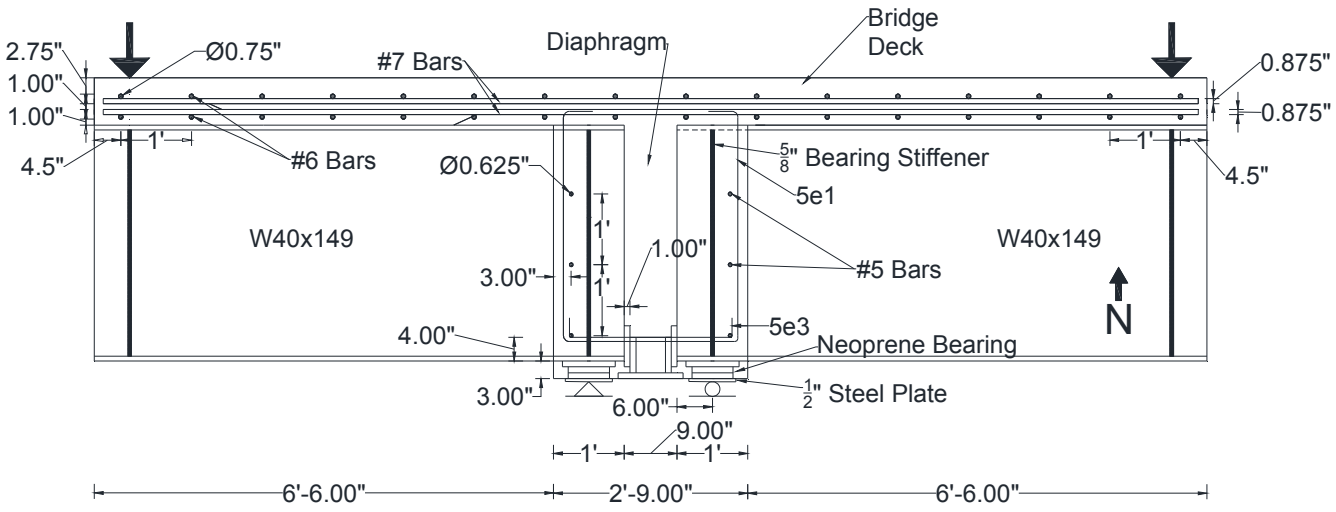

Figure 3-25. Details of Specimen I

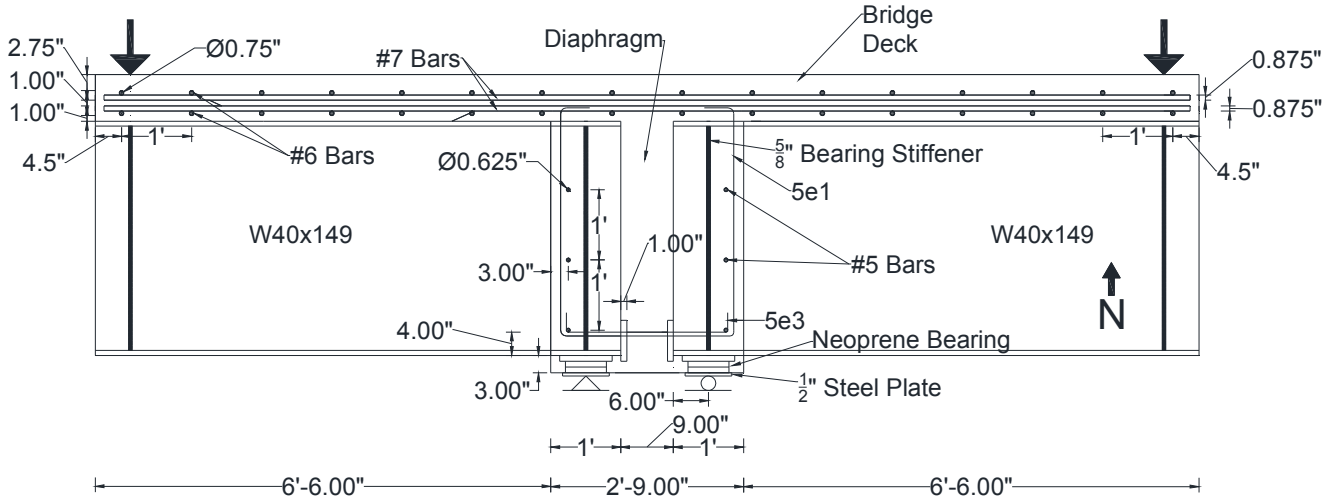

Figure 3-26. Details of Specimen II

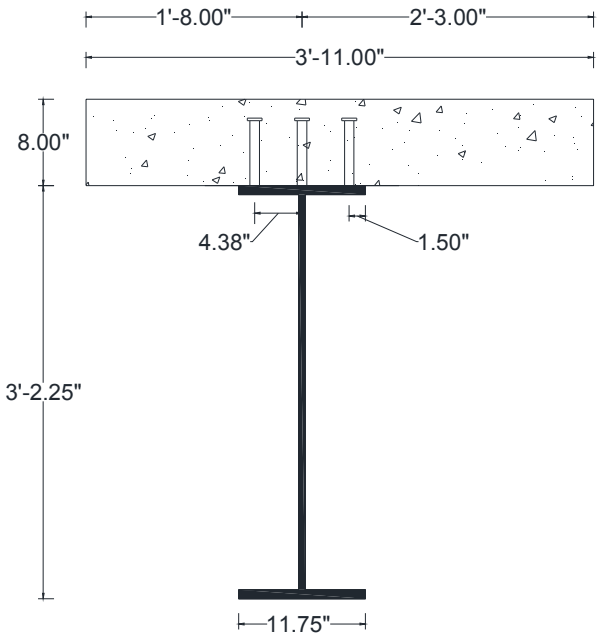

Figure 3-27. Cross Section Details

3.3.2 Fabrication Procedure

The specimens were fabricated in the Structural Engineering Laboratory at Iowa State University. Capital Contractors fabricated and donated the compression block, the

same company that fabricated all of the ones that were used for the Little Silver Creek Bridge. Both specimens were constructed at the same time.

All of the reinforcing steel mats were assembled first and then set aside until the formwork was completed. Locations of the shear studs were marked out on all of the girders. They were then attached using a stud welder and the process is shown in Figure 3-28. To make sure the proper heat was being used, a 45-degree bending test was performed prior to welding them on the girders.

Each specimen used a total of 16, 5/8 in. thick bearing stiffeners and they were positioned under each loading location and above the supports on each side of the web as shown in Figure 3-25 and Figure 3-26. They were tack welded in place and then sent to Howe Welding for full-length welding on each side. To replicate the bridge details, a 1 in. thick plate was also welded to the face of the girder on the diaphragm side as shown in Figure 3-29. Once the girders were delivered the lab, construction of the formwork was started. Figure 3-30 shows the formwork construction process for both specimens.

Figure 3-28. Placement of Shear Studs

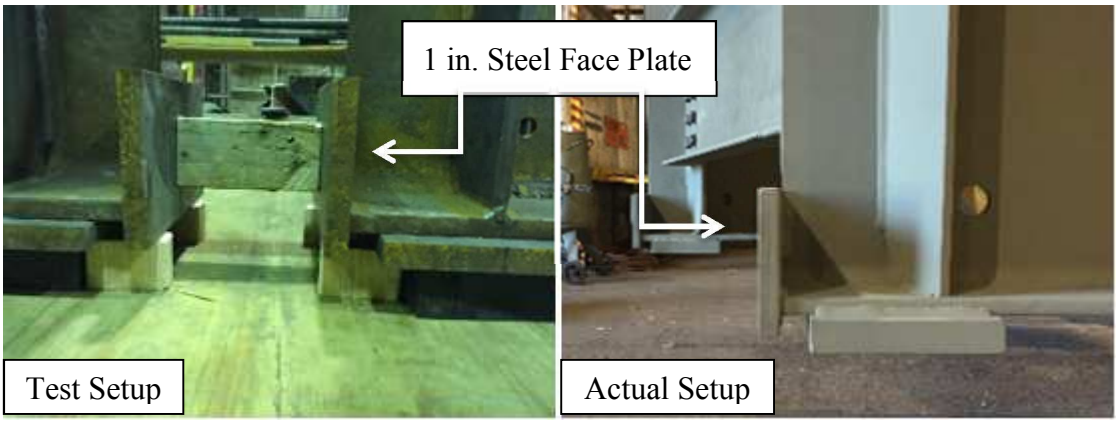

Figure 3-29. Diaphragm End of Girders

The specimen formwork was constructed out of both wood and steel. Plywood sheets were laid out to form the base. The sides for the diaphragm were constructed and slid into place forming a tight fit with the bottom flange as shown in Figure 3-30. Due to the pressures that were going to be seen when placing the concrete, threaded rods were used to stiffen the diaphragm formwork and prevent any possible blowouts. Figure 3-30 also shows the steel braces that were used to support the overhangs of the decks. After all of the formwork was assembled, the forms were oiled down one last time and the reinforcing steel mats were lifted into place. The vertical diaphragm reinforcement could now be secured and attached. 15 uniaxial strain gauges were installed on the top of the longitudinal bars near the diaphragm location as shown in Figure 3-31. Both specimens were formed right next to one another. The concrete for the two specimens was placed using concrete from a single source and placed at the same time. Before the specimens could be tested, Iowa DOT required a compressive strength of 5 ksi. 7 days after placement of the concrete the forms were removed and the first specimen, Specimen II, was positioned in the testing setup. The specimens were tested after 28-days of curing and the 28-day compressive strength of the concrete was measured to be 5.5 ksi.

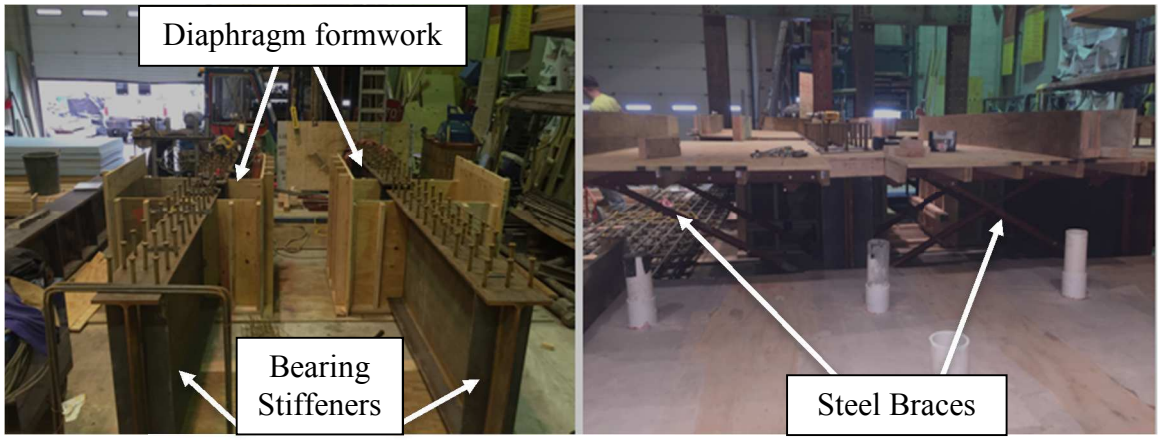

Figure 3-30. Formwork Construction

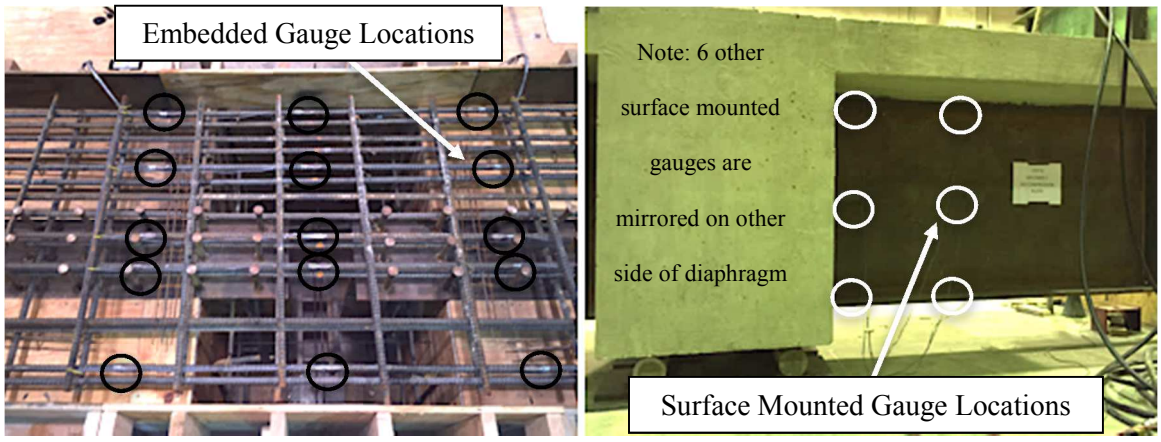

Figure 3-31. Embedded and Surface Mounted Gauges

3.3.3 Instrumentation Plan

The instrumentation plans for both specimens were exactly the same except for the two gauges placed on the compression block as shown in Figure 3-32 through Figure 3-35. Only uniaxial strain gauges were used in this study. For each specimen, there were fifteen embedded strain gauges located in the deck panel, and twelve surface mounted strain gauges located on the girders. As previously mentioned, there were an additional two gauges installed on the compression block of Specimen I. These gauges were located on the outside face of the compression block, as shown in Figure 3-34. For the strain

gauges on the steel bars embedded in the deck panel, five gauges were mounted in the center of the diaphragm and five gauges were installed 6 in. away from each side of the diaphragm as shown in Figure 3-32 and Figure 3-33.

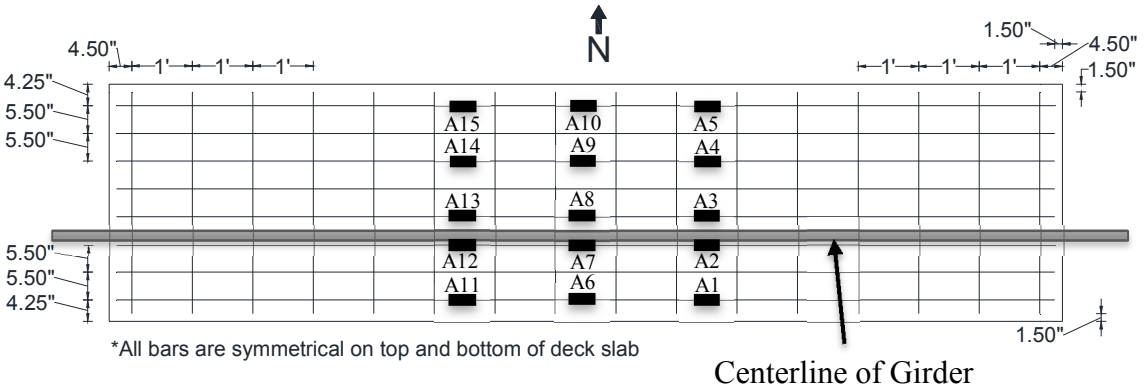

Figure 3-32. Embedded Instrumentation for Specimen I

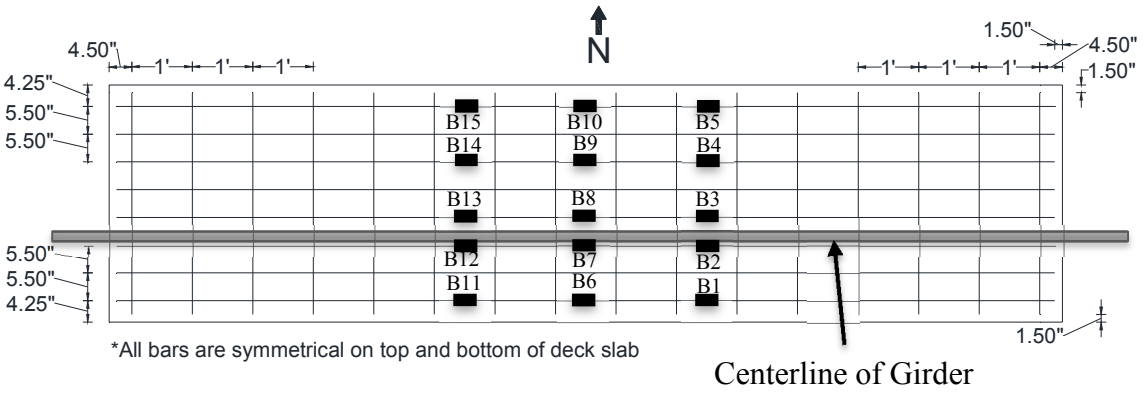

Figure 3-33. Embedded Instrumentation for Specimen II

The surface mounted strain gauges on the girder were positioned on the bottom of the top flange, center of the web, and top of the bottom flange. Locations of these gauges were 6 in. outside the diaphragm and midpoint of each girder for both the west and east side and are shown in Figure 3-34 and Figure 3-35. Note that the gauges with the letter "A" were installed on Specimen I and the gauges with the letter "B" were installed on specimen II. The locations that were used for the strain gauges made it possible to determine how the stresses were transferred through the diaphragm.

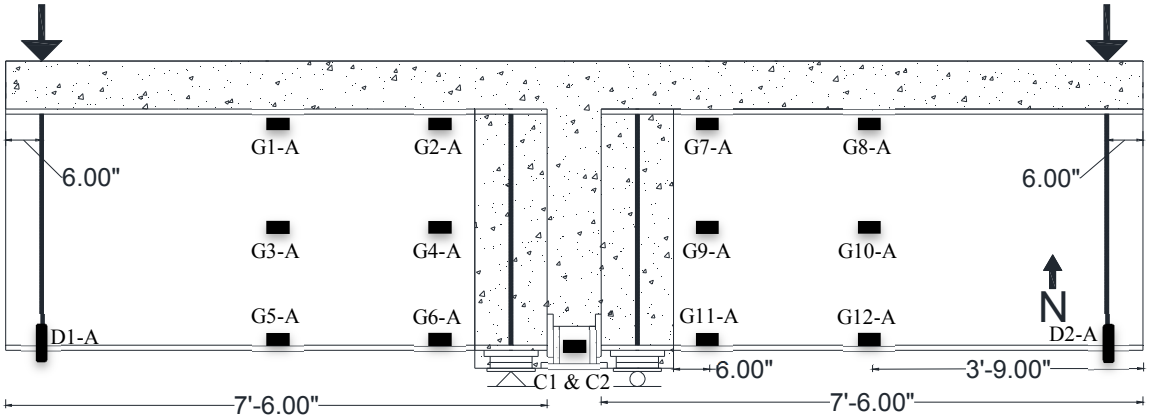

Figure 3-34. Surface Mounted Instrumentation for Specimen I

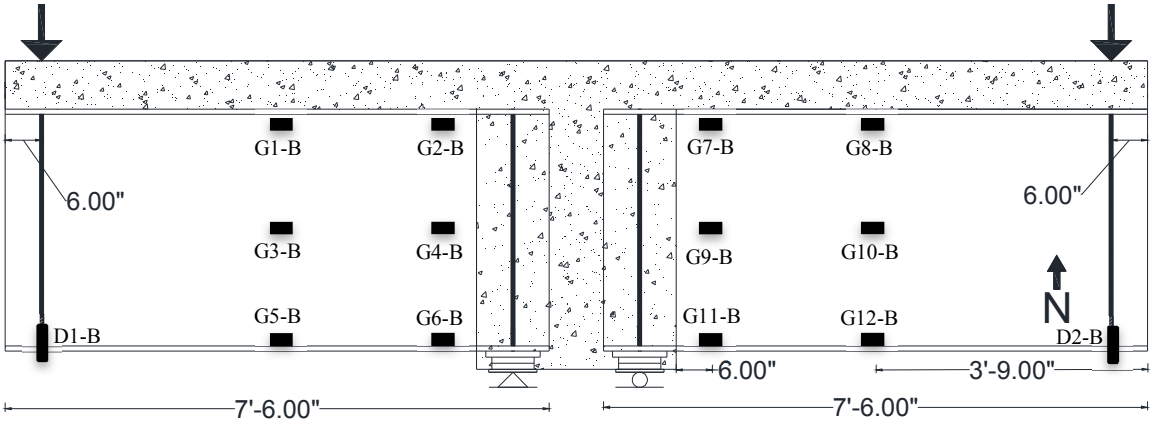

Figure 3-35. Surface Mounted Instrumentation for Specimen II

3.3.4 Strength Tests

Strength tests, shown in Figure 3-36 and Figure 3-37, were conducted on both of the specimens and performed using the same configuration. The goal was to determine how the compression block altered the performance of the specimen. In particular, strains were measured at several locations to determine how the compressive forces were being transferred through the diaphragm. To closely replicate the boundary conditions of the actual bridge, supports were placed under the bearing pads to simulate the contact points between the diaphragm and the pier. The supports were centered under the bearing pads

and therefor located directly under the centerline of the girders. Figure 3-36 through Figure 3-38 shows the testing setup that was used.

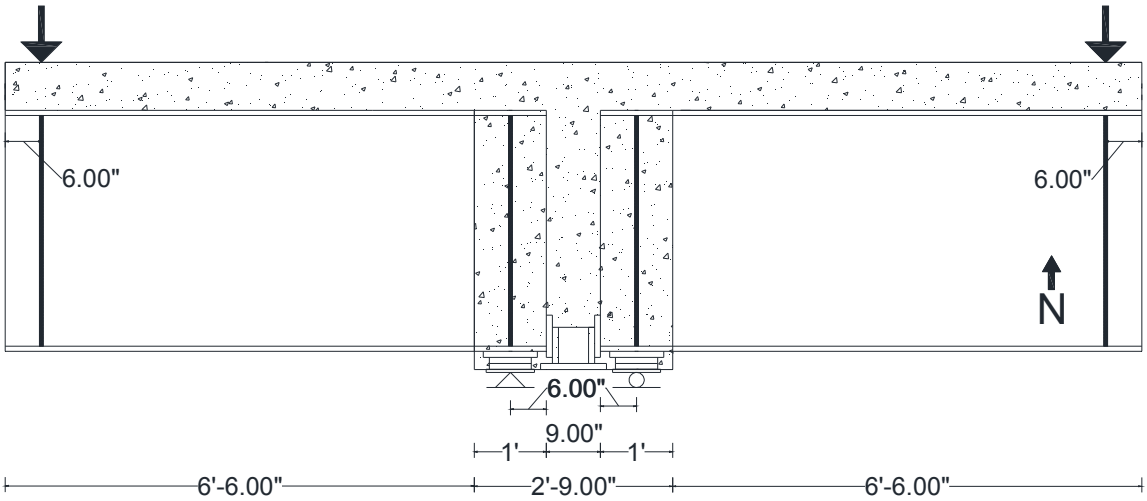

Figure 3-36. Testing Setup for Specimen I

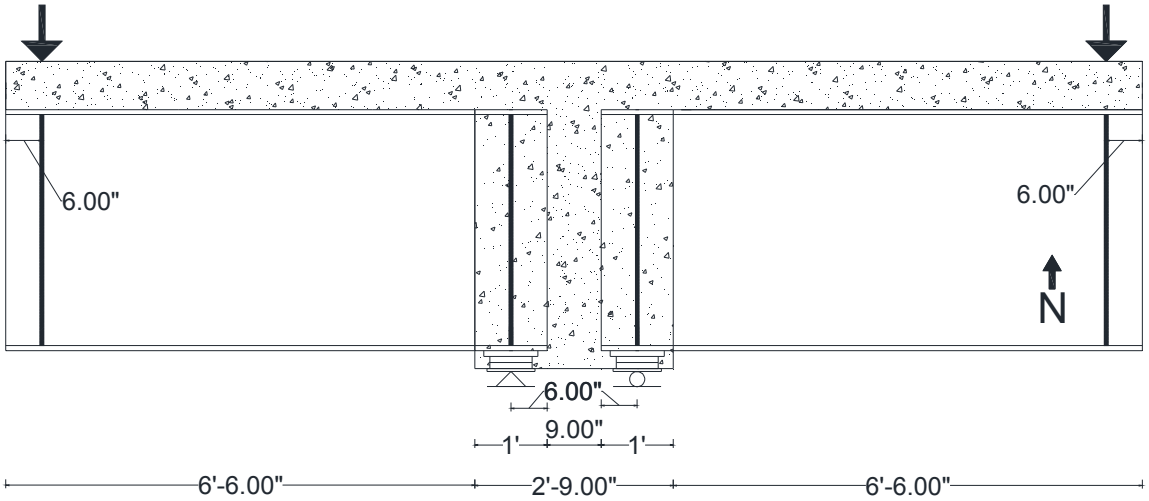

Figure 3-37. Testing Setup for Specimen II

Loading of the specimens was applied by a series of hydraulic actuators as shown in Figure 3-38. To produce the negative moment region at the diaphragm, two point loads were applied 6 in. from the outside edges of the specimens. The west side consisted of one 400 kip actuator mounted to a test frame while the east side consisted of two 200 kip hallow-core actuators secured to tie down rods. Due to the setup, the west actuator

pressed down directly on a loading plate that was centered over the girder and the east actuators pressed down on a load beam that was positioned over a loading plate. A load cell was placed on each side and measured the applied load throughout the testing process. The loading configuration for both sides is shown in Figure 3-39.

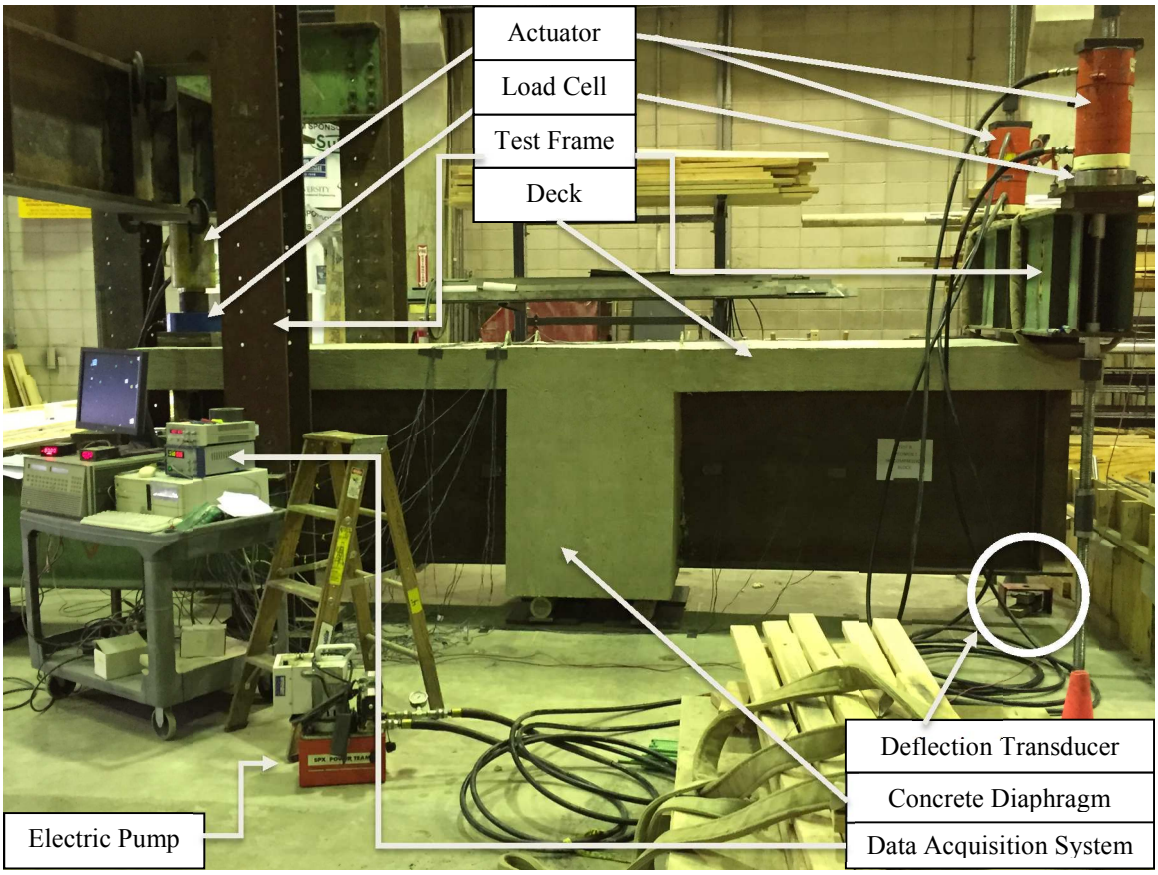

Figure 3-38. Laboratory Test Setup

During the testing process the loading was stopped periodically to monitor crack formations. Conventional crack mapping techniques were used to document the crack patterns of each specimen. This was performed until the loading on each side reached approximately 300 kips and it was deemed no longer safe to approach the specimen. Cracks that formed after this point were marked after the load was removed and labeled with the maximum load applied.

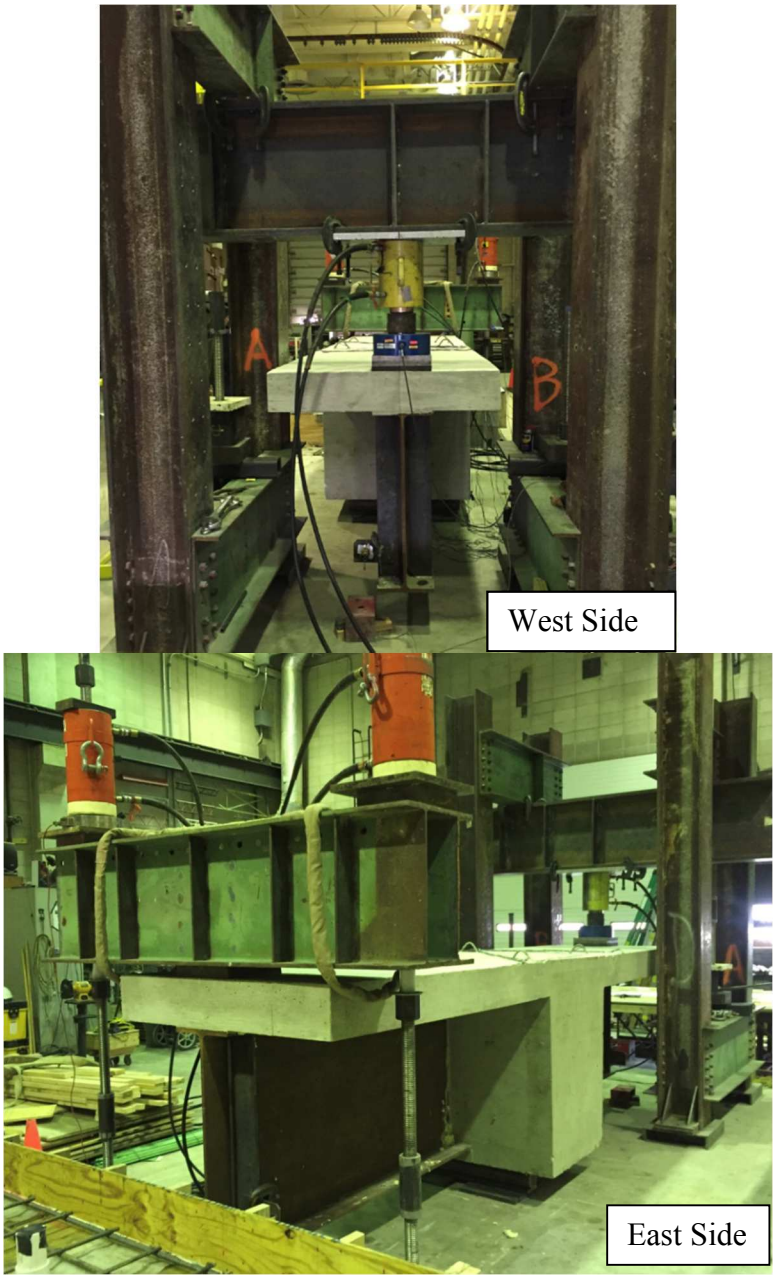

Figure 3-39. West and East Side Loading Configuration

CHAPTER 4. RESULTS AND DISCUSSIONS

4.1 Test A: Longitudinal Joints

4.1.1 Curing and Ponding Tests

During curing of the UHPC, no cracks were found at the interface between the UHPC (either K-UHPC or Ductal-UHPC) and the HPC. During the ponding test, no leakage was found at the two sides and bottom of the connection as shown in Figure 4-1. As a result, it was concluded that a good bond was achieved at the interface between the concrete and UHPC and the deformation due to early-age drying shrinkage and temperature change did not cause any cracks in the connection and interface.

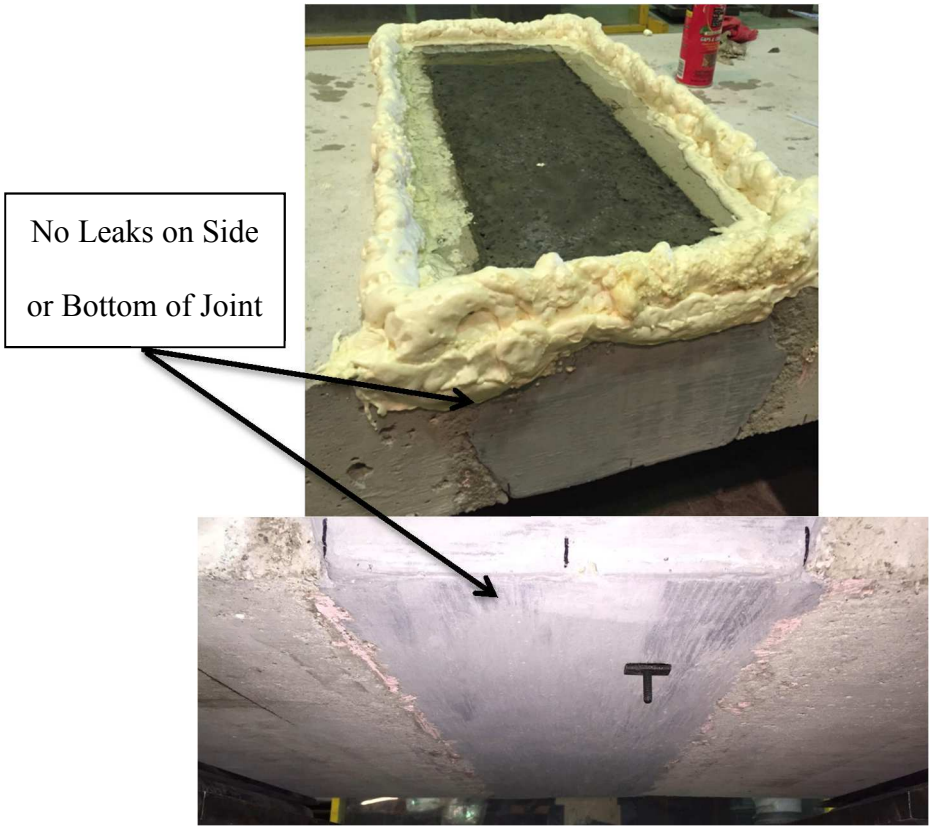

Figure 4-1. Examination of Ponding Test

4.1.2 Crack and Failure Patterns

Crack mapping was used during all tests to track crack initiation and crack growth patterns. The loading on each specimen was stopped and cracks were marked at approximately every 50 kips until it was no longer safe to be close to the test apparatus. Cracking for all of the specimens originated in the negative moment region over the two interior supports, as shown in Figure 4-2. The first cracks ran continuously over the entire length of the specimens. Then, cracks were found at the first and third spans and some of the initial cracks become noticeably wider. Around this time, cracking was also observed on the bottom and side surfaces of the specimen between the two interior supports and at the joint interface as shown in Figure 4-3. Near the time that the steel yielded, vertical flexural cracks became visible on the sides of the specimens.

As shown in Figure 4-3, significantly more flexural cracks formed on the jointless specimens than both types of jointed specimens. Following the yielding of the steel bars, cracking started to form diagonally from the loading line to the interior supports. No crack was found in the joint materials (i.e., K-UHPC and Ductal-UHPC). In general, all specimens had a similar crack pattern.

At failure of each specimen, the specimens were subjected to a flexural-shear failure that included abrupt crushing of the top surface of the concrete deck and large diagonal cracking as shown in Figure 4-4. The angle of the major diagonal cracks for each specimen was approximately 35 degrees. In general, all specimens had a similar failure pattern.

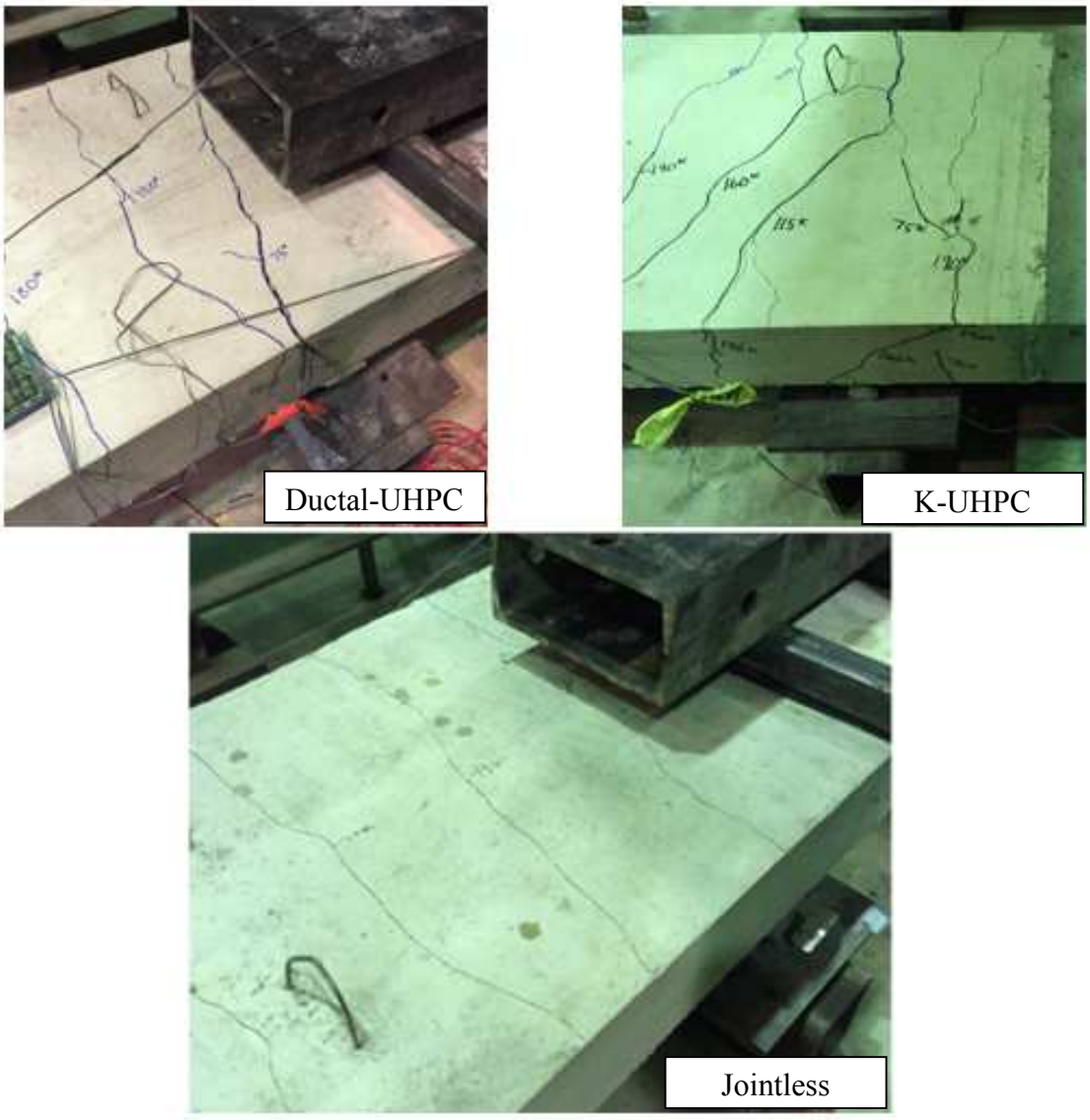

Figure 4-2. Crack Patterns

Both types of joint materials maintained a solid connection to the modules. After testing was finalized, the specimens were taken apart to examine the bond between the bars and the joint as shown in Figure 4-5. There was no observed slip between the reinforcing steel and the joint and no fracture was observed in the bar.

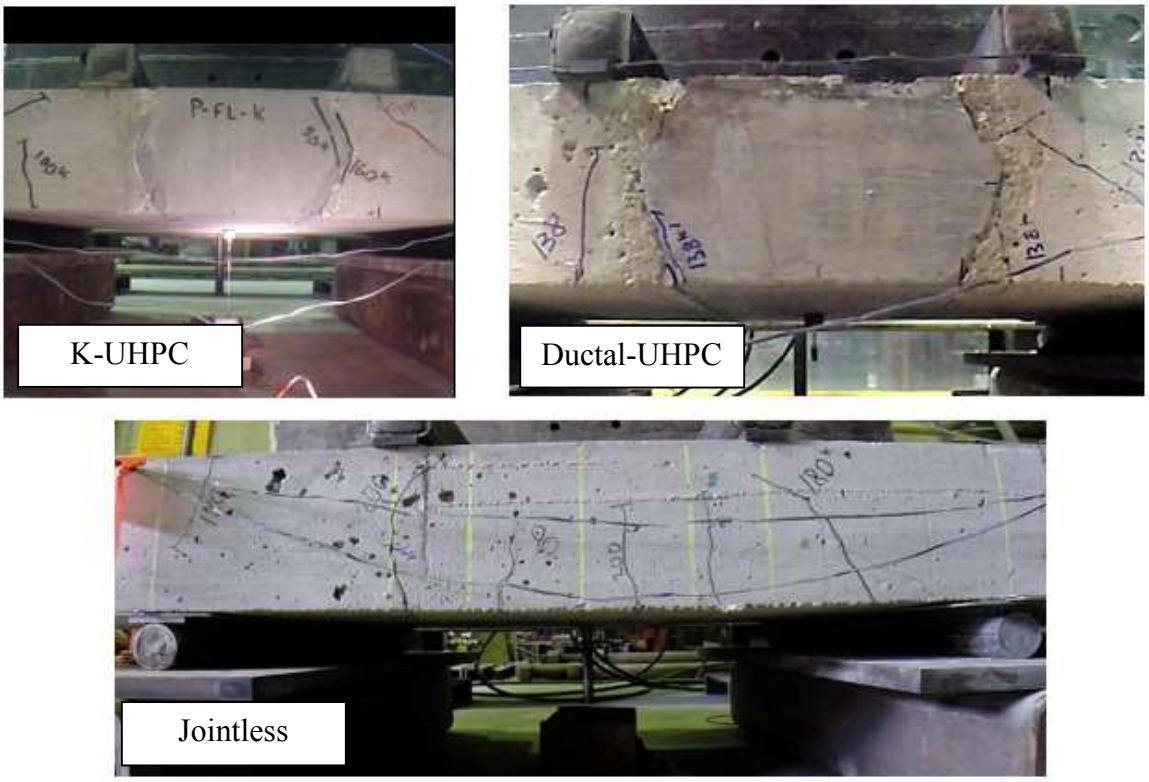

Figure 4-3. Flexural Cracking

Figure 4-4. Failure Cracks

Figure 4-5. Joint Investigation

4.1.3 Comparison of Surface Preparation Techniques

The three joint surface preparation techniques produced slightly different CSPs. The form-retarder produced the roughest surface profile, followed by the rubber formliner, and then the plastic formliner, which produced the smoothest as shown in Figure 4-6. The exposed aggregate surface is noticeably different between the specimens using the formliners and form-retarder respectively as shown in Figure 4-6.

The goal of using three different techniques was to select the best method to achieve the desired CSP. Applying the form-retarder was the easiest to construct method evaluated in this project. It was fairly simple to paint on, however, there were some spots that were hard to reach because of the layout of the reinforcing steel mats. After the forms were removed, the specimens were lifted outside the lab using a forklift. Once outside, the forms were power-washed to remove the chemical compound and provide the exposed aggregate finish. The rubber and plastic formliners were very similar in terms of constructability. Cutting and attaching the formliners to the joint forms was a fairly simple and quick task.

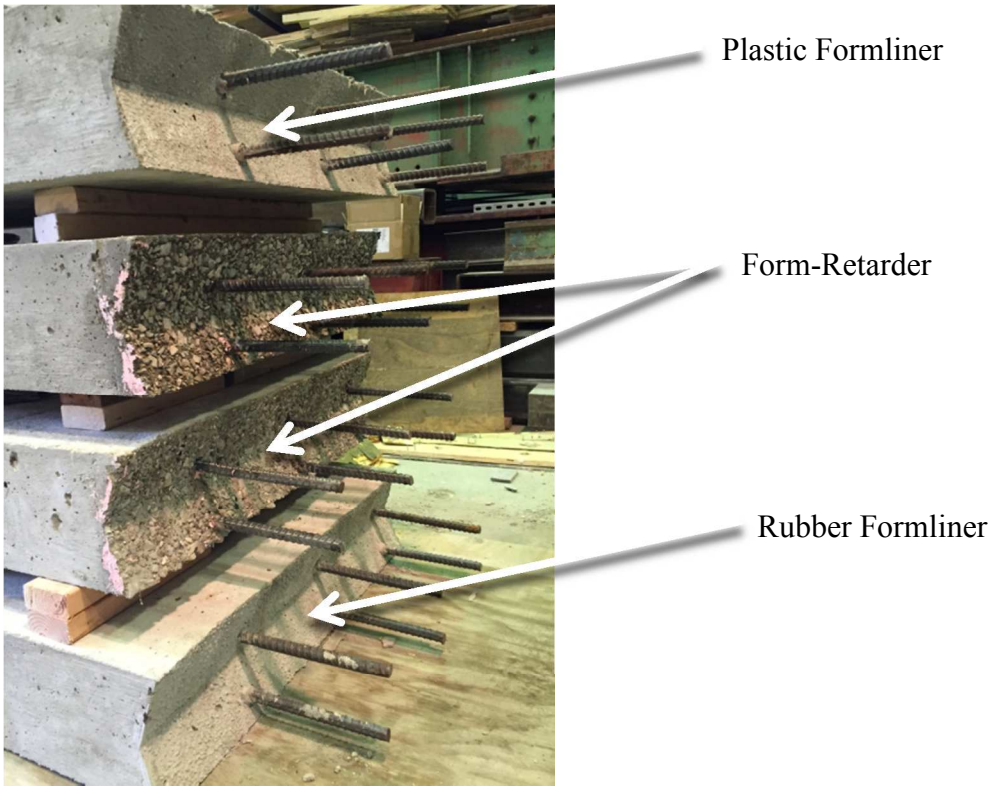

Figure 4-6. Comparison of Joint Surfaces

4.1.4 Load, Strains, and Deflections

Load-strain relationships were developed for each of the specimens and are shown in Figure 4-7 through Figure 4-16. Locations of the embedded gauges used for the figures were illustrated in Figure 3-16 and Figure 3-17. Through the developed relationships it was possible to determine several characteristics of the specimens including the cracking load, steel yielding load, and failure load. Note that only the strain from the four embedded bar gauges in each specimen were utilized for further analysis. The data produced from the concrete gauges was inconclusive and therefore left out of the overall comparison results. A solid bond did not form when attaching all of the gauges, which caused the results to be inconsistent between all of the tests.

The cracking load was estimated based on the load-strain relationships of the embedded strain gauges. The first point the strain value reached a plateau (an abrupt increase in strain) was recorded as the cracking load. For locations where the initial plateau was not as evident, the cracking load was determined once the first steel reinforcement in the deck reached a strain value equal to that of tensile cracking of concrete, which corresponds to about 135 micro-strains based on a linear stress-strain curve. Since the embedded strain gauges were very close to the surface of the deck, the results produced from strain gauge readings are assumed to closely represent the strain values seen on the deck surface. As for the yielding load, Grade 60 reinforcing steel was used for this project, which has a theoretical yield strain of 2,069 microstrain. The load at which the average strain in the cross section exceeded this limit was recorded as the yielding load of steel reinforcement. The maximum load that was reached prior to failure was recorded as the failure load.

Values for the cracking load, yielding load, and failure load are illustrated for each specimen in Figure 4-7 through Figure 4-16. All four embedded gauges for each specimen are included in each figure. The locations of the gauges are distingquished by linetype and the pattern for these are consistant throughout each figure. There is also a vertical line and circle on each figure that are used to display the yielding load and cracking load, respectively.

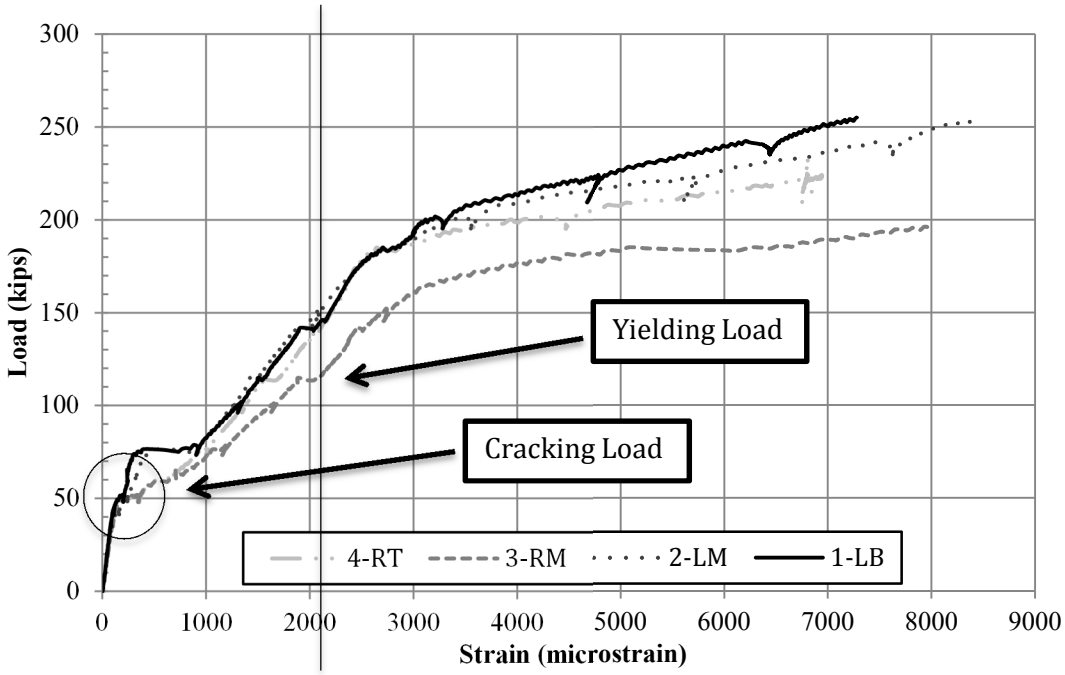

Figure 4-7. Load vs. Strain - Specimen C1 (1st Test)

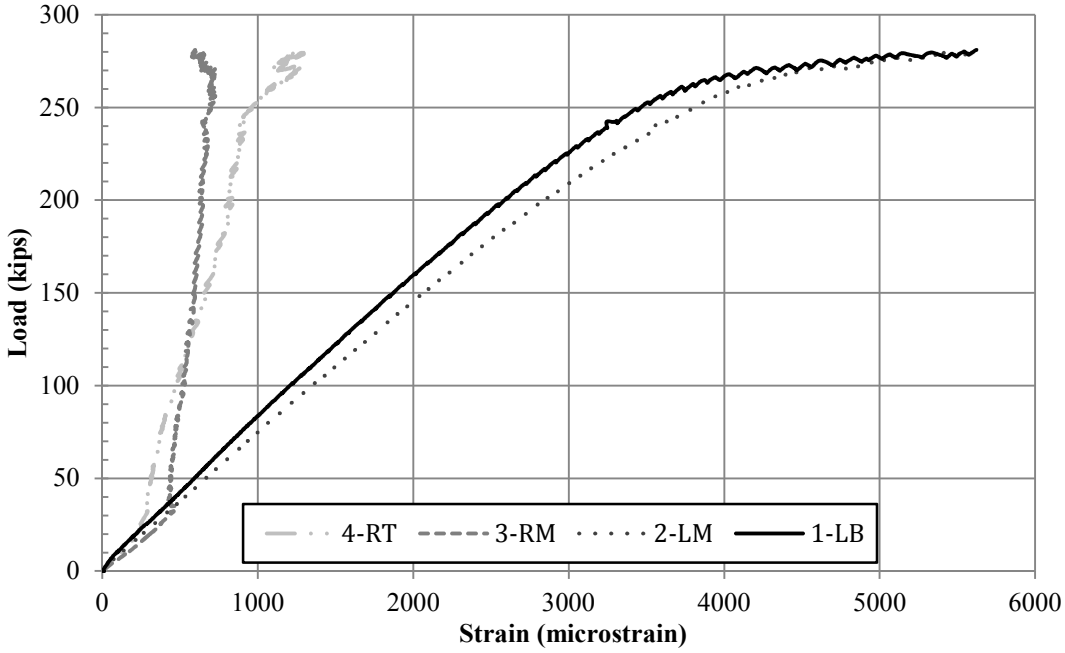

Figure 4-8. Load vs. Strain - Specimen C1 (2nd Test)

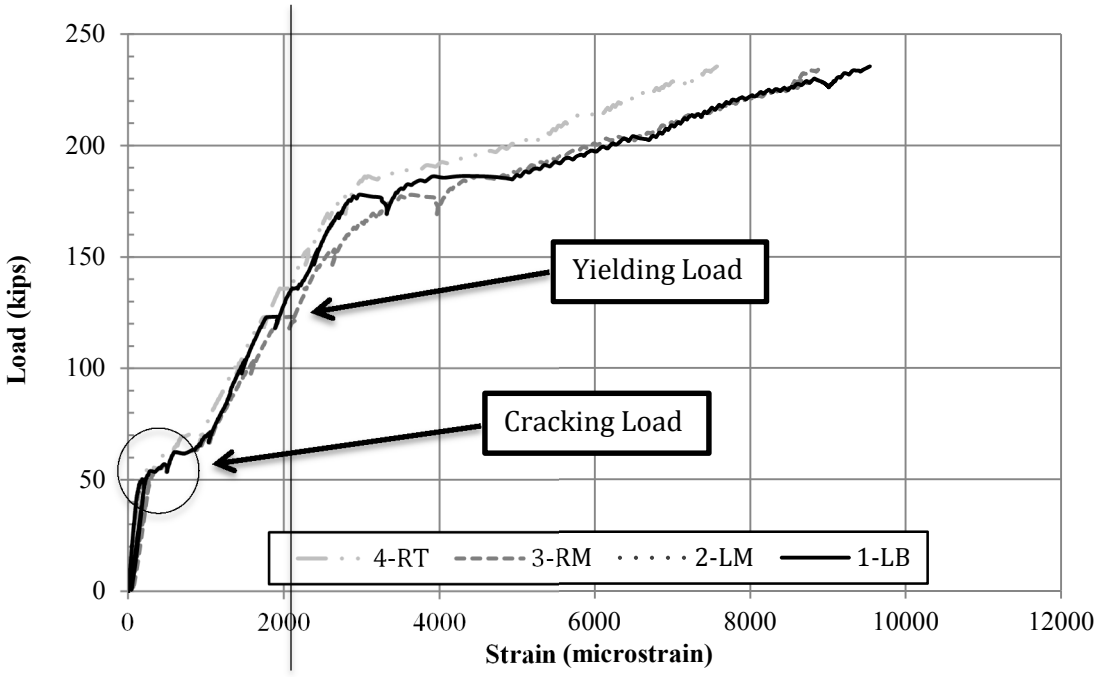

Figure 4-9. Load vs. Strain - Specimen C2

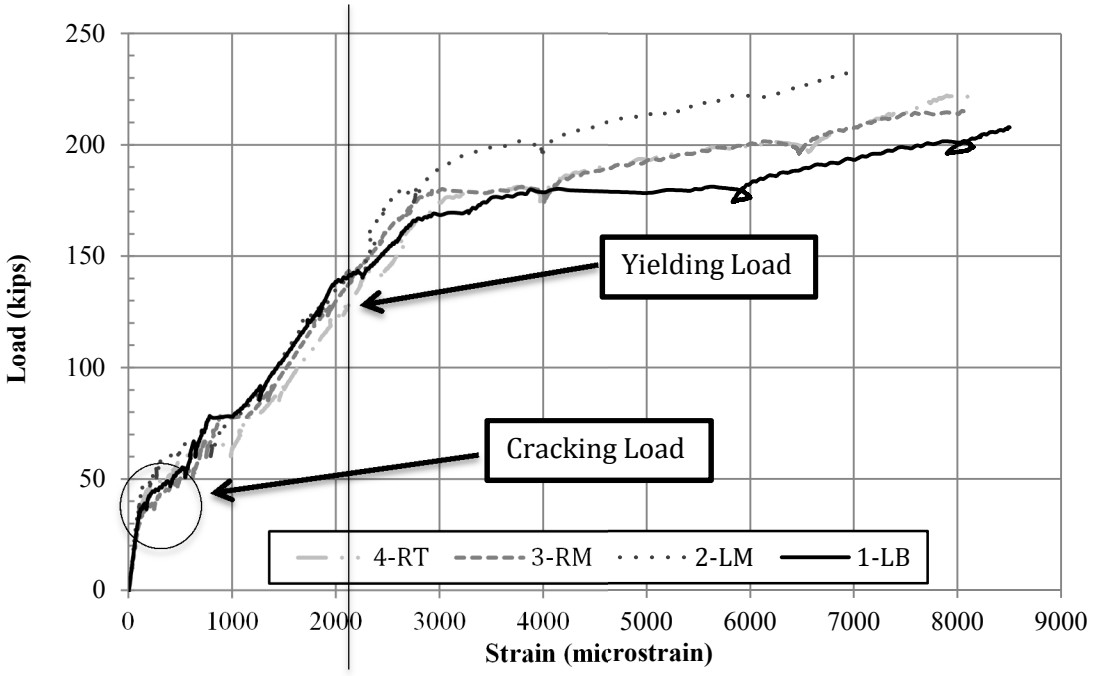

Figure 4-10. Load vs. Strain - Specimen C3

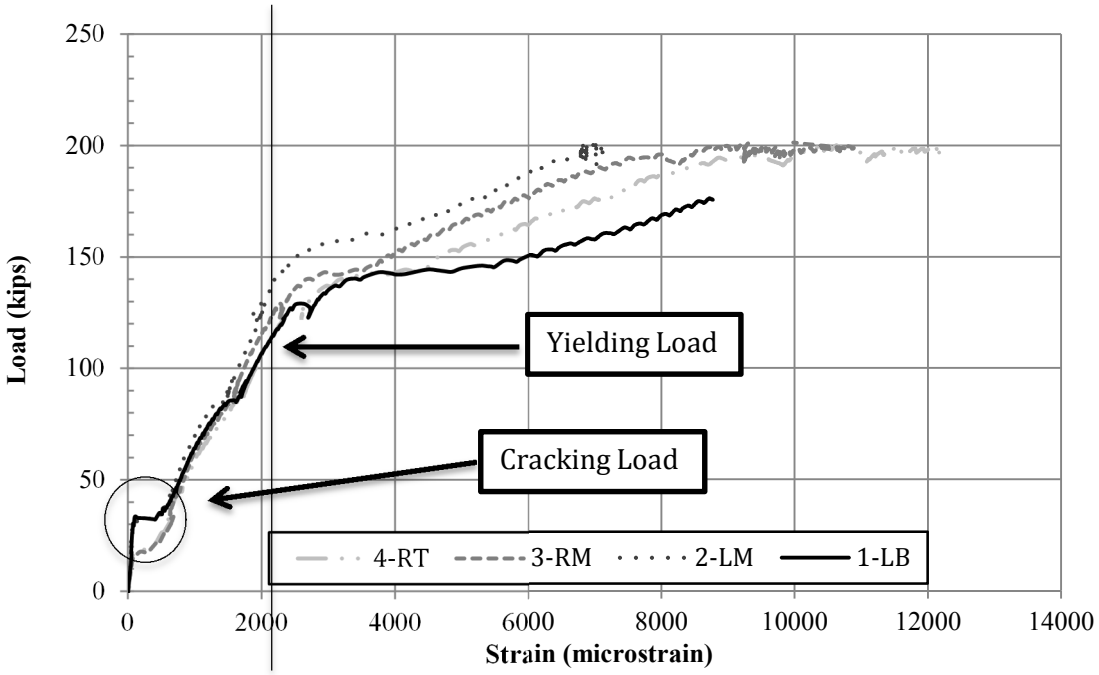

Figure 4-11. Load vs. Strain - Specimen J1 (Plastic Formliner-UHPC)

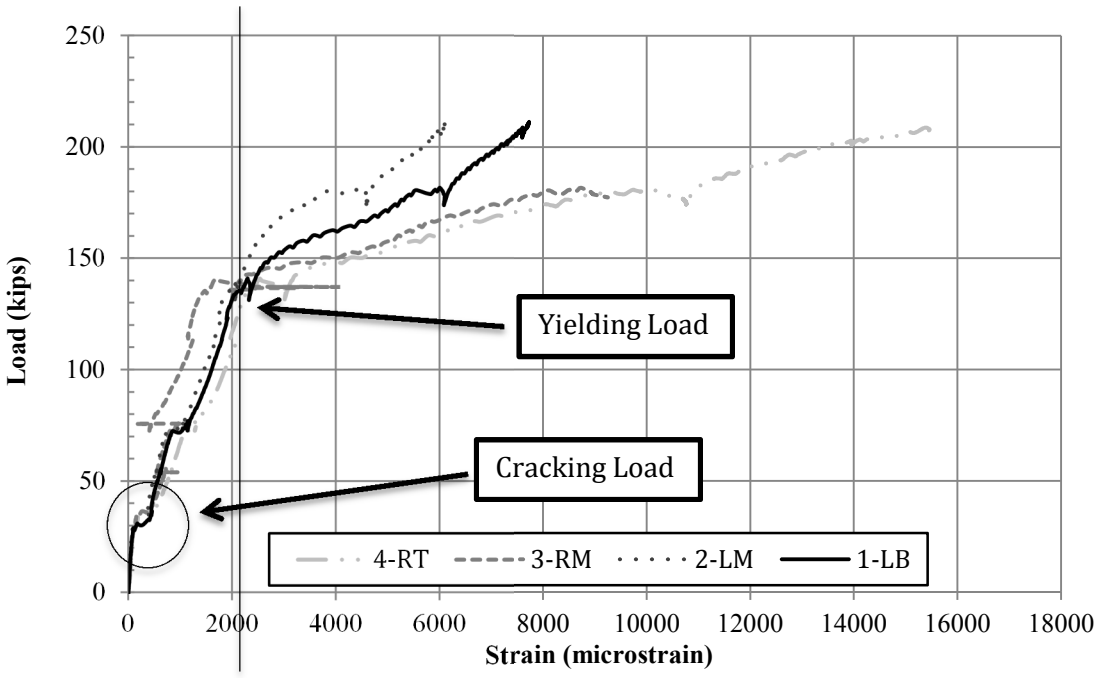

Figure 4-12. Load vs. Strain - Specimen J2 (Form-Retarder-UHPC)

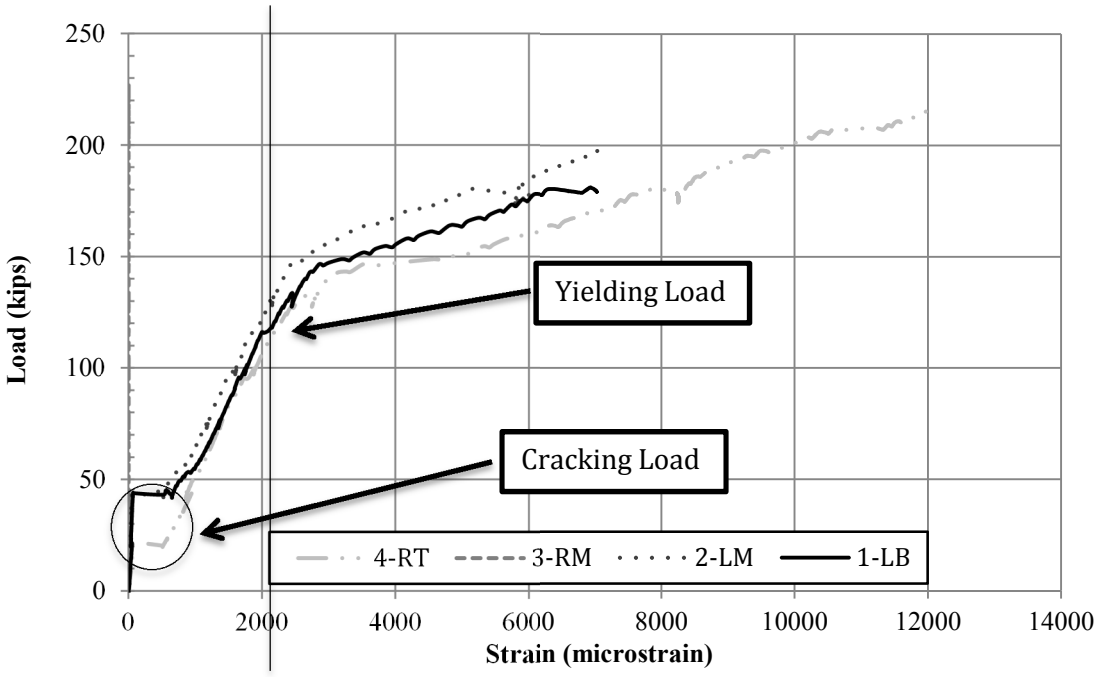

Figure 4-13. Load vs. Strain - Specimen J4 (Rubber Formliner-UHPC)

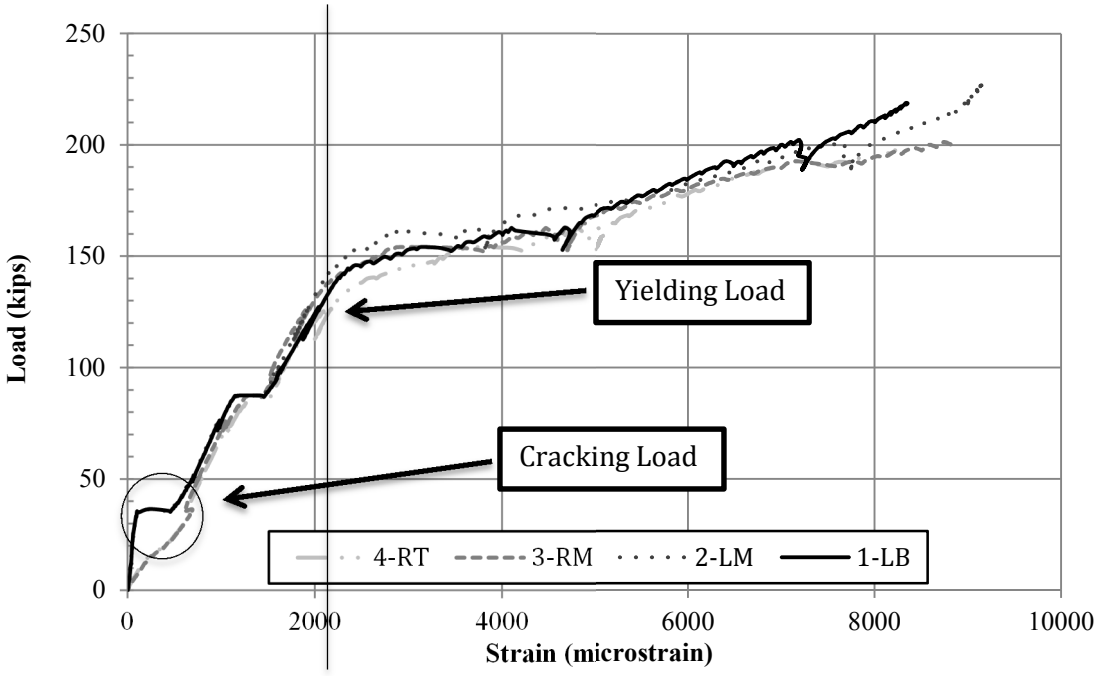

Figure 4-14. Load vs. Strain - Specimen K1 (Form-Retarder-K-UHPC)

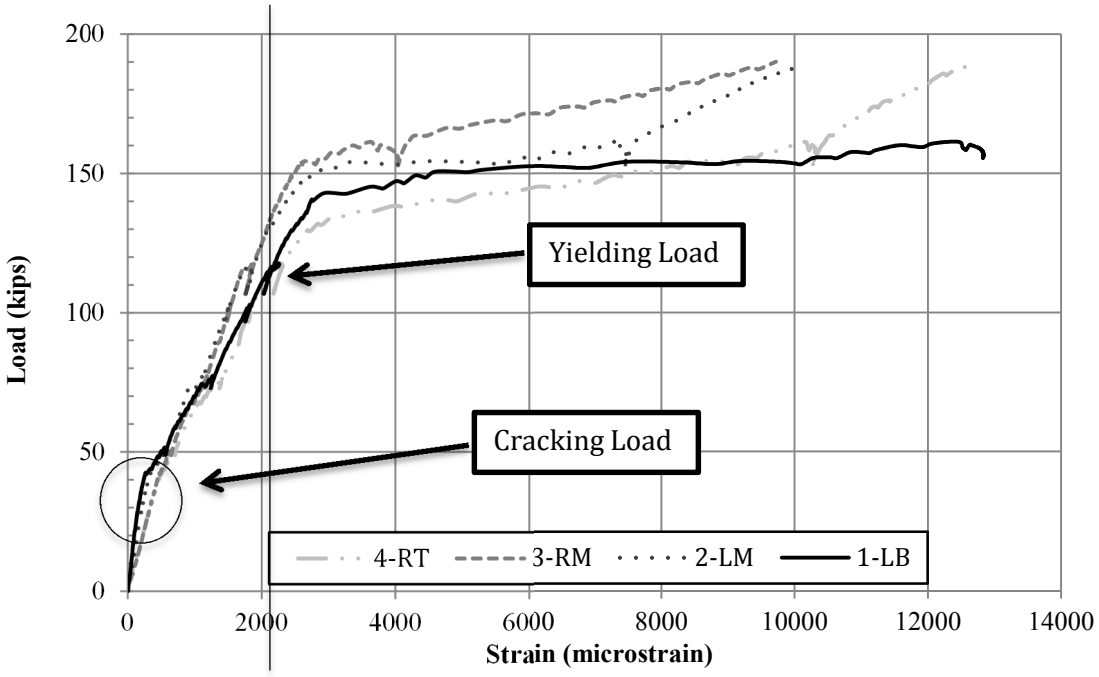

Figure 4-15. Load vs. Strain - Specimen K2 (Plastic Formliner-K-UHPC)

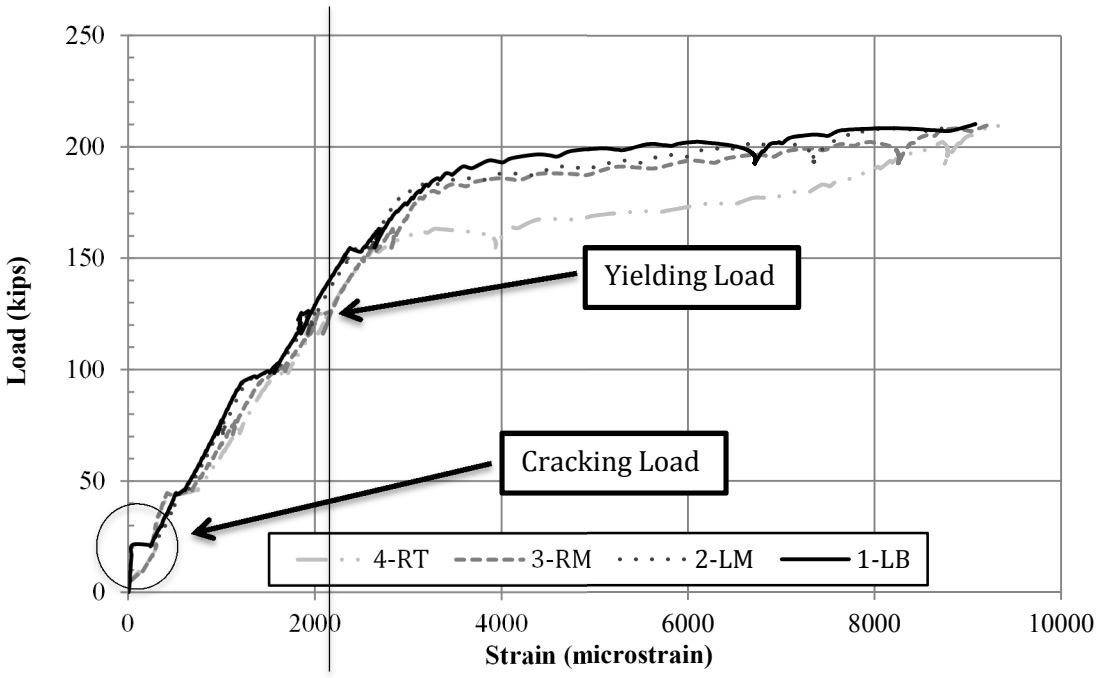

Figure 4-16. Load vs. Strain - Specimen K3 (Rubber Formliner-K-UHPC)

The results from all of the load-strain relationships were summarized and are shown in Table 4-1. These relationships were used to make several different comparisons between all of the specimens. Overall, it can be seen that there was a large deviation in the cracking load between the three types of specimens. The continuous specimens had a significantly higher load prior to cracking than the jointed specimens. It was also quite varied depending on what surface preparation technique was utilized. In general the plastic formliner resulted the highest crack load, then the form retarder, and lastly rubber formliner. There was not such a distinct pattern shown for the yielding load, however the jointless and the K-UHPC Specimens were able to sustain slightly higher loads prior to yielding than the Ductal-UHPC Specimens, on average. The specimens using the plastic formliner had the lowest yielding load for both types of joint material. The failure loads of the specimens followed a very similar pattern as the yielding loads. The jointless specimens showed to be stronger than the jointed specimens and once again sustained higher loads prior to failure. As far as the jointed specimens, the rubber formliner and the form-retarder outperformed the plastic formliner for ultimate strength.

Another particular interest for this testing was which method performed best to use for the joint surface. Overall, each joint surface preparation technique was used twice. The performance of each technique was determined based on the results from the strength tests and overall constructability including time and labor cost. The results from the strength tests for each technique are summarized in Table 4-2.

Table 4-1. Summary of all Test A Results

Type of Specimens		Joint Surface Preparation Technique	Load at Concrete Cracking (kips)	Load at Steel Yield (kips)	Load at Specimen Failure (kips)	Deflection at Failure Load (in.)
			Measured	Measured	Measured	Measured
Jointless specimens	C1	N/A	52	115	250	0.37
	C2	N/A	56	123	235	0.42
	C3	N/A	39	126	230	0.39
Jointed specimens (Ductal-UHPC)		Form-Retarder	31	114	210	0.38
		Plastic Formliner	34	110	195	---
		Rubber Formliner	20	112	225	0.39
Jointed specimens (K-UHPC)		Form-Retarder	35	125	228	---
		Plastic Formliner	39	114	190	0.33
		Rubber Formliner	22	125	210	0.29

Note: N/A – not applicable; --- – bad data

Table 4-2. Testing Results for each Surface Preparation Technique

Joint Surface Preparation Technique		Load at Concrete Cracking (kips)		Load at Steel Yield (kips)		Load at Specimen Failure (kips)		Deflection at Maximum Load (in.)	
		Measured	Average	Measured	Average	Measured	Average	Measured	Average
Form-Retarder	Ductal UHPC	31	33	114	119.5	210	219	0.38	0.38
	K-UHPC	35		125		228		---	
Plastic Formliner	Ductal UHPC	34	36.5	110	112	195	192.5	---	0.33
	K-UHPC	39		114		190		0.33	
Rubber Formliner	Ductal UHPC	20	21	112	118.5	225	217.5	0.39	0.34
	K-UHPC	22		125		210		0.29	

Note: --- – bad data

As shown in Table 4-2, the cracking loads for the three techniques were very inconsistent. The plastic formliner produced the most favorable results and was able to withstand a load of 36.5 kips prior to cracking. The form-retarder was close behind with 33 kips; followed by the rubber formliner which was only able to handle 21 kips before cracking. Yielding loads were very comparable between the three techniques all varying with just a few kips difference. It should be noted that the plastic formliner was the first to yield despite the fact that the initial performance appeared to be superior to the other two techniques. A similar pattern was followed for the failure load for each technique. The rubber formliner and the form-retarder performed the best and withstood just under 220 kips at the point of failure. The plastic formliner on the other hand, fell just short of the 200 kip mark. The results for each technique were very comparable regardless of joint material.

The performance of each joint material was also analyzed. The results were rearranged to directly compare the effect of the joint material and are summarized in Table 4-3. Keep in mind that there were some discrepancies in the results between the joint techniques that were used. However, as mentioned before the joint technique appeared to perform about the same for the two types of joint material. For this reason the results can directly be compared.

Table 4-3. Summary of Results by Joint Material

Type of Jointed Specimens	Joint Surface Preparation Technique	Load at Concrete Cracking (kips)		Load at Steel Yield (kips)		Load at Specimen Failure (kips)		Deflection at Maximum Load	
		Measured	Average	Measured	Average	Measured	Average	Measured	Average
Ductal-UHPC specimens	Form-Retarder	31	28.3	114	112	210	210	0.38	0.385
	Plastic Formliner	34		110		195		---	
	Rubber Formliner	20		112		225		0.39	
K-UHPC specimens	Form-Retarder	35	32	125	121.3	228	209.3	---	0.31
	Plastic Formliner	39		114		190		0.33	
	Rubber Formliner	22		125		210		0.29	

As shown in Table 4-3, several tests were ran and used to compare the different joint materials. A quick glance at the strength test results shows it is evident that the performance of the two materials is very similar. The average of the three specimens for each material cracked around 30 kips and failed after a load of 210 kips was applied. Based solely on these results one can conclude that either material would be suitable to use for the joints. However, another consideration taken into account was the constructability of the material, which the two mix designs varied in that aspect.

Both of the mixes were created on site using the same drum mixer. The mix design for the Ductal-UHPC was provided by the Iowa DOT and is referenced as SP-120245a. All of the procedures outlined in the mix design were followed during the mixing process. The actual mixing of the material went very smoothly. Several 3 in. by 6 in. cylinders were cast during the placement of the UHPC to track the strength throughout the curing process. This was particularly important with the minimum strength requirements for the project. The results from the compression test are shown in Table

4-4. The values listed in the table are the average strengths based on the three tests. In preparation for the compressive strength testing, the cylinders were removed from the plastic molds and then saw cut to form smooth ends. Wood shims were also used during the testing in hopes to better distribute the load across the whole specimen and fill any void spaces. It was anticipated that the strength requirements would be achieved on day four. For this reason, as well as volume limitations of the mixer, only 9 cylinders were cast. Three cylinders were to be tested on day three, four, and finally 28 days. As shown in the table, this was not plausible due to initially low strengths. The strength requirements were not reached until day seven, which is when testing began.

Korea Institute of Civil Engineering and Building Technology (KICT) provided the mix procedure for the K-UHPC. The mix procedure for the K-UHPC was very precise required time step sequences to be followed. Even with close attention to detail, the first round of mixing was not a success. Everything appeared to be running smoothly until suddenly, the material the material became very hard and appeared to lose all of its viscosity. Since all of the proper procedures were followed, it was assumed that the volume produced from the mix quantities that were given was too large for the mixer to handle. The second round of mixing was split into three separate batches. Only enough material to fill one specimen was mixed at a time. Everything went as planned for this round of mixing. Several 3 in. by 6 in. cylinders were cast for each of the three mixes. The average compressive strength between the three mixes was determined and shown in Table 4-4. It should be noted that all three mixes produced very consistent strength results. The required 15-ksi strength of the K-UHPC was achieved in 6 days, but the specimens were tested on the seventh day to keep the cure times consistent.

Table 4-4. Compressive Strength Testing Results for Joint Materials

Days	Ductal-UHPC (psi)	K-UHPC (psi)
0	0	0
4	12,950	13,099
5	14,015	N/A
6	N/A	15,697
7	16,864	16,102
28	N/A	19,300

Note: N/A – no data was collected

Load deflection relationships were also produced from the deflection transducer that was attached to the bottom surface in the center of each specimen are shown in Figure 4-17. Note the location of the transducer can be seen in Figure 3-16 through Figure 3-15. There was error in the instrumentation for two of the specimens. As a result, the data produced from Specimen J1 (Plastic Formliner-UHPC) and K1 (Form-Retarder-K-UHPC) are not included. It can be seen that all results were very comparable. The deflections at failure for each specimen are shown in Table 4-1. Some of the specimens experienced additional load after failure, but the graph only shows deflection up until failure to keep it consistent. Deflection of almost all specimens appeared to be just over 1/3 inch at the time of failure. This was the case for the continuous specimens as well as all jointed specimens. As shown in Table 4-3 the K-UHPC specimens produced smaller deflection results than the Ductal-UHPC ones. However, they were very close and less than 1/10-inch difference. It appeared the surface preparation technique had little effect on deflection, which is shown in Table 4-2.

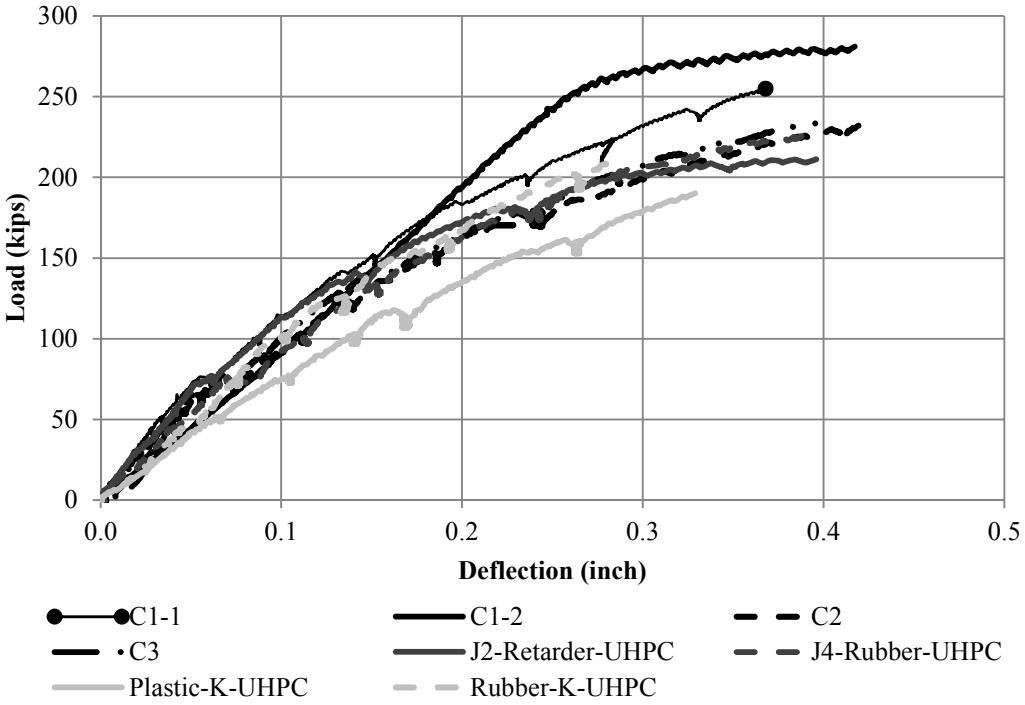

Figure 4-17. Load vs. Deflection for all Test A Specimens

4.2 Test B: Transverse Joints

The compressive strength of the concrete was tested to ensure adequate strength was attained for the specimens. A total of twelve 4 in. × 8 in. cylinders were cast during the placement of the HPC that was used for the concrete deck and diaphragm. Three cylinders were tested at a concrete age of 7, 14, and 28 days, respectively. The results for these tests are provided in Table 4-5. Specimen II was tested after the concrete had a 28-day cure, since the HPC had exceeded the 5-ksi requirements. Due to the removal and set up process, Specimen I was tested one week later after a 35-day cure time. For comparison purposes, all calculations were completed with an assumed average concrete compressive strength of 5,531 psi.

Table 4-5. Compressive Strength Tests Results

Concrete Age	Test 1 (psi)	Test 2 (psi)	Test 3 (psi)	Average (psi)
7	3582	3605	3389	3525
14	4750	4770	4630	4717
28	5540	5462	5590	5531

4.2.1 Crack and Failure Patterns

Conventional crack mapping techniques were used to monitor crack formations on both specimens. Locating the initial cracks and tracking their progression made it possible to determine how the stresses were transferred through the diaphragm. Cracks were mapped after load increments of 50 kips were applied to each end. All of the loads that were noted during testing are referenced here in terms of moments based on the locations for the point of interest. This was done for ease of the reader and to allow the moment capacity of the section to be directly analyzed. The distance of the moment arm for several key locations on the specimen is referenced in Table 4-6.

Table 4-6. Distance from Loading to Gauge Locations

Location	**Moment Arm (ft)**
6 in. West of the Diaphragm	5.5
Center of Diaphragm	6.5
6 in. East of Diaphragm	5.5
Midpoint of Girder	3.25
Edge of Diaphragm (lifting hooks)	6.0

Cracking for both specimens originated in the top of the deck slab right on the outside edges of the diaphragm as shown in Figure 4-18. Cracking of Specimen II was

first noticed when a load of about 50 kips was applied to each side, which corresponds to a moment around 300 ft-kip at the crack location. The first cracks ran across the width of the specimen along the same line as the lifting hooks. As the loading increased, cracks were formed 1 ft outside the edges of the diaphragm followed by cracks located in the center of the diaphragm. Vertical cracks on the sides of the specimen became noticeable around 100 kips (650 ft-kip). These cracks extended down the specimen towards the supports and opened as the yielding load was approached. Cracking down the vertical face of the diaphragm varied on each side. The short overhang side showed significantly more cracking than the long side did. Figure 4-19 and Figure 4-20 shows the crack formations for the short and long sides of the diaphragm of each specimen, respectively. Cracks on the long side did not continue down the vertical face of the diaphragm, but continued to the bottom on the short side. Almost all of the cracking on the specimen ran in the transverse direction, along the width of the specimen. After the maximum load was reached and the specimen was unloaded, a few longitudinal cracks were noticed. Specimen II had a localized failure due to concrete crushing under the loading on the east side as shown in Figure 4-21. The reinforcing steel mat over the diaphragm had yielded, but did not reach its ultimate strength. This implies that the concrete diaphragm would have been able to carry some amount of additional load before reaching its capacity. The diaphragm was also subject to permanent deformation since the reinforcing steel reached strain levels past the yielding point. No fracture was observed in the steel reinforcement as shown in Figure 4-22.

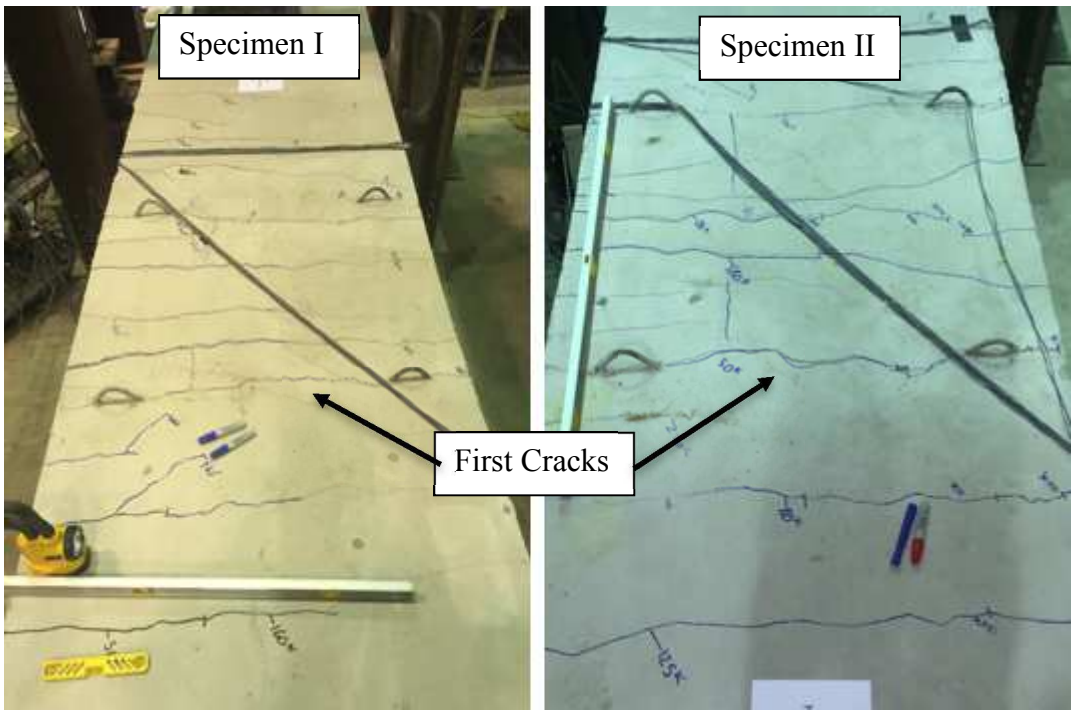

Figure 4-18. Crack Formations on Deck Slab for Each Specimen

Cracking and failure patterns for Specimen I were very similar to those of Specimen II. Again, the first cracks were noticed around a load of 50 kips (300 ft-kip) applied to each side and spanned along the width of the specimen in line with the lifting hooks as shown in Figure 4-18. Cracking then followed the same pattern; showing up 1 ft outside the diaphragm, in the center of the diaphragm, and along the vertical face of the deck. Cracking of Specimen I appeared to be more spread out from the loading locations than Specimen II. The cracks on the face of the diaphragm were also very similar. Minimal cracking was observed on the long overhang side, but cracks extended all the way down the face to the supports on the short side, which is shown in Figure 4-19 and Figure 4-20. Small cracks formed on the bottom of the diaphragm and spread to the neoprene bearing pads as shown in Figure 4-23. A larger plate was used at the loading locations to prevent concrete crushing as shown in Figure 4-24. Ultimate failure was

taken as the maximum loading that was withstood during testing. At this load, deflection continued to increase rapidly while the actual load was not increasing. The steel reinforcement over the diaphragm had yielded and the specimen was subject to permanent deformation.

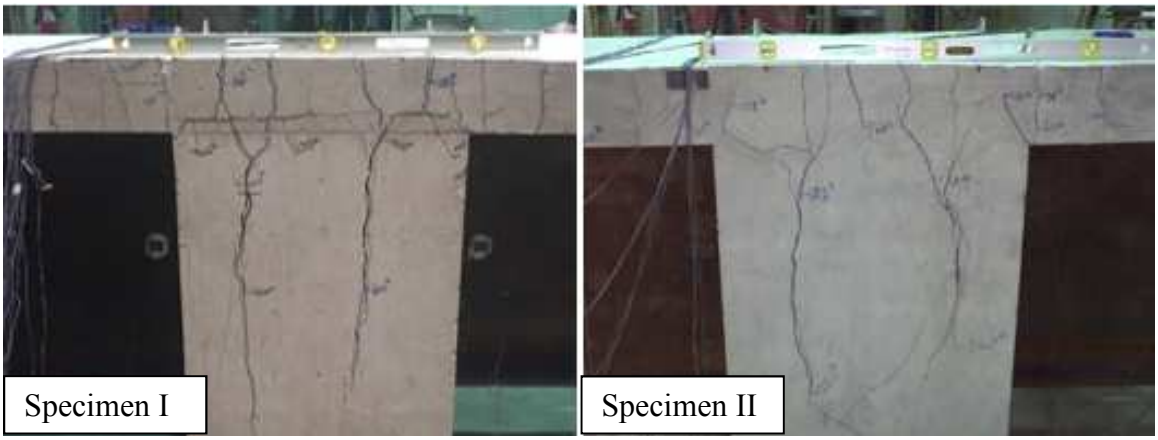

Figure 4-19. Diaphragm Cracks on Short Side for Each Specimen

Figure 4-20. Diaphragm Cracks on Long Side for Each Specimen

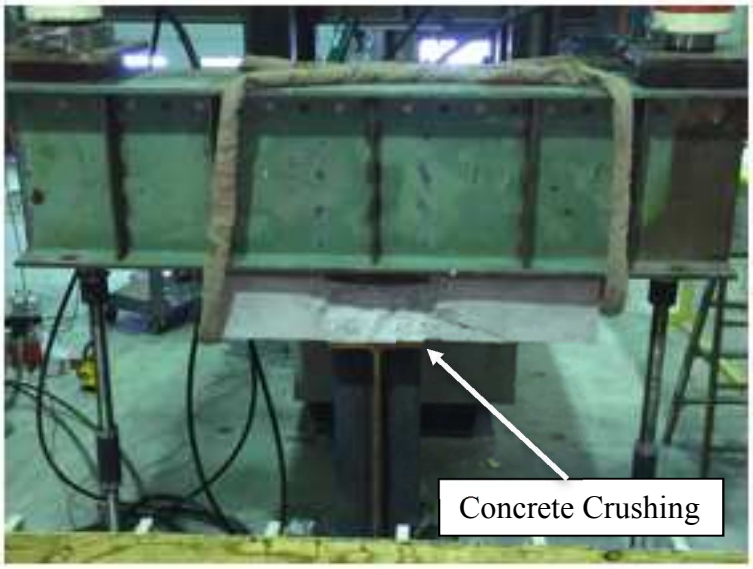

Figure 4-21. Localized Failure of Specimen II Under the Loading Point

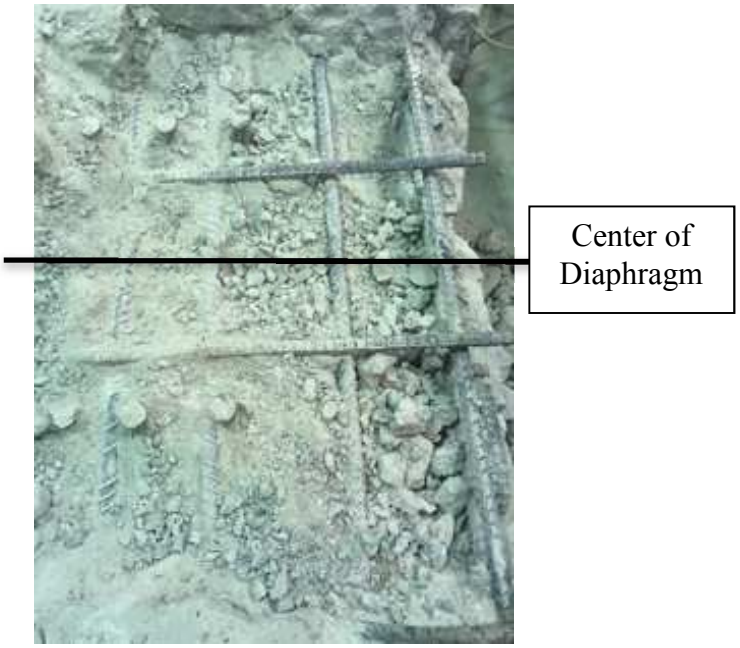

Figure 4-22. Reinforcing Steel Examination

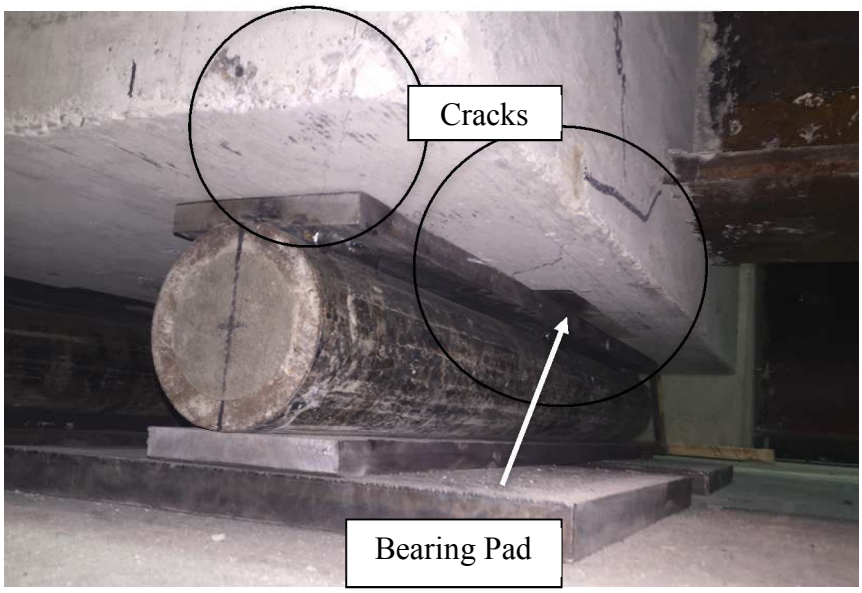

Figure 4-23. Cracking of Diaphragm for Specimen I

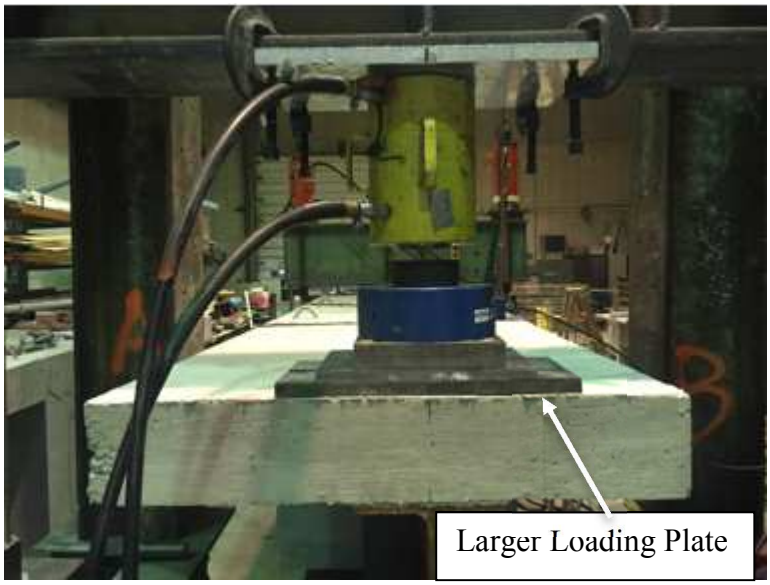

Figure 4-24. Revised Loading Configuration of Specimen I

4.2.2 Loads, Strains, and Deflections

For both specimens, the concrete-cracking load, steel-yielding load, ultimate load, and deflection at maximum load were determined. Again, these loads were referenced to in terms of moments using the moment arm for each section as noted in Table 4-6. For

comparison purposes, strain results were discretized by location: 6 in. west of the diaphragm, center of the diaphragm, 6 in. east of the diaphragm, and midpoint of the girders. The cracking load was estimated based on the load-strain relationships of the embedded strain gauges, which are shown in Figure 4-25 through Figure 4-30. The first point the strain value reached a plateau (an abrupt increase in strain) was recorded as the cracking load. For locations where the initial plateau was not as evident, the cracking load was determined once the first steel reinforcement in the deck reached a strain value equal to that of tensile cracking of concrete, which corresponds to about 135 micro-strains based on a linear stress-strain curve. Since the embedded strain gauges were very close to the surface of the deck, the results produced from strain gauge readings are assumed to closely represent the strain values on the deck surface. As for the yielding load, Grade 60 reinforcing steel was used for this project, which has a theoretical yield strain of 2,069 microstrain. The load at which the average strain in the cross section exceeded this limit was taken as the yielding load of steel reinforcement. Grade 50 steel was used for the W40x149 girders. The corresponding yielding strain is 1,724 microstrain, which will be tracked by the surface mounted gauges that are positioned along each girder. The largest values during the test for load and deflection were recorded as the ultimate load and maximum deflection, respectively. The following load-strain relationships were developed from the embedded strain gauges attached to the top mat in the bridge deck. The cracking and yielding load along with the moment arm to each section are illustrated in in Figure 4-25 through Figure 4-30.

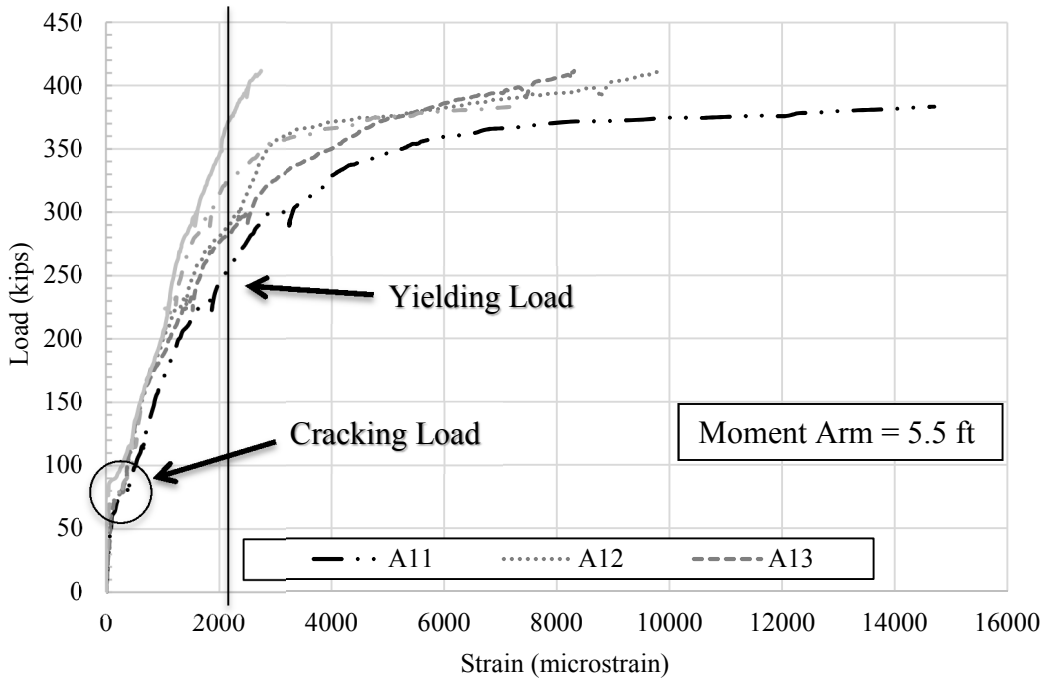

Figure 4-25. Load vs. Strain 6 in. West of the Diaphragm - Specimen I

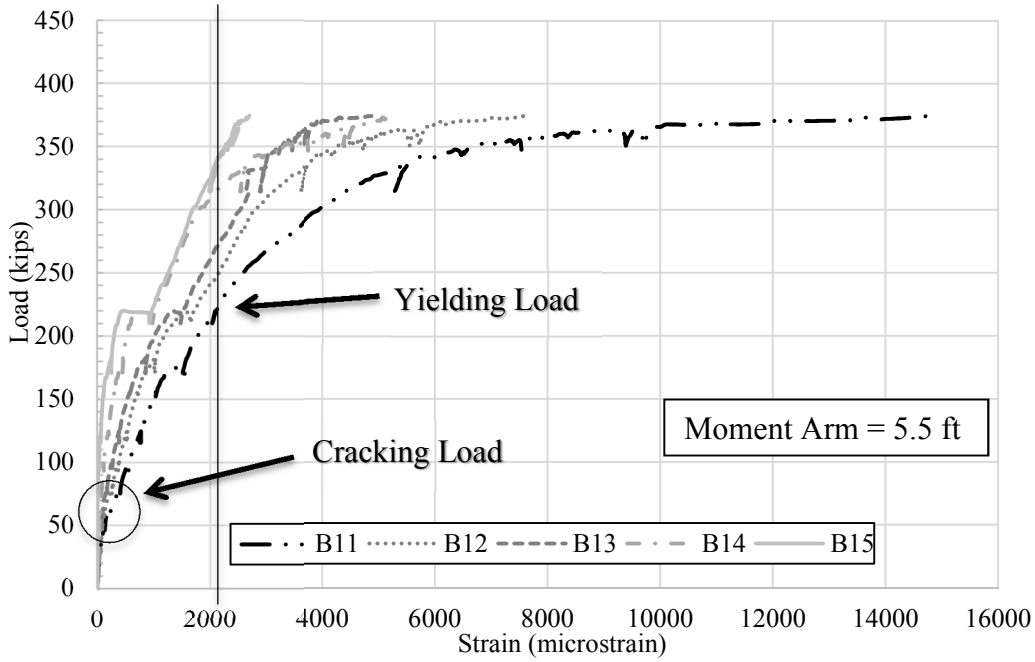

Figure 4-26. Load vs. Strain 6 in. West of the Diaphragm - Specimen II

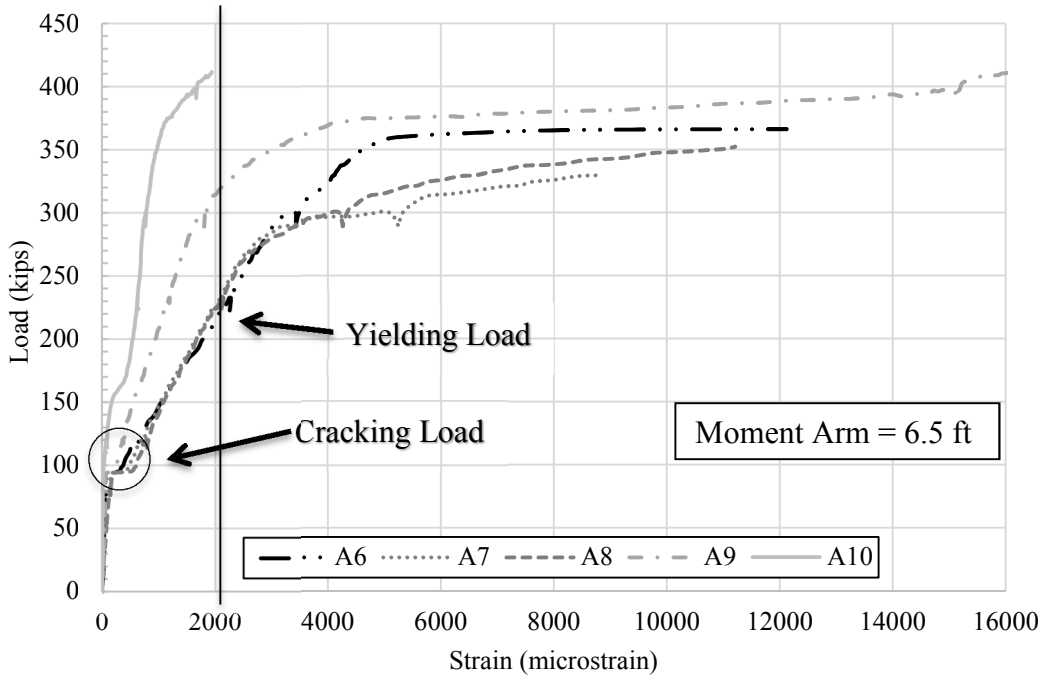

Figure 4-27. Load vs. Strain Center of the Diaphragm - Specimen I

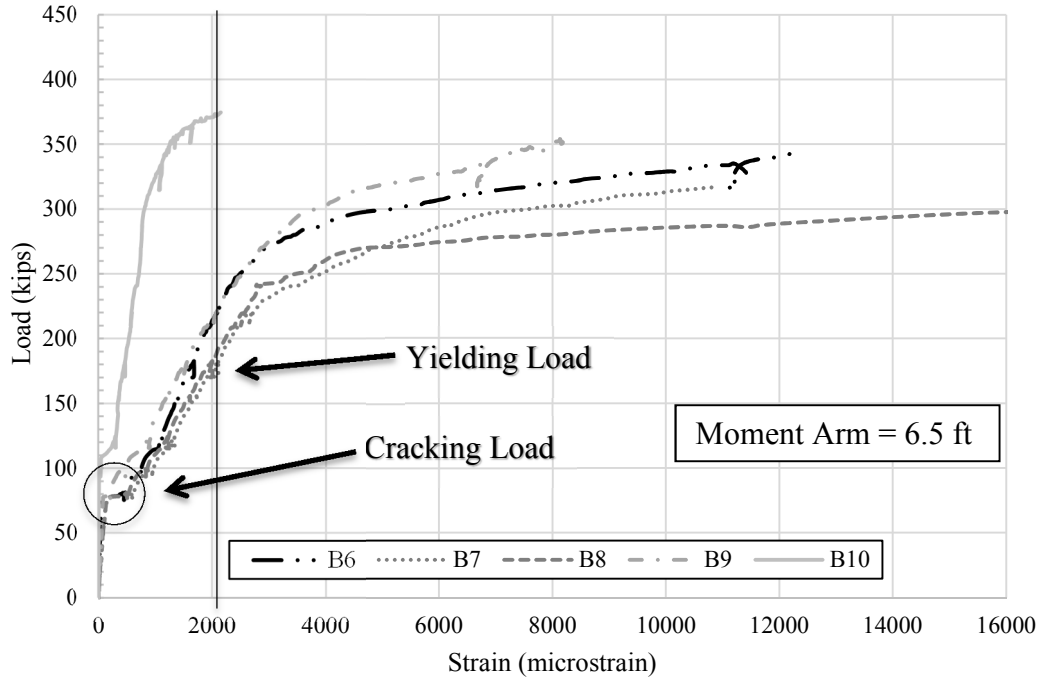

Figure 4-28. Load vs. Strain Center of the Diaphragm - Specimen II

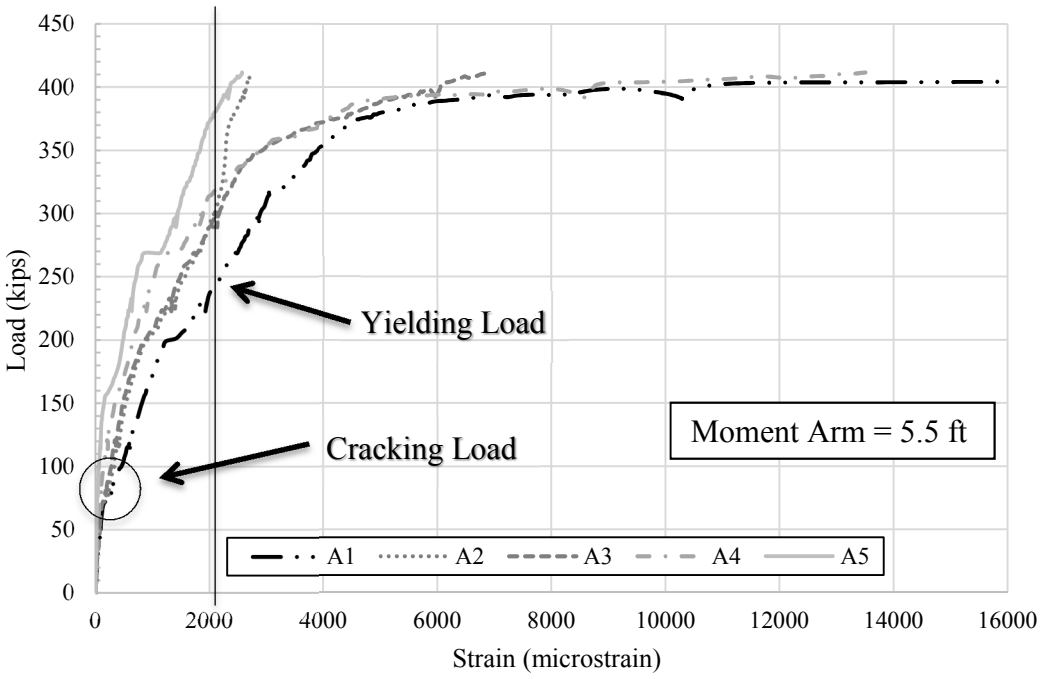

Figure 4-29. Load vs. Strain 6 in. East of the Diaphragm - Specimen I

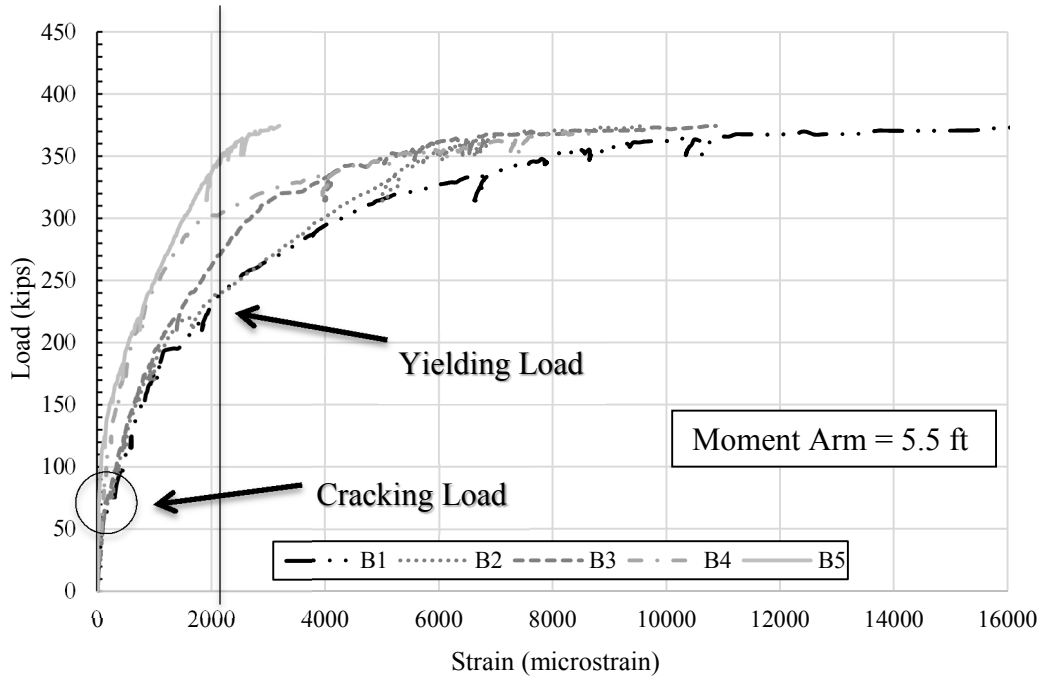

Figure 4-30. Load vs. Strain 6 in. East of the Diaphragm - Specimen II

A review of Figure 4-25 through Figure 4-30 reveals that Specimen I was able to sustain higher loads than Specimen II prior to the different failure points, such as cracking and yielding. For quicker comparison between the different sections for the two specimens, the minimum values produced in these figures are shown in Table 4-7. Again, the load values for the failure points will be referenced back to as moments based on the locations of the section.

Table 4-7. Summary of Tests Results at Each Cross-Section

	Cracking Load (kip) (Moment / ft-kip)		**Yielding Load (kip) (Moment / ft-kip)**	
	Specimen I	***Specimen II***	***Specimen I***	***Specimen II***
6 in. West of the Diaphragm (Moment Arm = 5.5 ft)	65 (357.5)	55 (302.5)	255 (1402.5)	220 (1210)
Center of Diaphragm (Moment Arm = 6.5 ft)	90 (585)	75 (487.5)	225 (1462.5)	180 (1170)
6 in East of the Diaphragm (Moment Arm = 5.5 ft)	70 (385)	65 (357.5)	245 (1347.5)	240 (1320)
Minimum Load	**65**	**55**	**225**	**180**
Corresponding Moment (ft-kip)	***357.5***	***302.5***	***1462.5***	***1170***

The overall load required for cracking was higher for Specimen I than for Specimen II. As previously discussed, the first cracks were noticed just outside of the diaphragm and worked there way towards the load lines before appearing in the center of the diaphragm. This pattern is also confirmed by the data, which show that the center of the diaphragm sustained a significantly higher load prior to cracking than the locations 6 in. outside. For Specimen I, this difference is clearly shown by comparing Figure 4-25 to Figure 4-27, which are strain relationships 6 in. west of the diaphragm and center of the diaphragm, respectively. Based on the strain values and a cracking strain of 2,069

microstrain, the first cracks for Specimen I were formed around a load of 65 kips - which relates to a moment of 357.5 ft-kip. Cracks for Specimen II formed earlier around a load of 55 kips - which relates to a moment of 302.5 ft-kip. However, these loads are the minimum loads to produce cracking at the section the embedded gauges were located (see Figure 3-32 and Figure 3-33).

Specimen I also sustained higher loads at the point of the first bar yielding. The yielding of both specimens occurred first at the center of the diaphragm. Specimen I was able to withstand a total load of 225 kips prior to the first bar yielding, while Specimen II was only able to handle a load of 180 kips. This corresponds to a yielding moment of 1,462.5 ft-kip for Specimen I and 1,170 ft-kip for Specimen I. However, as shown in Figure 4-25 through Figure 4-30 there is a large deviation of strain results produced throughout each section. To better understand how the forces were distributed throughout the specimen, transverse strain values across the width of the specimen were plotted for all three different longitudinal cross-sections; 6 in. west of the diaphragm, center of the diaphragm, and 6 in. east of the diaphragm. Note the gauge locations for these cross-sections are shown in Figure 3-32 and Figure 3-33 and the strain distributions are shown in Figure 4-31 through Figure 4-33. For reference the moment arm at each cross section are given in Table 4-6.

The transverse strain relationships were developed individually for each cross-section. For example, once the first bar reached the theoretical yield limit of 2069 microstrain all other strain values at that point of time were used for each section. The same goes for cracking strain.

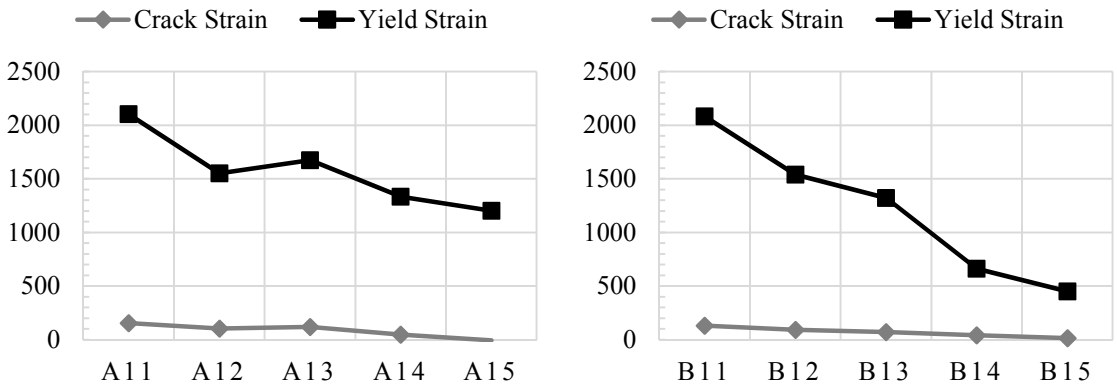

Figure 4-31. Strain Values 6 in. West of the Diaphragm

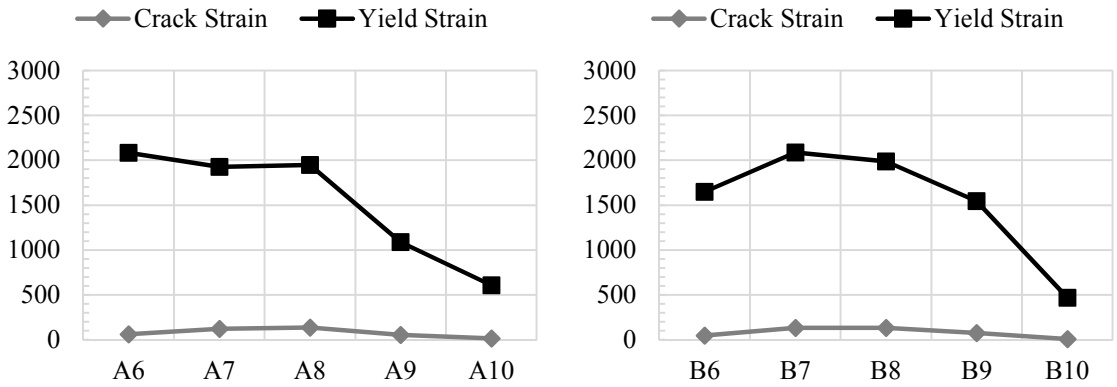

Figure 4-32. Strain Values Center of Diaphragm

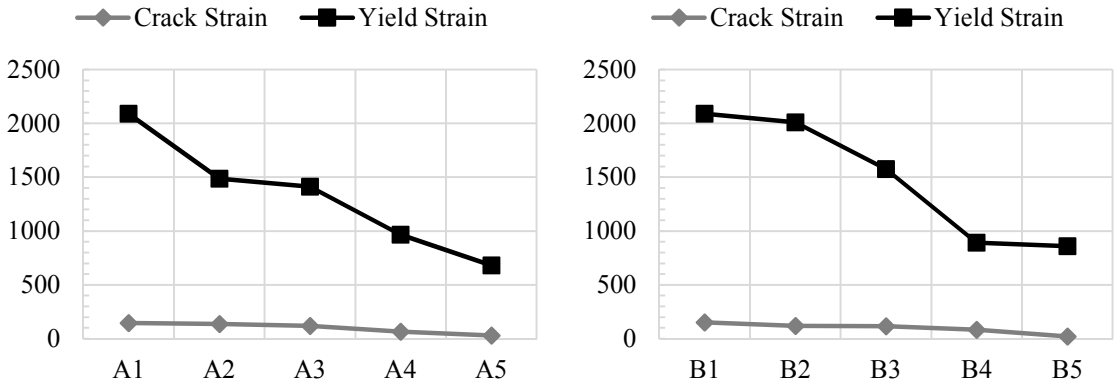

Figure 4-33. Strain Values 6 in. East of the Diaphragm

As shown in Figure 4-31 and Figure 4-33, both the east and west side of the diaphragm produced very similar results (see Figure 4-38 for loading rates). Strain readings were highest towards the edge of the short overhang side and decreased along the width of the specimen to the edge of the long overhang side. This pattern was consistent for both crack and yield strains for the sections outside of the diaphragm. The center of the diaphragm, shown in Figure 4-32 showed slightly different results. The strain readings were highest toward the centerline of the girder, where the load was applied, and gradually become smaller as they got further away. The short overhang side still experienced about three times the strain as that seen on the long side. Relating back to the visual crack mapping that was previously discussed, it makes sense why several more cracks were noticed on the short overhang side. The gauges towards the edge of the long overhang side had substantially lower strain readings throughout the whole length of the specimen. The individual results for these three cross sections are summarized in Table 4-7. The lowest load out of the three sections was used for the overall comparison in Table 4-8.

Relationships for loading and girder strains were also developed and are shown in Figure 4-34 and Figure 4-35. Both the east and west gauges are included in each figure. Locations of the strain gauges used for the comparisons are displayed in Figure 3-34 and Figure 3-35. The figures were setup to present a pairwise comparison between Specimen I and II and are separated into two figures, midpoint of the girder and 6 in. outside of the diaphragm. For quick identification different line types were used based on whether the gauge was installed on the top flange (dots), middle of the web (dashed), or the bottom

flange (solid). The darker line represents all of the gauges on the west girder and the lighter line represents all of the gauges on the east girder.

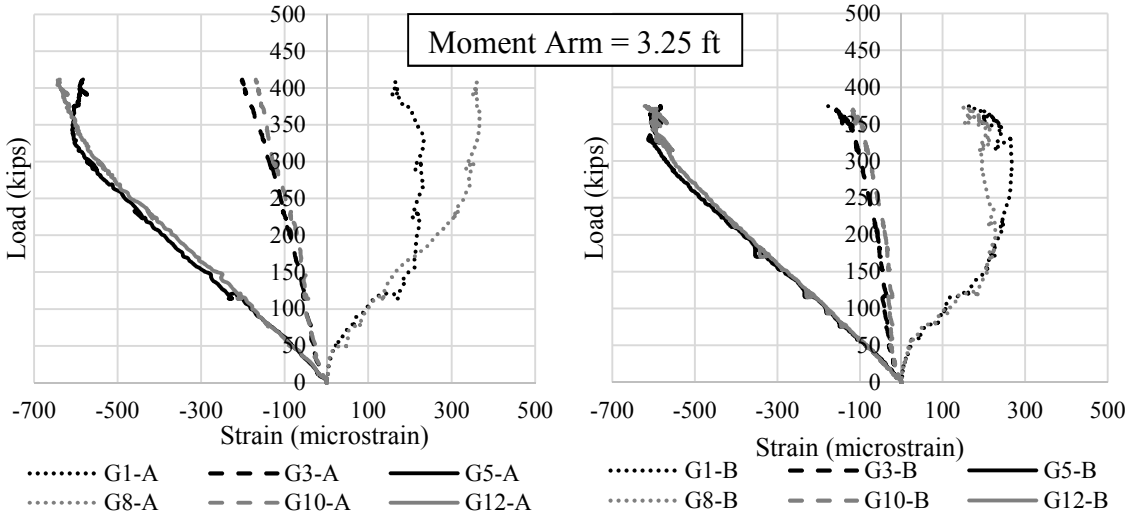

Figure 4-34. Load vs. Strain on Girder at Midpoint

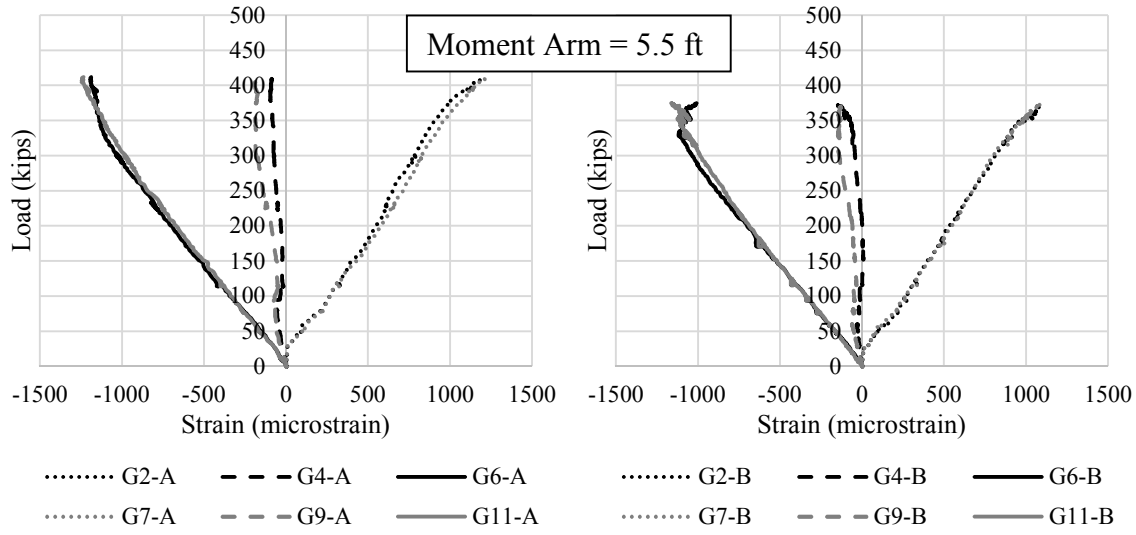

Figure 4-35. Load vs. Strain on Girder 6 in. Outside of Diaphragm

Strains on both the west and east side of the diaphragm were comparable for both specimens at matching locations. When comparing absolute strain values for both specimens, the results are almost identical. All of the gauges mounted to the middle of

the web had very small strain readings. These readings were almost always negative indicating compressive forces and confirming the location of the neutral axis is just above the center of the girders. Specimen II showed very small readings of tensile forces for a short period of loading, but for the most part only compressive forces were seen in the center of the web. With a maximum strain around 1,200 microstrain, all locations remained elastic, as the yield limit of 1,724 microstrain was not reached for the girders.

Load-strain relationships for the compression block were very similar to those of the bottom flange of the girder. As shown in Figure 4-36 only compressive forces were transferred through the compression block. Based on visual observation after testing was concluded, it is evident that the concrete diaphragm never failed under compression and was still able to transfer some of the compressive forces.

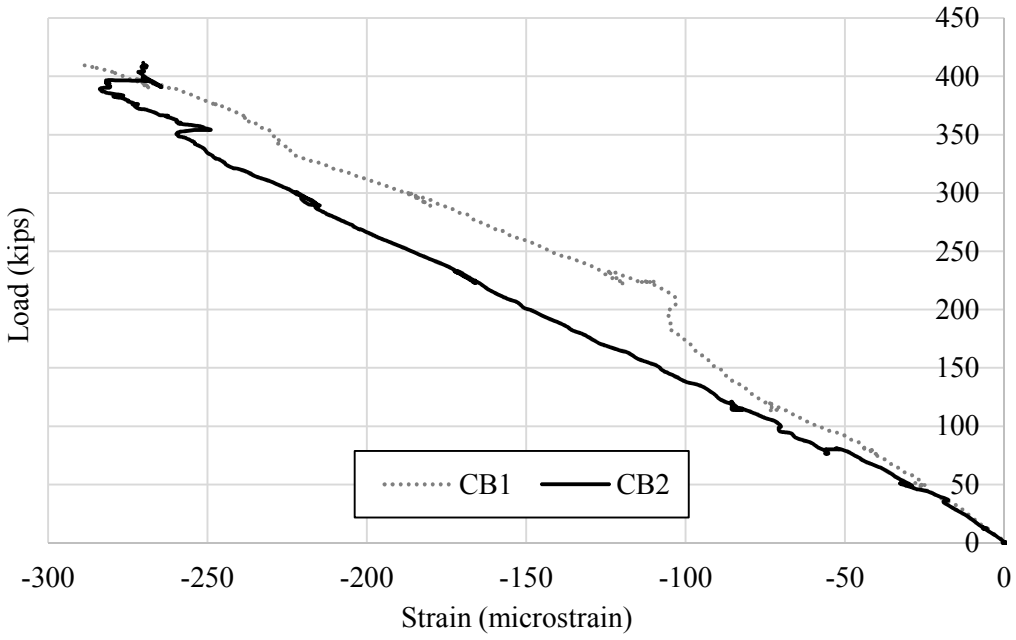

Figure 4-36. Load vs. Strain on Compression Block

Load-deflection relationships for both specimens are shown in Figure 4-37. It should be noted that deflection during early stages of loading was very sensitive. Since an electric pump applied the east load and a hand pump applied the west load, it was hard to keep the load rates constant at the beginning. For this reason, the average displacements for both sides were used to compare the specimens. Loading rates for both sides are shown in Figure 4-38. Both specimens had very similar deflection results. The specimens appeared to have a linear deflection until the steel bars in the center of the diaphragm had yielded. After yielding of the steel bars, the deflection of both specimens continued to increase due to smaller increments of loading. Specimen I was able to withstand a greater load than Specimen II at the same deflection. Towards the end of testing it appeared that both specimens would not be able to handle much additional load but the deflection significantly increased.

Based on the results provided in this section, it is evident that Specimen I, which included the compression block, produced more favorable results. The overall results are summarized in Table 4-8.

Table 4-8. Summary of Critical Tests Results

	Cracking		**Yielding**		**Ultimate**		**Maximum Deflection**
	Load (kip)	***Moment (ft-kip)***	***Load (kip)***	***Moment (ft-kip)***	***Load (kip)***	***Moment (ft-kip)***	***(in)***
Specimen I	65	357.5	225	1462.5	412	2678	1.20
Specimen II	55	302.5	180	1170	375	2437.5	1.28

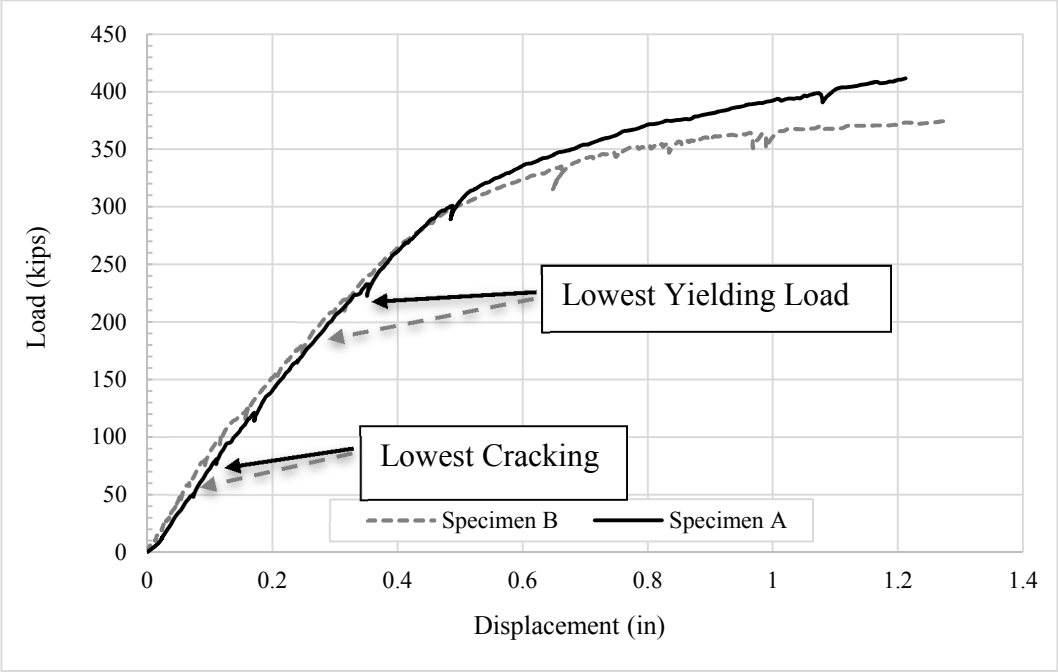

Figure 4-37. Load vs. Displacement of both Specimens

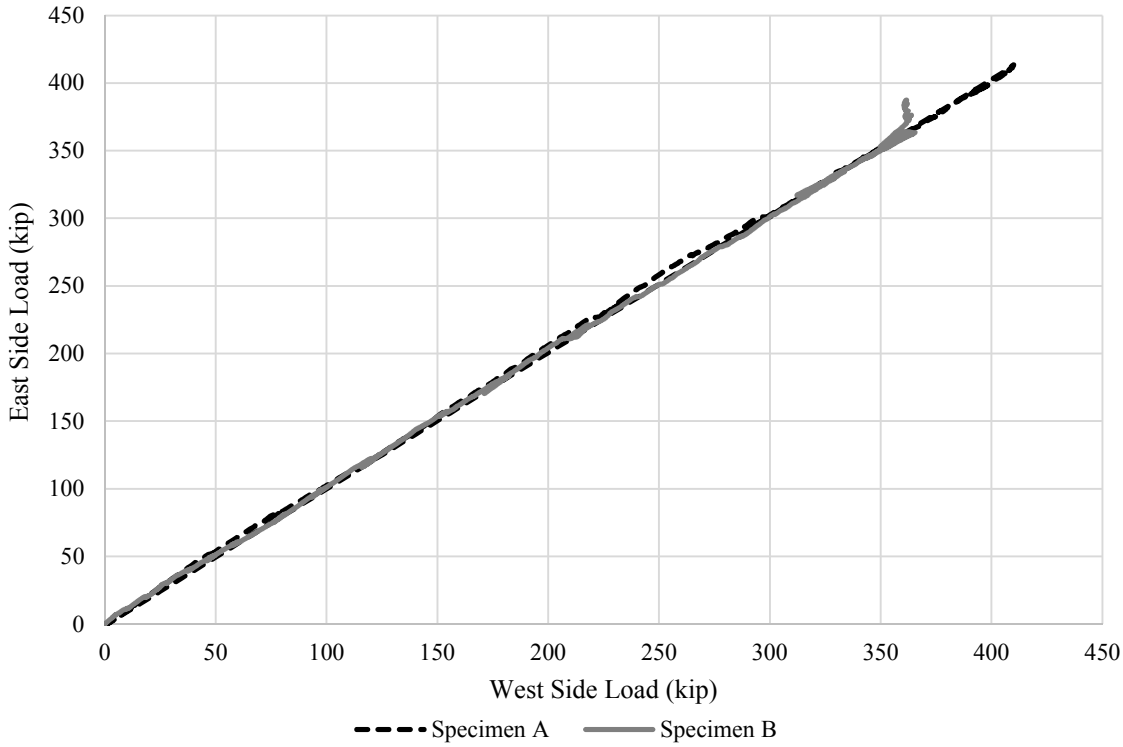

Figure 4-38. West vs. East Loading Rates

CHAPTER 5. SUMMARY, CONCLUSIONS, AND RECOMMENDATIONS

In this project, the performance and benefits of using Prefabricated Bridge Elements and Systems (PBES) connect by closure pour connections were evaluated. The recent project consisting of the replacement of a bridge located on Iowa 92 over Little Silver Creek in Pottawattamie County, Iowa was used to demonstrate this Accelerated Bridge Construction (ABC) technique. To further verify the adequacy of this technique, the performance of an ultra-high performance concrete (UHPC) longitudinal joint detail and a high performance concrete (HPC) transverse joint detail used for the Little Silver Creek Bridge were studied through laboratory testing.

A total of 11 specimens were designed, instrumented, and tested to evaluate the performance of two types of joints that are used for modular construction. Both the longitudinal and transverse joints were under consideration for this research. The following subsections will provide a brief summary of the overall project and the conclusions that were formed.

5.1 Longitudinal Joints

Nine specimens were designed, fabricated, instrumented, and tested in the Iowa State University Structural Engineering Laboratory (i.e., three jointed specimens fabricated using K-UHPC, three jointed specimens using Ductal-UHPC, and three jointless specimens designed to replicate a continuous bridge deck and as a baseline to evaluate the performance). The jointed specimens were designed with comparable details to those used for the jointless specimens. Three types of surface preparation techniques

(i.e., rubber formliner, plastic formliner, and form retarder) were utilized for the three jointed specimens using K-UHPC or Ductal-UHPC. All specimens were tested in an identical test setup with three spans. Ponding tests were performed by adding a pond at the mid-center span to demonstrate the joint's resistance to water infiltration. Strength tests were conducted by applying a two-line loading at the center-span until failure to evaluate the strength and ductility of specimens. The applied load, strain in concrete and steel, and deflection at the mid-center span were collected and cracks were mapped during testing. The performance was compared between the specimens using different types of surface preparation techniques, between the jointed and jointless specimens, and between the specimens using different joint materials (i.e., K-UHPC and Ductal-UHPC). The following conclusions were made based upon the work described herein:

5.1.1 Curing and Ponding Tests

- No leakage cracks were identified at the joint or at the interface of the K-UHPC and Ductal-UHPC specimens due to early-age drying shrinkage. A good bond was achieved at the interface between the concrete and K-UHPC and between the concrete and Ductal-UHPC.

5.1.2 Crack and Failure Patterns

- All specimens had a similar crack pattern under the application of simulated live loads. Cracking in all of the specimens originated in the negative moment region over the two interior supports and then developed in the first and third spans. Cracks also were noticed on the bottom and side surfaces of the specimens between the two interior supports and at the bottom joint interface. Following

yielding of the steel bars, cracking started to form diagonally from the loading line to the interior supports. No cracks were found in the UHPC joints.

- All specimens had a similar failure pattern. The specimens were subjected to a flexural-shear failure including abrupt crushing of the concrete top surface and large diagonal cracking.

- No slip was found between the reinforcing steel and the joint and no fracture was observed in the reinforcing steel.

- The strength and ductility of the jointed specimens with a longitudinal closure pour connection are comparable to those of the jointless specimens.

5.1.3 Surface Preparation Techniques

- The specimens using the three joint surface preparation techniques had similar yield and failure loads. There was a lot of variation in the cracking load between the three techniques.

- The plastic formliner initially performed the best, allowing the highest load prior to cracking. The performance then suddenly dropped and the results for yielding and failure load were the lowest of the three techniques.

- The constructability of the two formliners (plastic and rubber) was essentially the same. They both had to be cut to size, attached to the forms, and then drilled to allow the joint reinforcement to pass through. The process was simple was a procedure was established. The plastic forms were meant for single time use, but

the rubber ones could be used several times, assuming the reinforcing steel layout matches up.

- The form retarder was the easiest to apply. It simply required a paint like substance to be brushed on the forms prior to the placement of the material. It was hard to ensure that the same amount of material was applied to every area. This would definitely be a concern with a complex reinforcing steel configuration. Another downfall of this procedure is that the finished product needs to be power washed to produce the final exposed aggregate surface.

5.1.4 Loads, Strains, and Deflections

- The compressive strengths for the Ductal-UHPC and the K-UHPC appeared to increase at the same rate and both types appear to reach the minimum 15 ksi on the sixth day.
- Both the ductal-UHPC and K-UHPC specimens had similar ductility and strength.
- The jointless specimens were slightly stronger than the jointed ones. This is largely due to the fact that the tensile strength of the HPC was greater than that of the bond formed at the interface. The steel yield load was essentially the same between the two types.
- All specimens experienced about 1/3 inch deflection at the time of failure.

5.2 Transverse Joints

Two specimens were designed, fabricated, instrumented, and tested in the Iowa State University Structural Engineering Laboratory. The specimens designed simulated

two adjacent modules connecting over the pier locations. The first specimen, Specimen I, incorporated the use of a compression block that was placed tightly between the two adjacent ends of the girders. The second specimen, Specimen II, was designed with the same exact details but did not include the compression block. Concrete was instead used to fill the location where the compression block would have been. Both of the specimens were tested using the same boundary conditions. Negative moment flexural strength tests were conducted by applying point loads to both cantilevered ends. The applied load, deflections under loading points, and the strains in both the steel bars and girders were measured and recorded. Having the use of the compression block as the only variable between the two specimens, made it possible evaluate the effect the compression block had on the specimen.

5.2.1 Crack and Failure Patterns

- Both specimens had a similar crack progression throughout testing. The first cracks formed on the top of the bridge deck right on the edges of the diaphragm. Cracks then started working their way out towards the loading points followed by cracks appearing in the center of the diaphragms.
- For both specimens, significantly more cracks formed on the short overhang portion of the diaphragm than on the long overhang side due to the offset of the girders and loading points. Cracks on the short overhang side continued all the way down the face of the diaphragm and eventually worked their way towards the bearing pads.

- Yielding of the top reinforcing steel mat in the deck originated at the center of the diaphragm for both specimens. The three bars positioned over the top of the girder were the first to yield.

5.2.2 Loads, Strains, and Deflections

- Cracking load for Specimen II was lower than that of Specimen I by 10 kips. The corresponding cracking moments were 357.5 ft-kip for Specimen I and 302.5 ft-kip for Specimen II. The section just outside of the diaphragm would have cracked at slightly lower loads due to the 6 in. extension in the moment arm.
- Specimen I also required an additional 45 kips more than Specimen II to reach its yielding point. The yielding moment for Specimen I and II was 1462.5 ft-kip and 1170 ft-kip, respectively. By the end of testing, all of the reinforcing steel in the top of the deck had yielded for both specimens.
- Deflection measured at the maximum load was very similar for both specimens. Specimen I was slightly less than Specimen II at 1.20 in. and 1.28 in., respectively. Deflection up until the yielding point was essentially the same.
- The factored load for the diaphragm section is 1428 ft-kip. Specimen II had several bars that yielded prior to this load. None of the reinforcing steel for Specimen I had yielded at this point.
- Based on cracking load, yielding load, and ultimate deflection results, Specimen I produced more favorable results. The compression block increased the performance of the specimen and served as an effective transfer mechanism for the compressive forces.

REFERENCES

AASHTO. (2004). AASHTO LRFD Bridge Design Specifications . Washington, DC: American Association of State Highway and Transportation Officials.

American Society of Civil Engineering (ASCE). (2015). *Iowa Infrastructure 2015 Report Card*. Retrieved from Infrastructure Report : www.infrastructurereportcard.org/bridges/

Azizinamini, A. (2005). *Development of a Steel Bridge System - Simple for Dead Load and Continuous for Live Load.* University of Nebraska, Licoln.

Bridge Engineering Center. (2015). Investigation of Negative Moment Reinforcing in Bridge Decks. Ames, Iowa: Bridge Engineering Center, Iowa State University.

Bryant, J., & Ford, C. (2013, June). A Toolkit for Accelerated Bridge Construction. *A Renewal Project Breif* . Washington, DC: Transportation Research Board.

Culmo, M. P. (2009). *Connection Details for PBES.* CME Associates, Inc. East Hartford: Federal Highway Administration.

Federal Highway Administration. (2014). *The Second Strategic Highway Research Program (2006-2016).* Retrieved March 2, 2016, from Transportation Research Board: trb.org

Hartwell, D. R. (2011). *Laboratory testing of Ultra High Performance Concrete deck joints for use in accelerated bridge construction.* Ames, Iowa.

Iowa Department of Transportation. (2016). *Little Silver Creek Bridge*. Retrieved March 11, 2015, from Iowa DOT: http://www.iowadot.gov/LSCBridge/index.html

Iowa Department of Transportation. (2016). *U.S. 6 bridge over Keg Creek*. Retrieved March 12, 2015, from Iowa DOT: http://www.iowadot.gov/us6kegcreek/

Johnson, R. (2015). *Simple Made Continuous Bridges with Steel Diaphragms: Tension and Compression Transfer Mechanisms.* Fort Collins, Colorado.

Mulholland, D. (2015). *Iowa Infrastructure 2015 Report Card.* (ASCE, Ed.) Retrieved June 6, 2016, from Infrastructure Report Card: www.infrastructurereportcard.org

Shoup, L., Donohue, N., & Lang, M. (2011, March 30). *The fix we're in For: The State of Our Nation's Bridges.* Retrieved March 2, 2016, from Transportation for America: t4america.org